HIGHWAY RESEARCH RECORD

Number 44

Concrete Pavement Design

5 Reports

Presented at the
42nd ANNUAL MEETING
January 7-11, 1963

HIGHWAY RESEARCH BOARD
of the
Division of Engineering and Industrial Research
National Academy of Sciences—
National Research Council
Washington, D. C.
1963

Department of Design

T.E. Shelburne, Chairman
Director of Research, Virginia Department of Highways, Charlottesville

COMMITTEE ON RIGID PAVEMENT DESIGN

William Van Breemen, Chairman
Research Engineer, Engineering Research
New Jersey State Highway Department, Trenton

Harry D. Cashell, Secretary
Chief, Concrete and Concrete Pavement Branch, Physical Research Division
U. S. Bureau of Public Roads, Washington, D.C.

Henry Aaron, Chief Engineer, Reinforced Concrete Pavement Division, Wire Reinforcement Institute, Washington, D.C.

Robert F. Baker, Director, Office of Research and Development, U.S. Bureau of Public Roads, Washington, D.C.

Phillip P. Brown, Consultant, Soils, Mechanics and Paving Bureau of Yards and Docks, Department of the Navy, Washington, D.C.

Paul F. Carlton, Engineer, Headquarters, Army Materiel Command, Washington, D.C.

W. E. Chastain, Sr., Assistant Engineer of Research & Planning, Research Branch, Illinois Division of Highways, Springfield

E. A. Finney, Director, Research Laboratory Division, Michigan State Highway Department, Lansing

W. S. Housel, University of Michigan, Ann Arbor

F. N. Hveem, Materials and Research Engineer, California Division of Highways, Sacramento

W. H. Jacobs, Executive Secretary, Rail Steel Bar Association, Chicago, Illinois

C. D. Jensen, Director, Bureau of Materials, Pennsylvania Department of Highways, Harrisburg

Wallace J. Liddle, Chief Materials Engineer, Materials Testing Laboratory, Utah State Department of Highways, Salt Lake City

Ernest T. Perkins, Executive Director, East Hudson Parkway Authority, Pleasantville, New York

Thomas B. Pringle, Chief, Civil Engineering Branch, Engineering Division, Military Construction, Office, Chief of Engineers, Department of the Army, Washington, D.C.

Gordon K. Ray, Manager, Paving Bureau, Portland Cement Association, Chicago, Illinois

James P. Sale, Assistant Chief, Special Engineering Branch, Research and Development, Military Science Division, Department of the Army, Office, Chief of Engineers, Washington, D.C.

F. H. Scrivner, Pavement Research Engineer, Texas Transportation Institute, A & M College of Texas, College Station

M. D. Shelby, Research Engineer, Texas Highway Department, Austin

W. T. Spencer, Soils Engineer, Materials and Tests, Indiana State Highway Commission, Indianapolis

Otto A. Strassenmeyer, Associate Highway Engineer, Research and Development, Connecticut State Highway Department, Wethersfield

K. B. Woods, Head, School of Civil Engineering and Director, Joint Highway Research Project, Purdue University, Lafayette, Indiana

Contents

Warping Stresses and Deflections in Concrete Pavements: Part III

A. S. REDDY, G. A. LEONARDS, and M. E. HARR, respectively, Research Assistant, School of Civil Engineering; Professor of Soil Mechanics; and Associate Professor of Soil Mechanics, Purdue University

The role of theoretical analyses in the development of reliable design criteria for concrete pavements is reviewed. Available theories are examined in the light of performance records. As the underlying assumptions are incomplete, the usefulness of these theories is limited; moreover, the concepts involved have restricted planning of field experiments to the point where significant variables have not been measured, with the result that interpretation of the data is confused and the findings inconclusive.

A theory is presented which accounts for warping produced by nonlinear temperature and moisture variations of sufficient magnitude to result in a partly supported slab, and the subgrade support characteristics are generalized to include time-dependent deformations. The behavior of concrete pavements predicted by this theory is found to be compatible with field performance; its use as a basis for designing more significant field experiments is recommended.

•ACCORDING to Farrell and Paterick (1), expenditures for all types of surfacing on primary and secondary roads have comprised about 40 percent of the construction funds for highways as compared with about 25 percent, each, for grading and structures. In 1960, about 4,000 miles of new concrete pavements were constructed in the United States (2), an increase of approximately 60 percent over that being constructed during the previous five years. Thus, expenditures for concrete pavements represent an important and increasing fraction of the nation's highway investment. The need for improved design criteria is now more pressing than ever.

DEVELOPMENT OF DESIGN CRITERIA

Over a period of some 50 years, each of the following approaches has aided materially in the development of design procedures for concrete pavements: (a) laboratory experiments, (b) controlled field experiments—test sections and test roads, (c) observations of prototype performance, and (d) theoretical analyses. The relative utility of these techniques will be reviewed briefly.

Highway pavements are among the most complex structures with which the civil engineer has to deal. The loads are variable in magnitude, space, and time, and large numbers of load repetitions must be taken into account; major changes in topography, subgrade materials, ground water and drainage conditions are common; the behavior of layered systems with widely different strength and displacement tolerances must be evaluated; and local variations in climatic conditions affect performance to a greater extent than in virtually any other structure of concern to the civil engineer.

Faced with such variety of significant variables, laboratory tests in which it is feasible to control only a limited number of variables and geometries can be of value primarily for the purpose of elucidating specific phenomena, such as, the effects of

Paper sponsored by Committee on Rigid Pavement Design.

repeated loads on cumulative deflections, the pumping characteristics of various types of subbases, the relative shear strength of subgrade soils, and the effects of compaction. Although such studies are very useful, in the absence of a mechanism for combining the interactions of these properties with other factors affecting pavement performance, laboratory tests are inherently incapable of leading to the formulation of more reliable overall design procedures.

Test sections and test roads permit control of a number of variables under specific prototype conditions. Highway engineers have had the foresight to use this tool to a greater extent than their counterparts in structural and foundation engineering, yet these efforts have not led to the development of generally valid design criteria. This is because prototype conditions vary widely from locality to locality and adequate procedures for translating behavior—and the interactions contingent upon this behavior—from one locality to another are not yet available. Perhaps the most valuable aspect of a test road is its use to assess the validity of a design procedure. Comparisons of this nature have almost invariably demonstrated that large disparities exist between predicted and observed behavior. It is still widely believed that the stronger the support beneath a concrete pavement the better the performance of the pavement for a given set of loading conditions. Table 1 is an abbreviated summary of the rigid pavement survival data obtained at the AASHO Road Test (3). It is apparent that subbase thickness had a minor influence on performance. In contrast to the behavior of flexible pavements, single-axle loads were hardly more damaging than their (theoretically) equivalent tandem-axle loads, but what assurance can be given that this will also be the case under a different set of prototype conditions? On the other hand, if an analysis were available that could predict such performance, and this prediction could be verified in a test road under another set of conditions, designs for other environments and loading arrangements could subsequently be made with confidence. These considerations illustrate the strength and weaknesses of the test road approach in furthering the development of reliable design concepts.

Observation of prototype performance still remains a primary basis of pavement design procedures. Investigation of failures has led to a gradual evolution in design practices so that today satisfactory pavements can be constructed to suit local conditions almost anywhere in the United States. However, this approach has many drawbacks. In the 1940's, when vehicle loads and numbers were increasing rapidly, experience could not keep pace with changing conditions. The situation has been partly remedied by enacting laws to limit vehicle loads, yet evidence is lacking to the effect

TABLE 1

ABBREVIATED SUMMARY OF PERFORMANCE DATA, NONREINFORCED CONCRETE PAVEMENTS AT AASHO ROAD TEST

Loop	Axle Load (kips)	Subbase Thickness (in.)	Axle Applications (1,000's) to Failure[a]					
			5-In. Surface	6½-In. Surface	8-In. Surface	9½-In. Surface	11-In. Surface	12-In. Surface
3	12S	3	(3.7)	(3.9)	(4.4)			
		6	(3.1)	(4.1)	(4.3)			
		9	(3.7)	(4.2)	(4.0)			
	24T	3	705	(4.0)	(4.3)			
		6	901	(4.1)	(4.3)			
		9	771	(4.0)	(4.2)			
4	18S	3	716	(3.8)	(4.5)	(4.2)		
		6	353	(4.3)	(4.4)	(4.5)		
		9	291	(3.0)	(4.3)	(4.1)		
	32T	3	343	687	(4.2)	(4.0)		
		6	328	1,000	(4.2)	(4.2)		
		9	289	722	(4.1)	(4.2)		
5	22.4S	3		760	(4.2)	(4.3)	(4.1)	
		6		898	(4.1)	(3.7)	(4.5)	
		9		705	1,111	(4.5)	(4.5)	
	40T	3		335	(4.2)	(4.2)	(4.3)	
		6		369	(4.2)	(4.0)	(4.5)	
		9		698	898	(3.8)	(4.4)	
6	30S	3			878	(3.6)	(4.4)	(4.2)
		6			(3.9)	(4.3)	(4.2)	(4.0)
		9			(3.4)	(4.2)	(4.3)	(4.2)
	48T	3			(1.8)	(3.1)	(4.3)	(4.3)
		6			(4.1)	(4.3)	(4.3)	(4.2)
		9			1,114	(4.3)	(4.3)	(4.4)

[a] Failure is taken at a serviceability index of 1.5. Numbers in parentheses are serviceability indices at end of test (no failure). S = single axle, T = tandem axle.

that current legal restrictions represent an optimum combination of road costs and vehicle efficiency and experiments with vehicle design (as related to pavement design) have been greatly restricted. Furthermore, due to changes in local conditions, virtually every state uses a different design procedure, hampering exchanges in experience between states and greatly limiting the possibilities of utilizing 50 years of road-building experience in this country in the design of equally satisfactory roads abroad. Most serious of all, although a number of current designs have proven satisfactory, there is no basis for deciding that they are necessarily the most economical. Some recent designs have been disappointing, and proposals for radical changes in pavements sections, such as the use of insulating layers for the purpose of attenuating the detrimental effects of frost action, cannot be fully accepted until a record of satisfactory performance based on trial and error techniques has been developed.

It is apparent, therefore, that the lack of adequate theory has been the largest single factor hampering further progress in highway pavement design. The validity of a theory can readily be assessed, partly in the laboratory, but principally by the use of test sections or by observations of prototype behavior. If a theory embraces the significant aspects of the problem, it can form the strongest link possible for translating experience from one locality to another. No restrictions need be placed on changing conditions, and the most economical (yet satisfactory) design can quickly be arrived at for any specific set of conditions. The history of technological development in every area of human endeavor bears eloquent testimony to the validity of these facts. A sustained and concerted effort to develop more reliable theories of pavement design is urgently needed if the public is to receive the fullest possible benefits from its highway dollar.

REVIEW OF AVAILABLE THEORIES

In earlier papers (4, 20,), the factors that influence the performance of concrete pavements were reviewed. Although it was recognized that the development of cracks in concrete pavements was not necessarily indicative of impending failure, cracks in existing roads generally reflect deficiencies in design and construction practices. The occurrence of these cracks may not be injurious initially from the standpoint of driving comfort, but rather from the danger of water penetration (and subsequent loss of support), from the loss of effective load transfer and reduced mass of the individual slabs, and from the danger of spalling and increased pavement deterioration. The gradual elimination of diagonal (corner) and longitudinal cracks in concrete pavements was traced, and it was shown that (except in special cases) failure of modern concrete pavements could not be attributed to weak subgrade support, pavement pumping, frost action, poor load transfer at joints, or deterioration of unsound concrete. Extensive performance data were cited to show that by far the major proportion of cracks were oriented transversely to the direction of the road and that they were caused primarily by the combined effects of pavement warping and superimposed traffic loads. Unequivocal evidence was presented to the effect that, for typical ambient conditions, variations in temperature and moisture with slab thickness induced warping of sufficient magnitude to result in partially supported slabs.

Although Goldbeck (5) in 1919 and Older (6) in 1921 independently derived a "corner formula" for the required thickness of concrete pavement slabs (to account for loss of support at the corners due to weak subgrades and temperature and moisture differentials), the first completely rational theoretical analysis was contributed by Westergaard (7) in 1926. In 1927 Westergaard (8) extended his analysis to the consideration of stresses and deflections induced in the slab by uniform temperature gradients. With modifications to account for the effects of adjacent loads (9), impact (10), load repetitions (11, 12) and warping effects (10, 11, 13, 14, 15), Westergaard's analysis still serves as a framework around which current design procedures for concrete pavements are built. It is pertinent, therefore, to review the basic assumptions made in this theory; namely, (a) that the temperature gradients are uniform, (b) that the slab remains at all times in full contact with its support, and (c) that the support can be represented by independent elastic springs of constant stiffness, as suggested earlier by Winkler (16).

The consequences of these assumptions has been the development of a conceptionally inadequate basis for predicting the behavior of concrete pavements. They suggest that the critical stresses will produce diagonal cracks at the corners, whereas the majority of cracks are now transverse. They indicate that, for a given set of conditions, an increase in subgrade modulus would permit the use of a reduced slab thickness, whereas it has been known for some time that concrete pavements placed on rock break up rapidly. The general lack of correlation between subgrade modulus and pavement performance is now well documented (3). Moreover investigations to evaluate the behavior of concrete pavements have generated considerable confusion, as deflections and strains have been measured without full knowledge of the actual support conditions at the time the measurements were taken.

In 1959, Harr and Leonards (4, 40) solved the "slab on ground" problem to include the (more common) case where warping due to temperature and/or moisture gradients results in partly supported slabs. For the first time, it was shown analytically that high values of the subgrade modulus (K) can result in increasing (rather than decreasing) critical stresses due to warping and that interactions between slab size and thickness, degree of subgrade support, and concrete quality may result in either increasing or decreasing critical (tensile) stresses with increasing values of K. However, the concept of a subgrade modulus (Winkler foundation), and the assumption of a uniform temperature gradient was retained.

The Winkler type foundation lacks continuity in the medium (shear stresses are neglected) and poses severe problems in determining appropriate values of K (17). For this reason, a number of investigators have preferred to replace the Winkler foundation with an elastic continuum (18). Hetenyi (19) observed: "Though the first type [Winkler foundation] is mathematically simpler, one should not regard it, as some investigators do, as an approximate or elementary solution for the elastic solid foundation, because of its own physical characteristics and significance."

Full scale experiments (20) on a slab warped by temperature gradients to a condition of partial support corroborate this view for short-term loadings. However, under sustained loadings (such as the weight of the slab), most subgrade soils suffer time-dependent deformations due to consolidation or creep processes, or to a combination of these factors. (Depending on the relative rates of these processes, creep in the concrete slab may also be important.) Such time-dependent deformations may be simulated by viscoelastic models (21, 22).

A variety of mechanical models has been proposed (23) to simulate the behavior of the viscoelastic materials. These generally consist of various combinations of three fundamental types: (a) Maxwell element, (b) Kelvin element and (c) standard solid element (Fig. 1). Freudenthal and Lorsch (24) discussed the three mechanical models and compared the behavior of these models with the actual behavior of soil. Graphs were presented to indicate that the standard solid model gives the best approximation to the actual behavior of soil.

For problems whose geometry does not vary with time, the time dependency of the viscoelastic problem can be removed by taking the Laplace transform of the differential equations and boundary conditions. This operation transforms the viscoelastic problem into an elastic problem, and the inverse transform of the solution gives the solution to the viscoelastic problem. Using this method, Freudenthal and Lorsch (24) solved the problem of an infinite beam on a viscoelastic foundation; Hosken and Lee (25) solved the problem of an infinite elastic plate on a viscoelastic foundation; Pister and Williams (26) solved the problem of an infinite plate on a viscoelastic foundation taking into account Reissner's (27) shear interactions; and Kerr (28) solved the problem of a rigid circular plate on a viscoelastic foundation taking into account shear interactions. Lee (29), and Boley and Weiner (30), discuss other methods of solving viscoelastic problems and include excellent bibliographies. For the special case where the slab is in full contact with its support, the principle of superposition may be applied and the use of the Laplace transform method is justified. However, for the more common case of partial support, superposition is not applicable (even though the differential equations are linear) because each component of loading has an independent effect on the distance to the point of zero support (Fig. 2).

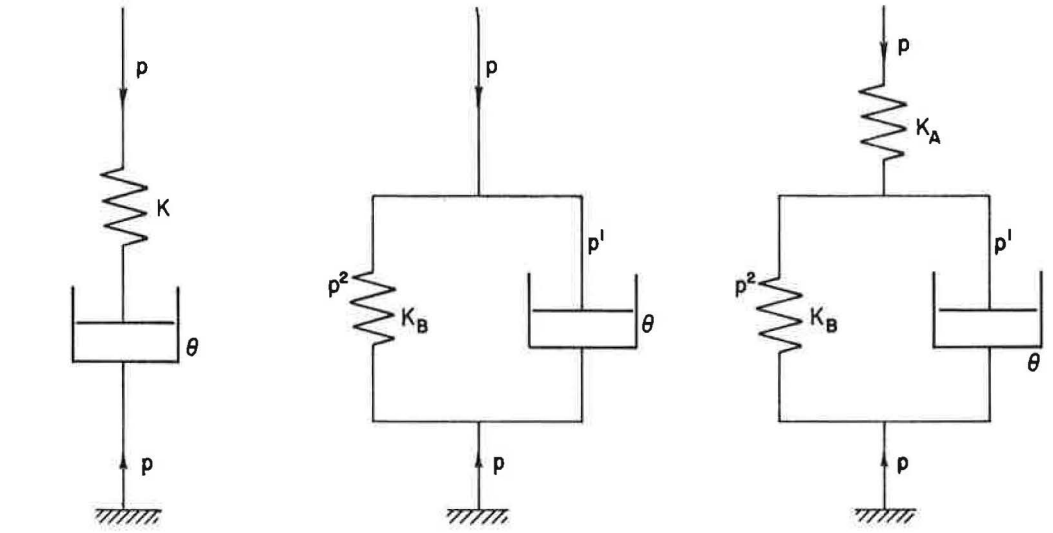

Figure 1. Basic elements of viscoelastic models.

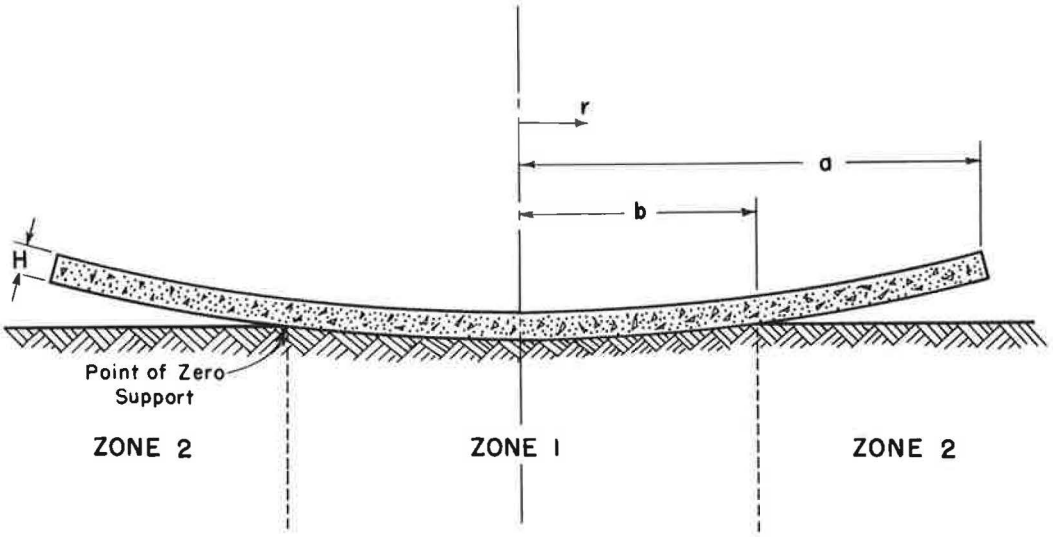

Figure 2. Simplified diametral section of a warped slab.

In their solution of the partly supported slab on a Winkler foundation Harr and Leonards (4, 20) assumed linear temperature (or moisture) variations through the thickness of the slab, although observations by Teller and Sutherland (15), Lang (31), and the Corps of Engineers (32) showed that curved temperature variations represent the more usual distribution. This was based on the fact that Teller and Sutherland concluded from their observations that linear variations are more critical, and the fact that Thomlinson's analysis (33) of a simple harmonic variation in temperature at the top surface of the slab (which resulted in curved temperature variations) gave values of computed stresses less than those of Westergaard for a fully supported slab. However, once the solution to a partly supported slab on a viscoelastic foundation was ob-

tained, it was realized that non-linear temperature (or moisture) variations could be more critical than linear variations.

In summary, realistic analysis of the critical stresses and deflections that develop in concrete slabs on ground due to their weight, superimposed loads, and temperature (and/or moisture) variations must take into account at least the following three physical phenomena:

1. Warping of sufficient magnitude to result in only partial support of the slab by the ground;
2. Non-linear temperature (and/or moisture) variations as a function of slab thickness; and
3. Subgrade reactions that are time-dependent.

This report presents an analysis that includes all three of these factors. Numerical solutions were obtained for the Maxwell and standard solid models for linear (equivalent) temperature variations, and for the case where the temperature variations can be represented by the combination of a linear and a (symmetrically) curved variation. Comparisons are made with the solutions obtained by Leonards and Harr (4) and with field performance records. On the basis of these comparisons, the utility of the new theory is assessed.

THEORY

Assumptions

1. Homogeneous, isotropic, circular slab with a free edge boundary obeying Hooke's law.
2. The supporting medium is homogeneous and is represented at each point of contact by an independent viscoelastic element.
3. Deflections of the slab are small in comparison to its thickness.
4. External forces acting on the slab are those due to gravity and/or a uniformly distributed load acting normal to the surface of the slab. Inertia forces are neglected.
5. The slab is subjected to a temperature (and/or moisture) variation with depth that is independent of time. The variation in temperature is constant on all planes parallel to the upper and lower slab surfaces.

Notation

F = force
L = length
T = temperature
t = time
w = deflection, considered positive in the upward direction (L)
$w_{m,n}$ = deflection at the nodal point n after mth increment in the value of the radial distance to the point of zero deflection (L)
E = Young's modulus (F/L^2)
μ = Poisson's ratio
H = slab thickness (L)
y = any arbitrary distance from the center of the slab, positive down (L)
q = uniformly distributed load due to the weight of the slab and/or surface loading (F/L^2)
$D = \frac{E\,H^3}{12\,(1-\mu^2)}$ = flexural rigidity of the slab (FL)

$T(y)$ = temperature at depth y (T)
ΔT = temperature difference between top and bottom of slab
K = spring constant for Winkler foundation or Maxwell model (F/L^3)
K_A = spring constant of upper spring in standard solid model (F/L^3)
K_B = spring constant of lower spring in standard solid model (F/L^3)
$p(t)$ = upward reaction on the slab at time t (F/L^2)

$p^1(t)$ = reaction on dash pot at time t (F/L^2)
$p^2(t)$ = reaction on lower spring in standard solid model at time t (F/L^2)
θ = dash pot constant (Ft/L^3)
τ = dimensionless time factor (Kt/θ)
α = linear coefficient of thermal expansion (T^{-1})
λ = distance between two nodal points (L)
r = radial distance (L)
b = radial distance to point of zero deflection (L)
a = radius of slab (L)
t_m = time required for the mth increment in the value of b (t)
V (r) = shear at point r (F/L)
M (r) = radial bending moment at point r (FL/L)
σ (r) = radial stress at point r (F/L^2)

$$\nabla^2 r = \frac{\partial^2}{\partial r^2} + \frac{1}{r}\frac{\partial}{\partial r}$$

$$\nabla^4 r = \left(\frac{\partial^2}{\partial r^2} + \frac{1}{r}\frac{\partial}{\partial r}\right)\nabla^2 r$$

Analysis

The thermoelastic problem is first reduced to an equivalent elastic problem with initial and boundary stresses. Consider a slab that is initially at a uniform temperature. Let the temperature at any distance y from the center of the slab be changed by T (y). Stresses will be applied at the boundary to prevent deformations from occurring within the slab due to the change in temperature. For the strains at all points to be zero (30):

$$\frac{1}{E}(\sigma_r - \mu\sigma_\theta) + \alpha T(y) = 0 \qquad (1a)$$

$$\frac{1}{E}(\sigma_\theta - \mu\sigma_r) + \alpha T(y) = 0 \qquad (1b)$$

From Eqs. 1a and 1b,

$$\sigma_r = \frac{-\alpha E T(y)}{(1-\mu)} = \sigma_\theta \qquad (2)$$

Inasmuch as σ_r and σ_θ are equal, the values of the stresses in any other direction must also equal σ_r.

Thus, to prevent deformations at all points within the slab, stresses σ_r and σ_θ given by Eq. 2 must be applied at every point within the slab and at the boundary of the slab. However, since the boundary at r = a was initially assumed to be free, the radial stress $\frac{-\alpha E T(y)}{(1-\mu)}$ must be removed at the boundary. This can be done conveniently by substituting a statically equivalent force system (which has the same resultant force and moment per unit length) along the boundary but of opposite sign. The thermoelastic problem is reduced to an elastic problem with a moment at r = a and initial stresses at all values of r given by

$$M(r)\Big]_{r=a} = \frac{\alpha E}{(1-\mu)} \int_{-H/2}^{+H/2} T(y)\, y\, dy \qquad (3)$$

$$\sigma_r \text{ (initial)} = \frac{-\alpha E\, T(y)}{(1 - \mu)} + \frac{\alpha E}{H(1 - \mu)} \int_{-H/2}^{+H/2} T(y)\, dy \tag{4}$$

Invoking Saint-Venant's principle (30, 34), the solution obtained using this substitution is very accurate at distances from the free edge larger than the thickness of the slab.

The case where temperature increases with the depth of the slab (upward warping) is treated in this paper. The slab is divided into zones as shown in Figure 2. Zone 1 represents the region that is in contact with the viscoelastic foundation. Zone 2 represents the region having no contact with the foundation.

The differential equation for zone 1 is (35)

$$D\left(\frac{\partial^4 w}{\partial r^4} + \frac{2}{r}\frac{\partial^3 w}{\partial r^3} - \frac{1}{r^2}\frac{\partial^2 w}{\partial r^2} + \frac{1}{r^3}\frac{\partial w}{\partial r}\right) = q - p\,(t) \tag{5}$$

in which q is the superimposed axisymmetrical load and p (t) is the time-dependent subgrade reaction.

The differential equation for zone 2 is (35)

$$D\nabla^4 w = q \tag{6}$$

For the Maxwell model, p and w are related by

$$\frac{\partial w}{\partial t} = \frac{1}{K}\frac{\partial p}{\partial t} + \frac{p}{\theta} \tag{7}$$

For the standard solid model they are related by

$$\frac{\partial w}{\partial t} = \frac{1}{K_A}\frac{\partial p}{\partial t} + \frac{1}{K_B}\frac{\partial p^2}{\partial t} \tag{8a}$$

or

$$\frac{\partial w}{\partial t} = \frac{1}{K_A}\frac{\partial p}{\partial t} + \frac{p^1}{\theta} \tag{8b}$$

The equivalent elastic problem is solved by the finite-difference method. The central difference equations (36, 37) for the first four partial derivatives are (λ, the distance between nodal points):

$$\frac{\partial}{\partial r} \cong \frac{\cdots}{2\lambda} \qquad (-1)\;(0)\;(+1)$$

$$\frac{\partial^2}{\partial r^2} \cong \frac{\cdots}{\lambda^2} \qquad (1)\;(-2)\;(1)$$

$$\frac{\partial^3}{\partial r^3} \cong \frac{\cdots}{2\lambda^3} \qquad (-1)\;(2)\;(0)\;(-2)\;(1)$$

$$\frac{\partial^4}{\partial r^4} \cong \frac{\cdots}{\lambda^4} \qquad (1)\;(-4)\;(6)\;(-4)\;(1) \tag{9}$$

A difference equation will be obtained for each of the interior points within zones 1 and 2. It is apparent from Eq. 5 that a singularity occurs at r = 0. The difficulty is overcome by writing the differential equation in rectangular coordinates,

$$\frac{\partial^4 w}{\partial x^4} + \frac{2\partial^4 w}{\partial x^2 \partial y^2} + \frac{\partial^4 w}{\partial y^4} = \frac{q}{D} - \frac{p(t)}{D} \tag{10}$$

Taking the same origin for both polar and rectangular coordinates, due to radial symmetry at r = 0,

$$\frac{\partial w}{\partial x} = \frac{\partial w}{\partial y} = \frac{\partial w}{\partial r} \tag{11a}$$

$$\frac{\partial^2 w}{\partial x^2} = \frac{\partial^2 w}{\partial y^2} = \frac{\partial^2 w}{\partial r^2} \tag{11b}$$

$$\frac{\partial^4 w}{\partial x^4} = \frac{\partial^4 w}{\partial y^4} = \frac{\partial^4 w}{\partial x^2 \partial y^2} = \frac{\partial^4 w}{\partial r^2} \tag{11c}$$

Therefore

$$4\frac{\partial^4 w}{\partial x^4} = \frac{q}{D} - \frac{p(t)}{D} \text{ (at } r = 0) \tag{12a}$$

or

$$4\frac{\partial^4 w}{\partial r^4} = \frac{q}{D} - \frac{p(t)}{D} \text{ (at } r = 0) \tag{12b}$$

$$M_r = D\left(\frac{\partial^2 w}{\partial r^2} + \frac{\mu}{r}\frac{\partial w}{\partial r}\right) \tag{13a}$$

As $r \to 0$, $\frac{1}{r}\frac{\partial w}{\partial r} \to \frac{\partial^2 w}{\partial r^2}$

Therefore

$$M_r\Big]_{\text{at } r = 0} = D(1 + \mu)\frac{\partial^2 w}{\partial r^2} \tag{13b}$$

There are (n + 3) unknowns (Fig. 3); one nodal point at r = 0, n nodal points in the slab, and 2 nodal points representing the boundary conditions; n equations are obtained from interior points. At the boundary, two additional equations are obtained. For the nodal point that is common to zones one and two, another equation is obtained by equating the difference equations for the common point. (Alternately, the summation of vertical forces may be equated to zero (38). However, consideration of the difference equation for the nodal point common to zones 1 and 2 is much simpler from the standpoint of obtaining numerical results on the computer.) Therefore there are as many equations as unknowns.

If n is the nth nodal point, and using the sign conventions as shown in Figure 3,

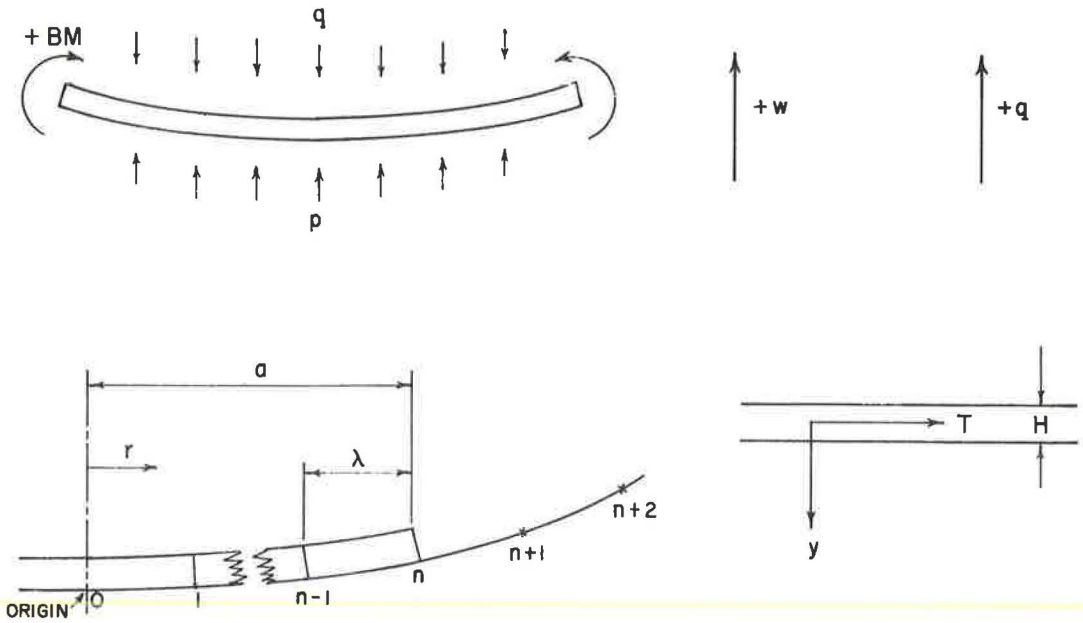

Figure 3. Nomenclature and sign convention for finite difference procedure.

$$\frac{\partial w}{\partial r} \cong \frac{w_{n+1} - w_{n-1}}{2\lambda} \tag{14a}$$

$$\frac{\partial^2 w}{\partial r^2} \cong \frac{w_{n+1} - 2w_n + w_{n-1}}{\lambda^2} \tag{14b}$$

$$\frac{\partial^3 w}{\partial r^3} \cong \frac{w_{n+2} - 2w_{n+1} + 2w_{n-1} - w_{n-2}}{2\lambda^3} \tag{14c}$$

$$\frac{\partial^4 w}{\partial r^4} \cong \frac{w_{n+2} - 4w_{n+1} + 6w_n - 4w_{n-1} + w_{n-2}}{\lambda^4} \tag{14d}$$

Taking the downward loading as q for zones 1 and 2:

$$D\ (\nabla^4 w) = -\ q + p\,(t) \tag{15}$$

For any nth nodal point the difference equations are given by

$$\frac{D}{2n^3\lambda^4}\Big[w_{m,\,n+2}\ (2n^3 + 2n^2) + w_{m,\,n+1}\ (-8n^3 - 4n^2 - 2n + 1) + w_{m,\,n}\ (12n^3 + 4n) + w_{m,\,n-1}\ (-8n^3 + 4n^2 - 2n - 1) + w_{m,\,n-2}\ (2n^3 - 2n^2)\Big] = -\ q + p_{m,\,n} \tag{16}$$

where m is the mth increment in the value of b, the common point for zones 1 and 2. For zone 2, p = 0 and for zone 1, p is a function of time.

The relation of p with deflection and time for a Maxwell element is given by Eq. 7. Writing the difference equation for this relation,

$$\frac{w_{m,n} - w_{m-1,n}}{\Delta t_m} = \frac{1}{K}\frac{(p_{m,n} - p_{m-1,n})}{\Delta t_m} + \frac{p_{m,n}}{\theta} \tag{17}$$

where $p_{m,n}$ is the contact pressure at the nth nodal point after mth increment of b and Δt_m is the time required for increasing b from (m-1)th increment to mth increment. Therefore,

$$K(w_{m,n} - w_{m-1,n}) = (p_{m,n} - p_{m-1,n}) + \frac{K\Delta t_m}{\theta} p_{m,n} \tag{18a}$$

$$K(w_{m,n} - w_{m-1,n}) = p_{m,n}\left(1 + \frac{K\Delta t_m}{\theta}\right) - p_{m-1,n} \tag{18b}$$

$$p_{m,n} = \frac{K(w_{m,n} - w_{m-1,n}) + p_{m-1,n}}{\left(1 + \frac{K\Delta t_m}{\theta}\right)} = \frac{Kw_{m,n}}{\left(1 + \frac{K\Delta t_m}{\theta}\right)} - \frac{Kw_{m-1,n}}{\left(1 + \frac{K\Delta t_m}{\theta}\right)} + \frac{p_{m-1,n}}{\left(1 + \frac{K\Delta t_m}{\theta}\right)} \tag{18c}$$

At $t = 0$, that is, for $m - 1 = 0$, $Kw_{o,n} = p_{o,n}$ (initial condition).

The relation of p with deflection and time of the standard solid element is given by Eqs. 8a and b. Proceeding in the same manner as for the Maxwell element (38)

$$p_{m,n} = \frac{K_A w_{m,n}}{1 + \frac{K_A}{K_B}\left(\frac{K_B\Delta t_{m/\theta}}{1 + \frac{K_B\Delta t_m}{\theta}}\right)} + \frac{\left(p_{m-1,n} - K_A w_{m-1,n}\right)}{1 + \frac{K_A}{K_B}\left(\frac{K_B\Delta t_{m/\theta}}{1 + \frac{K_B\Delta t_m}{\theta}}\right)} + \frac{K_A}{K_B} p^2_{m-1,n} \frac{\left(K_B\Delta t_{m/\theta}\right) \Big/ \left[1 + \left(K_B\Delta t_{m/\theta}\right)\right]}{1 + \frac{K_A}{K_B}\left(\frac{K_B\Delta t_{m/\theta}}{1 + \frac{K_B\Delta t_m}{\theta}}\right)} \tag{19}$$

At t = 0, that is, for m - 1 = 0, $p^2_{o,n} = 0$ (initial condition).

Difference Equations for Boundary Conditions

For the shear at r = a to be zero,

$$- D \frac{\partial}{\partial r} (\nabla^2 w) = 0 \tag{20a}$$

or

$$- D \left[\frac{\partial^3 w}{\partial r^3} - \frac{1}{r^2} \frac{\partial w}{\partial r} + \frac{1}{r} \frac{\partial^2 w}{\partial r^2} \right]_{r = a} = 0 \tag{20b}$$

for which the difference equation is (n = a/λ),

$$- D \left[\frac{w_{m, a/\lambda+2} - 2w_{m, a/\lambda+1} + 2w_{m, a/\lambda-1} - w_{m, a/\lambda-2}}{2\lambda^3} - \right.$$

$$\frac{1}{a^2} \frac{(w_{m, a/\lambda+1} - w_{m, a/\lambda-1})}{2\lambda} +$$

$$\left. \frac{1}{a} \frac{(w_{m, a/\lambda+1} - 2w_{m, a/\lambda} + w_{m, a/\lambda-1})}{\lambda^2} \right] = 0 \tag{21}$$

For the moment at r = a to be M_o, as given by Eq. 3

$$D \left(\frac{\partial^2 w}{\partial r^2} + \frac{\mu}{r} \frac{\partial w}{\partial r} \right) r = a = M_o \tag{22}$$

for which the difference equation is

$$D \left[\frac{(w_{m, a/\lambda+1} - 2w_{m, a/\lambda} + w_{m, a/\lambda-1})}{\lambda^2} + \right.$$

$$\left. \frac{\mu}{2a\lambda} \frac{(w_{m, a/\lambda+1} - w_{m, a/\lambda-1})}{\lambda^2} \right] = M_o \tag{23}$$

RESULTS

Computation Procedures

It is more convenient to work with increments in b, the radial distance to the point of zero deflection and to calculate the corresponding time increment Δt rather than to work directly with increments in time. In order to reduce the number of variables involved, the solutions are presented in terms of a dimensionless "time factor."

For the Maxwell model:

$$\tau = \frac{K}{\theta} \Delta t \tag{24}$$

For the standard solid model:

$$\tau = \frac{K_B \Delta t}{\theta} \tag{25}$$

The corresponding time increments can be obtained from a knowledge of the relaxation time, K/θ.

The starting point in the computations (t = 0) is the solution for a Winkler foundation (4). From this value of b, the first increment in b is taken to the immediately adjacent nodal point; thereafter, the increments in b equal the nodal point spacing λ. A decision must be made regarding the number of nodal points to be used in the numerical solution. The number must be large enough to give sufficiently precise results but not so large as to make the computational procedure too cumbersome. Furthermore, the value of λ must be small enough so that data can be obtained for a sufficient number of τ-values to show the effects of the viscoelastic foundation as a function of time.

For a = 240 in., a value of λ = 5 in. was selected; that is, a = 48 λ. Thus, the total number of nodal points is 48 + 1, the nodal point at r = 0. With the two difference equations representing the boundary conditions, the total number of simultaneous equations to be solved is 51. A flow diagram (Fig. 4) for the FORTRAN source program (39) is used in the solution; the complete program is given by Reddy (38). To examine the precision of the result, a comparison of the deflection and stress at r = 0 for a = 48 λ (51 equations), and a = 96 λ (99 equations), is given in Table 2. It is apparent that λ = 5 in. is a sufficiently small increment to give more than adequate precision for practical purposes.

Numerical Results

Due to the large number of variables involved, it is impractical to present the results as an assembly of charts similar to those prepared by Harr and Leonards (4) for the Winkler foundation. Numerical results are available (38) for the following combination of data for the case of linear variation in temperature with depth: a = 240 in.; H = 4, 12, and 24 in.; μ = 0.15; $\alpha = 6 \times 10^{-6}$ in./in./°F; ΔT = 30 F; and $E = 3 \times 10^6$ and 5×10^6 psi.

For the Maxwell model the values of K selected equal 100, 200, 400, and 700 pci; for the standard solid model computations were made for the ratio K_A/K_B equal to 0.5, 1.0, 3.0, and 10.0 with K_A = 100, 200, 400, and 700 pci.

For illustrative purposes, sets of three curves giving the deflection, radial stress at upper surface of slab, and subgrade reaction as a function of radius and time factor for a few combinations of the parameters listed above are shown in Figures 5 through 10. In spite of an extensive search of the literature, values of relaxation time K/θ appropriate to this problem were not found. Therefore, interpretation of the results in terms of actual times must await experimental determination of K/θ-values.

If the temperature distribution is nonlinear the procedure is the same, except that the initial stresses and deflections (at τ = 0) must be determined for the case of a slab on Winkler foundation with initial stresses and end moments as given by Eqs. 3 and 4 (40). If the temperature distribution can be approximated by

$$T(y) = A\, y^{2k} + B\, y \tag{26}$$

where, A and B are constants and k is any positive integer, the solution is greatly simplified. Eq. 26 can be separated into two parts:

$$T = B\, y \tag{27}$$

$$T = A\, y^{2k} \tag{28}$$

Eq. 27 represents a linear temperature distribution whose solution has already been

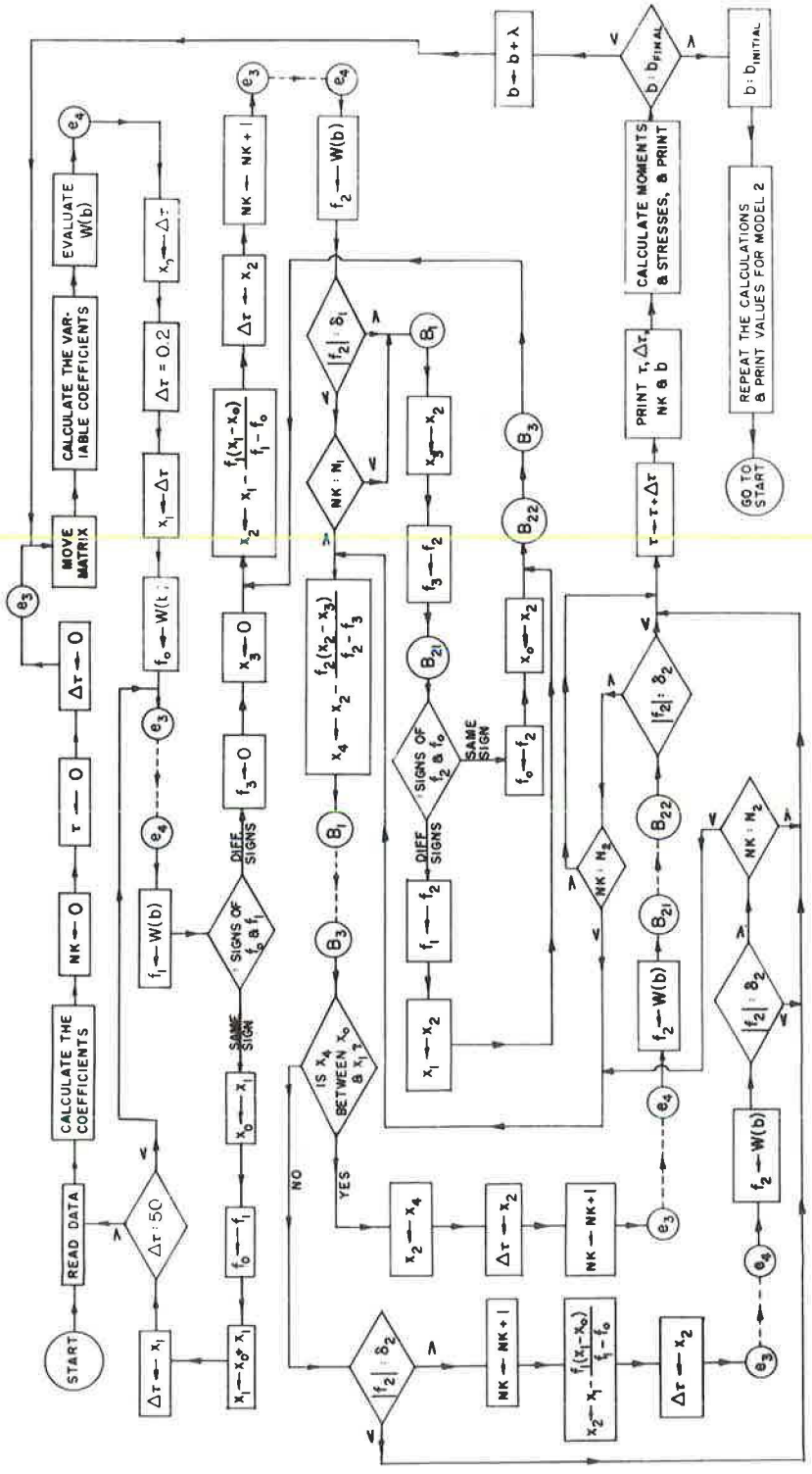

Figure 4. Flow diagram.

TABLE 2

COMPARISON OF DEFLECTIONS AND TENSILE STRESS AT r = 0

b (in.)	Time Factor		Deflection (in. × 10^{-3})		Stress (psi)	
	λ = 5 In.	λ = 2.5 In.	λ = 5 In.	λ = 2.5 In.	λ = 5 In.	λ = 2.5 In.
175	0.3204	0.3200	2.000	1.973	527.0	526.9
180	1.540	1.536	3.388	3.389	529.5	528.8
185	3.560	3.586	5.697	5.633	538.6	538.0
190	6.662	6.68	9.839	9.573	555.4	556.3
195	11.01	11.11	17.40	16.93	576.8	580.0
200	17.07	17.17	30.39	29.76	597.3	602.0
205	25.22	25.28	50.96	50.24	611.7	616.8
210	36.02	36.03	81.29	80.74	616.9	621.7
215	50.14	50.10	123.5	123.4	611.6	615.4
220	68.41	68.38	179.7	180.5	595.3	597.8

Maxwell model: K = 200 pci; a = 240 in.; E = 5,000,000 psi; ΔT = 30F; and H = 4 in.

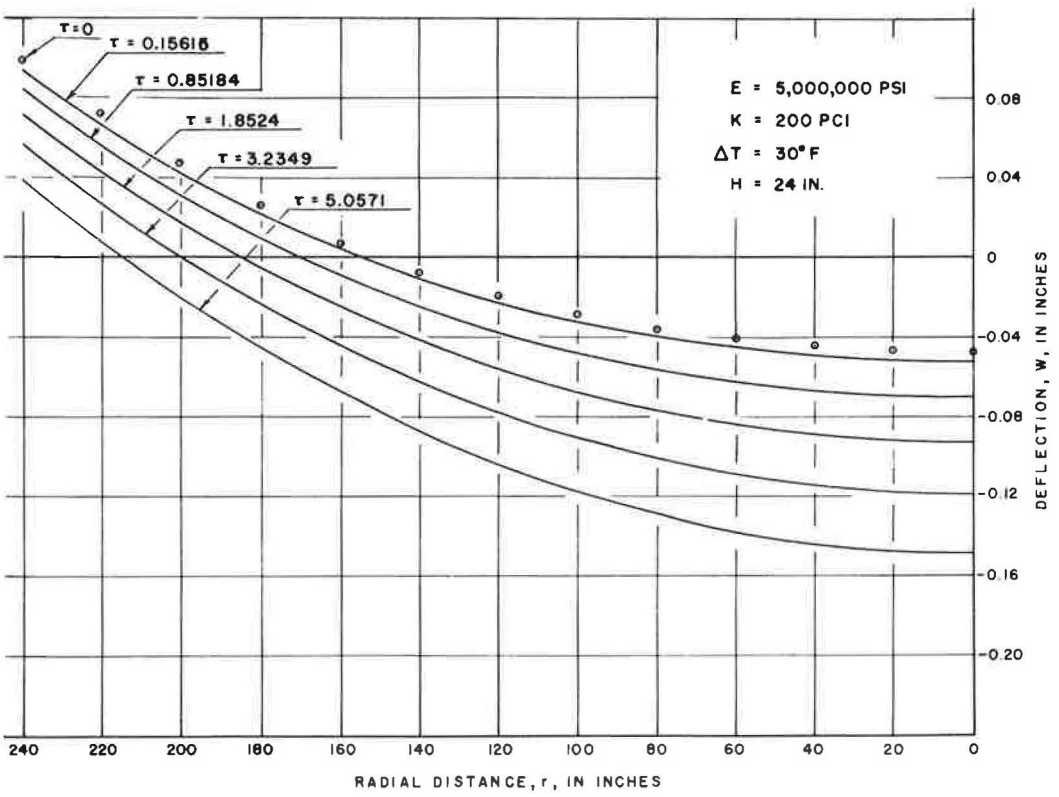

Figure 5. Deflection curves for slab on Maxwell foundation.

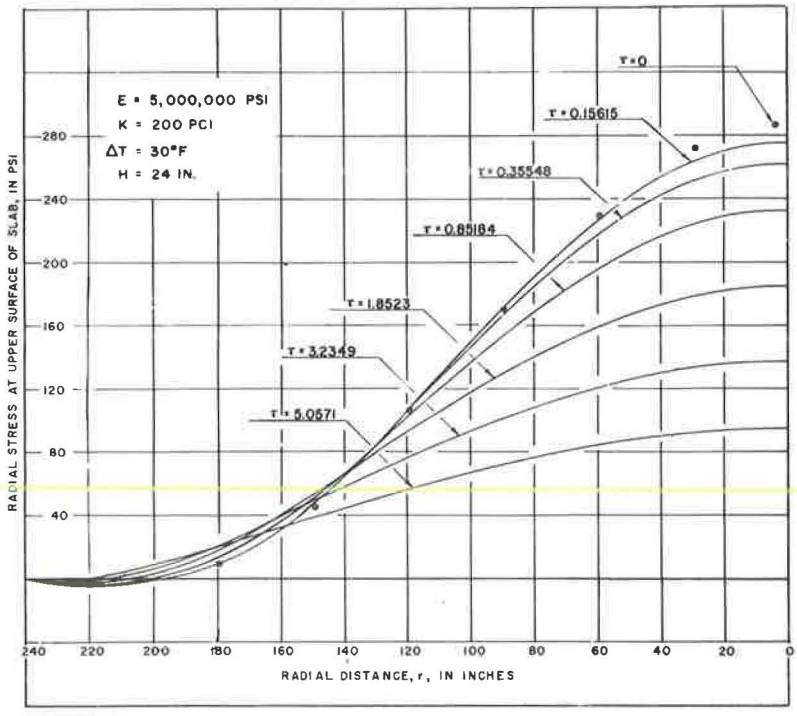

Figure 6. Radial stresses for slab on Maxwell foundation.

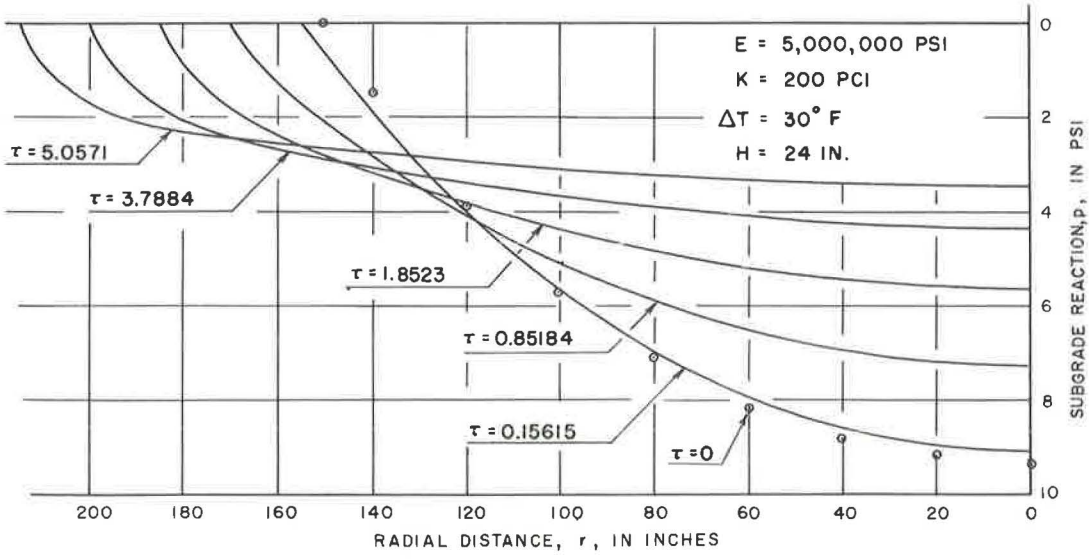

Figure 7. Subgrade reaction for slab on Maxwell foundation.

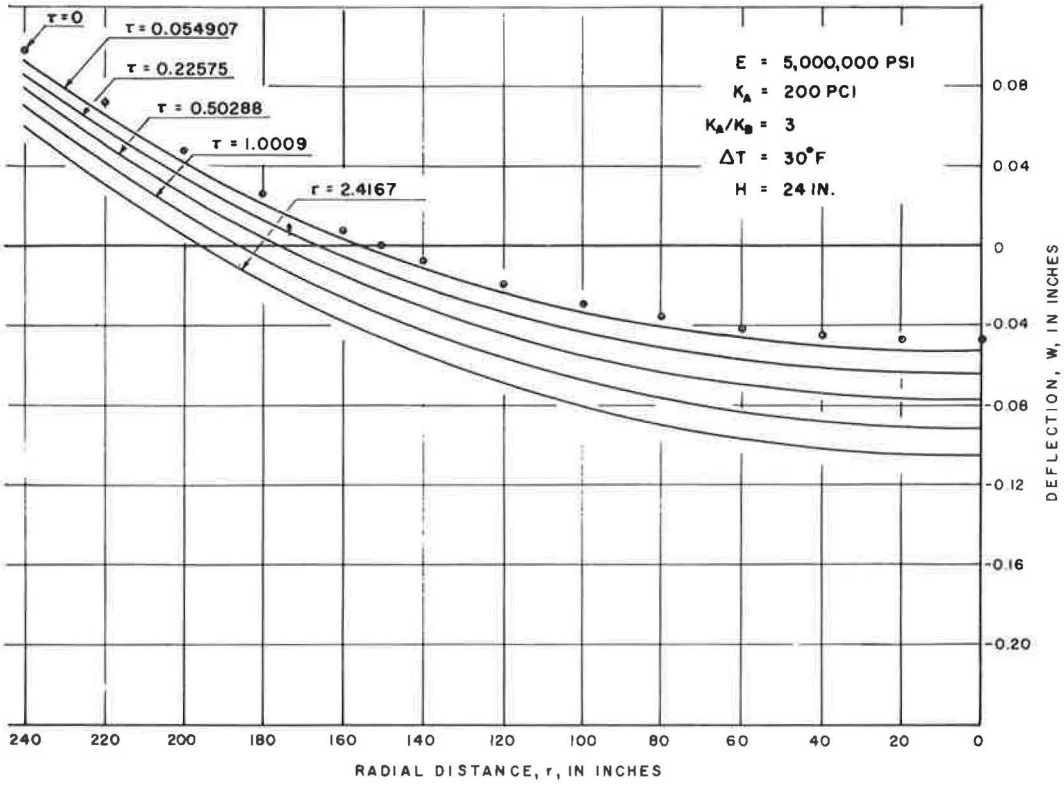

Figure 8. Deflection curves for slab on standard solid foundation.

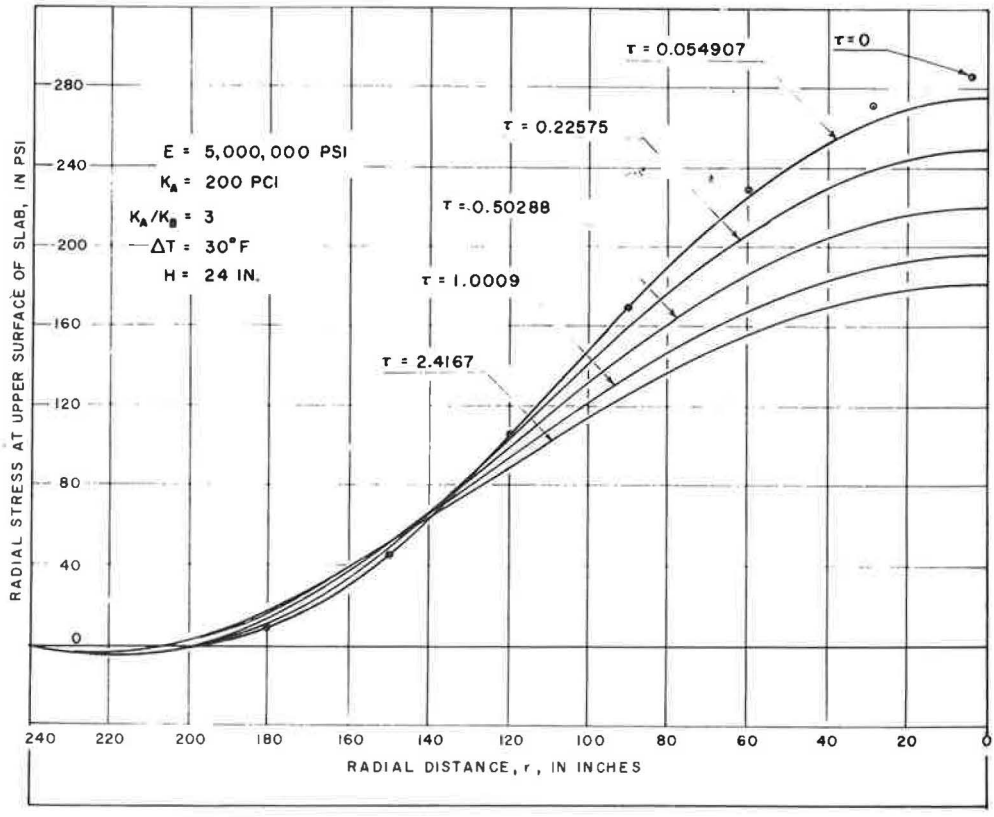

Figure 9. Radial stresses for slab on standard solid foundation.

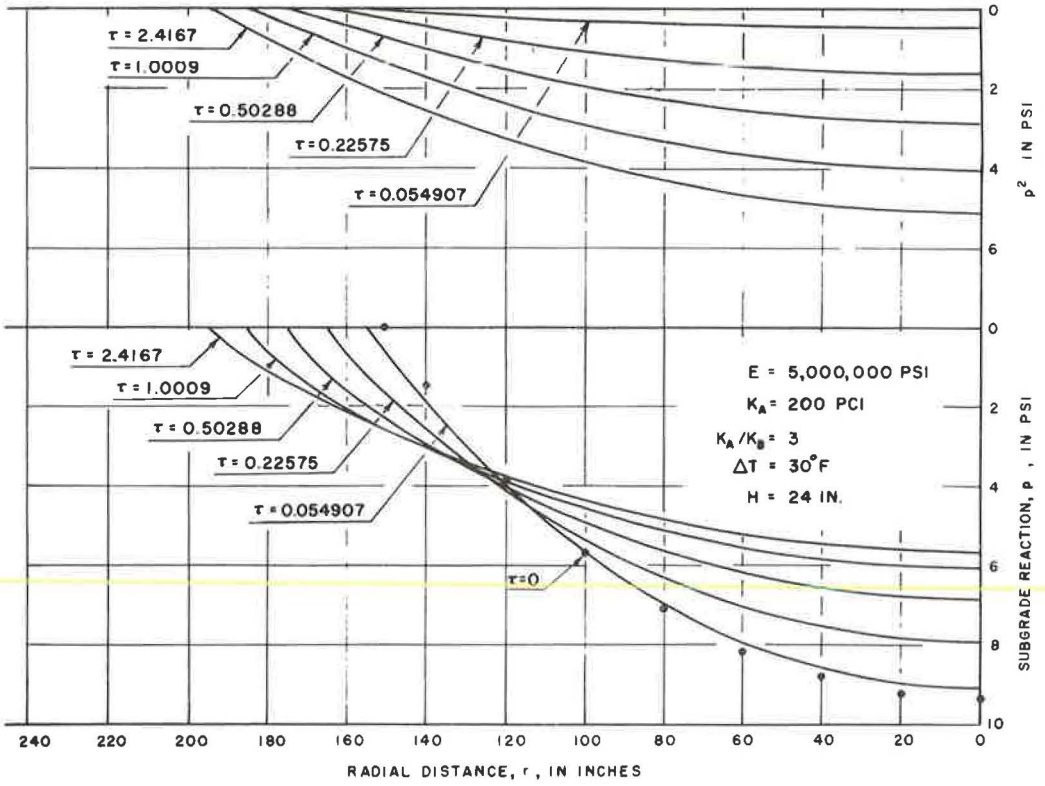

Figure 10. Subgrade reaction and p^2 for slab on standard solid foundation.

given. Eq. 28 gives a temperature distribution that is symmetrical about the mid-depth of the slab. The boundary moment (Eq. 3) is, therefore, zero; hence, this temperature distribution produces only initial stresses (Eq. 4) and no additional warping of the slab results. Because there is no change in geometry, the effects of the temperature distributions defined by Eqs. 27 and 28 are directly additive. For example, with a = 240 in.; H = 12 in.; K = 200 pci; E = 5,000,000 psi:

$$T(y) = \frac{30\,y}{H} - \frac{30\,y^2}{H^2} \tag{29}$$

the initial stress due to the temperature distribution given by Eq. 28 equals (Eq. 4):

$$\sigma_r \text{ (initial)} = \frac{\alpha E}{1-\mu}\left[-T(y) + \frac{1}{H}\int_{-H/2}^{+H/2} T(y)\,dy\right] =$$

$$\frac{\alpha E}{1-\mu}\left[+\frac{30\,y^2}{H^2} - \left(\frac{1}{H}\right)\left(\frac{30}{H^2}\right)\frac{H^3}{12}\right] \tag{30}$$

for $y = -6 = \frac{-H}{2}$ (top surface of slab):

$$\sigma_r \text{ (initial)} = \frac{\alpha E}{1-\mu}\left(+\frac{30}{4} - \frac{30}{12}\right) = \frac{(6 \times 10^{-6})\ (5 \times 10^{6})}{0.85}\left(+\frac{30}{6}\right) = 176.5 \text{ psi (tension)}$$

Therefore, a tensile stress of 176.5 psi is added to the stresses obtained for the linear temperature distribution (at y = -6, top surface of slab) for all values of r and τ. The deflections are identical with those obtained from the linear temperature distribution.

DISCUSSION OF RESULTS

Figure 11 shows the effect of the type of model assumed for the subgrade support on the maximum tensile stress in the slab. For a 24-in. slab on a relatively weak subgrade, the Maxwell model results in a very large reduction in the maximum tensile stress (compared to a Winkler foundation) at a time factor equal to 5. For large values of K_A/K_B, the standard solid model tends towards the Maxwell model; at very small values of K_A/K_B the standard solid model tends towards a Winkler foundation. Thus, in general, the Winkler foundation and the Maxwell model bracket the range in tensile stress likely to occur due to viscoelastic effects in the subgrade. An appropriate standard solid model may be assumed to approximate relaxation effects, as suggested by Freudenthal and Lorsch (24).

The effect of time on the maximum tensile stress in the slab is shown in Figure 12 for a weak subgrade, and in Figure 13 for a relatively strong subgrade. Two important deductions can be made:

1. Viscoelastic effects in the subgrade cause important reductions in maximum tensile stress with time in the case of thick slabs; for thin slabs, relaxation effects are relatively minor and may even result in an increase in the maximum tensile stress with time.
2. For thick slabs, the maximum tensile stresses are significantly lower for slabs on weak subgrades as compared with strong subgrades.

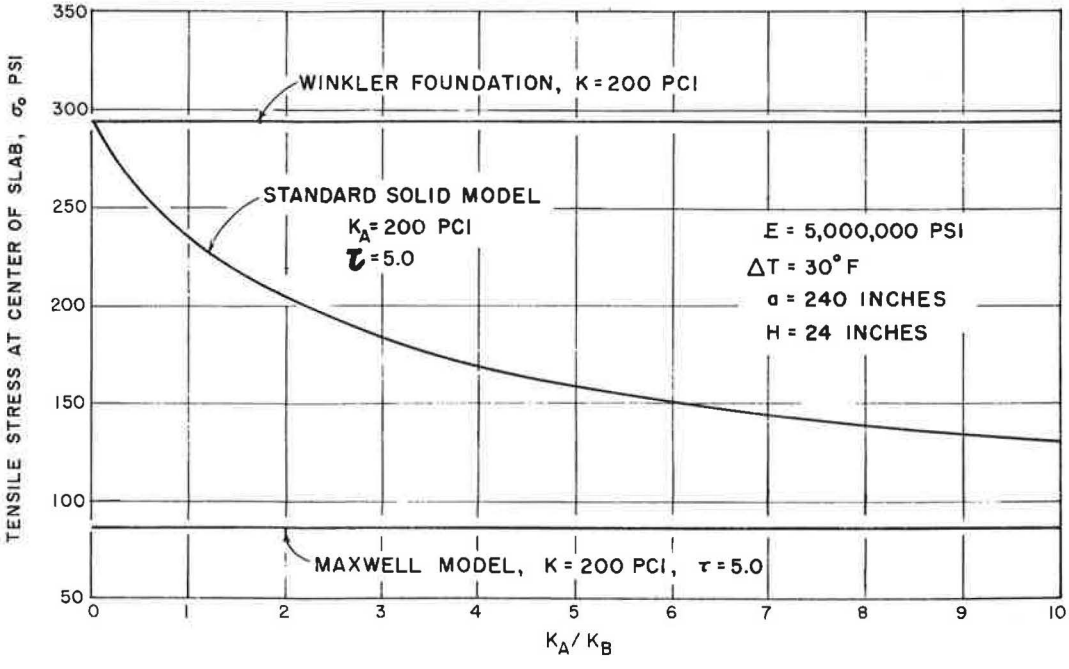

Figure 11. Effect of subgrade support on maximum tensile stress.

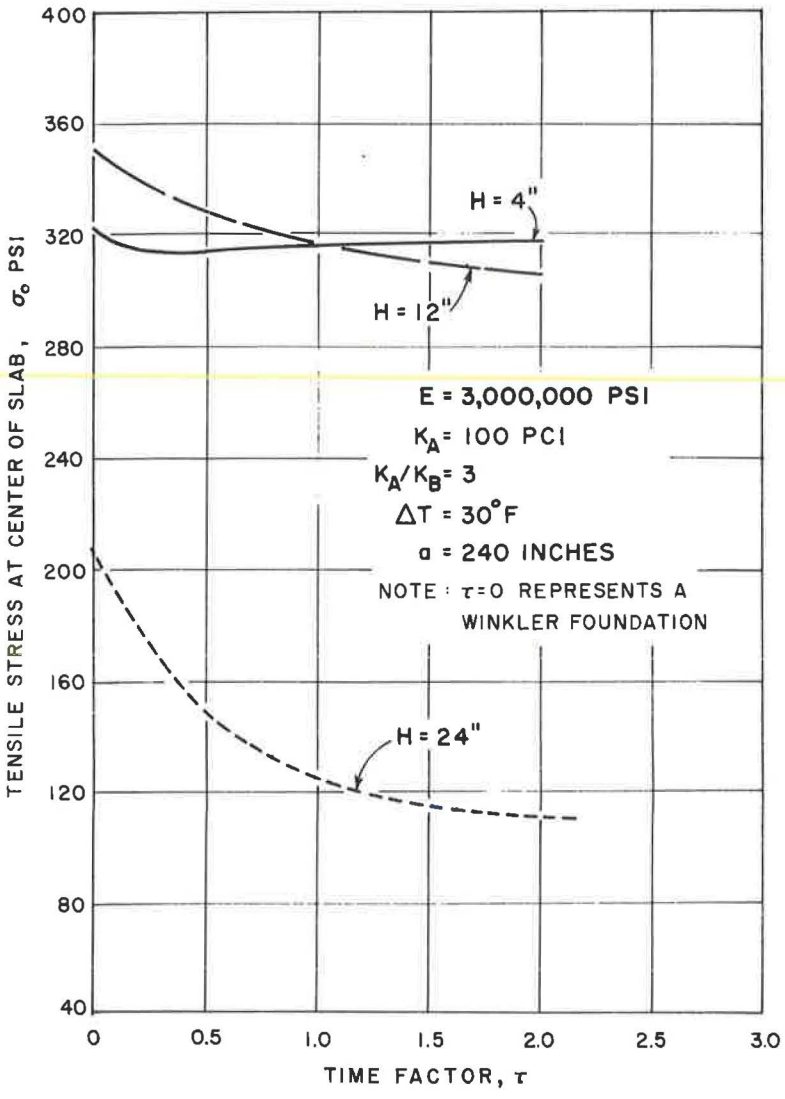

Figure 12. Effect of time on tensile stress at center of slab—standard solid model.

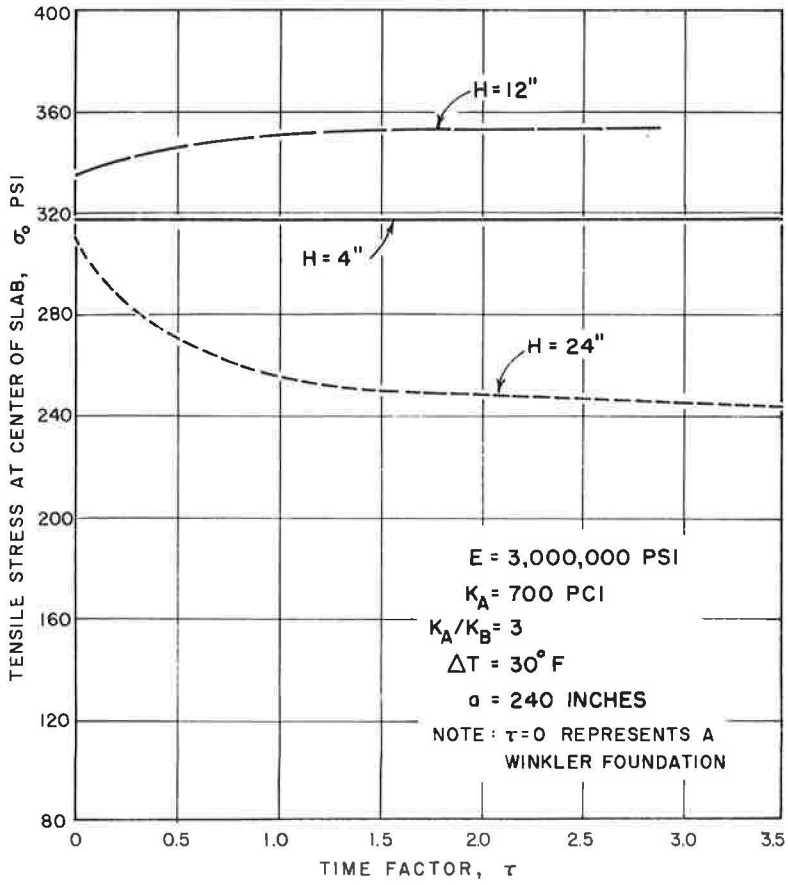

Figure 13. Effect of time on tensile stress at center of slab—standard solid model.

Pending experimental verification of the theoretical results, it appears that the combination of a thick slab and a weak subgrade will combat the detrimental effects of warping most successfully, as shown by Figure 14 where the ratio of the tensile stress at the center of the slab to the modulus of rupture is plotted for the three subgrade models as a function of the modulus of subgrade reaction. For the two viscoelastic models, values of τ were selected so that relaxation is virtually complete (i.e., the slabs have sunk into the ground until they are almost fully supported by the subgrade). Assuming that the standard solid model is a reasonable approximation to reality, it is seen that for thinner slabs little benefit is obtained as the stiffness of the subgrade is increased. This is compatible with performance records obtained at the AASHO Road Test (3). For thick slabs, increased subgrade stiffness is detrimental.

For a given temperature difference between the top and bottom of the slab, a non-linear temperature distribution results in larger tensile stresses than a linear temperature distribution if the gradients in the top half of the slab thickness are larger than in the bottom half (for the case of upward warping) and vice versa for downward warping. Since this type of non-linear temperature distribution commonly occurs in practice (15, 31, 32), the non-linear case is critical from a design standpoint.

The analysis presented herein is sufficiently general to provide a sound basis for significant field experiments. Procedures are available to measure temperature gradients and degree of subgrade support (20); in fact, considerable data on temperature variations have already been accumulated (15, 31, 32). Measurement of the

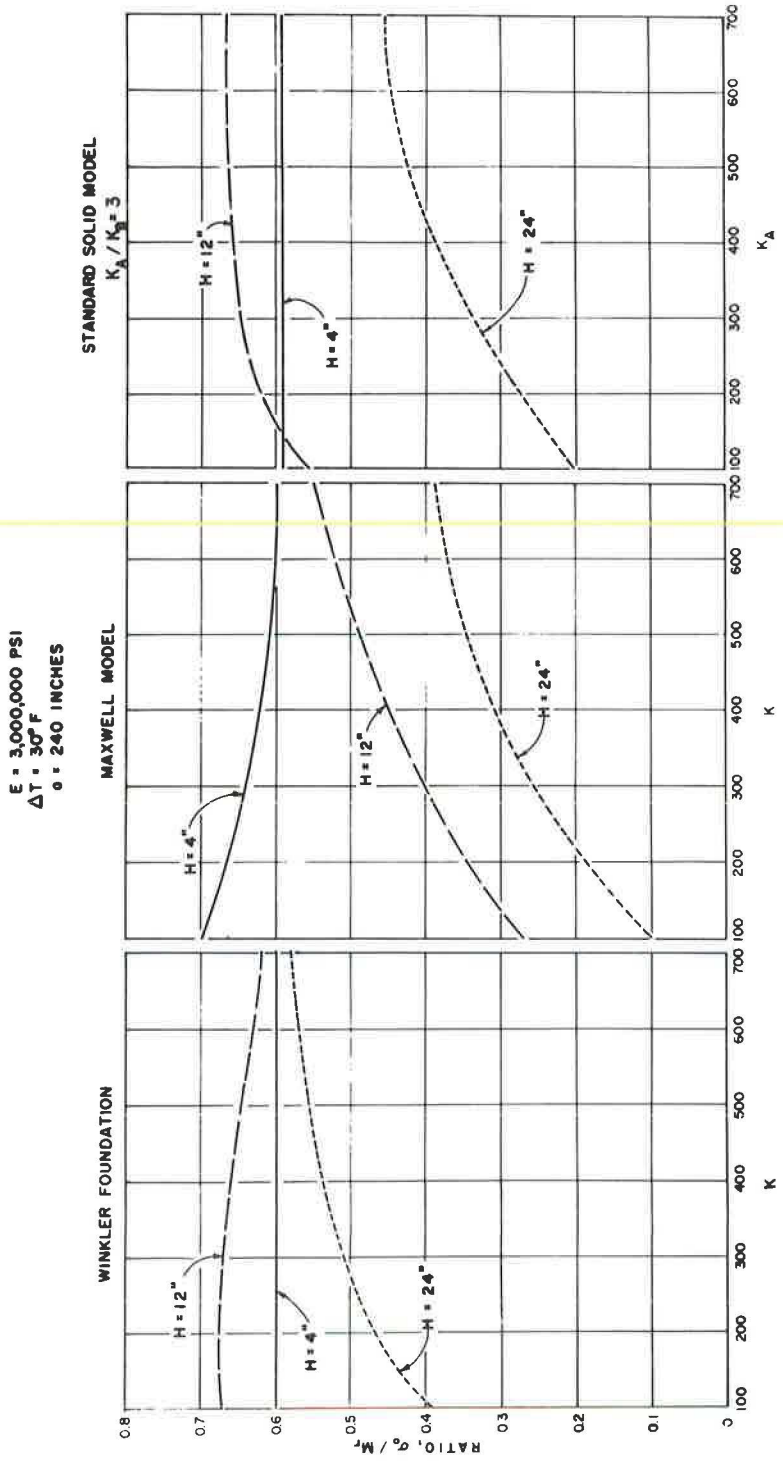

Figure 14. Effect of type and properties of subgrade support on maximum tensile stresses in the slab (relaxation virtually complete).

equivalent effect of transient moisture gradients is a more difficult problem, but considerable progress has recently been made in this connection (41). Experiments to determine the parameters K_A, K_A/K_B, and K_B/θ would permit a full appraisal of the practical utility of the theory presented. Extension of the analysis to account for the effects of moving loads over (partly supported) warped slabs, and for creep effects in the slab itself, would establish the final link between theory and reality in the concrete pavement design problem.

CONCLUSIONS

1. On the basis of the assumptions stated herein, a theory has been developed whereby the stresses, deflections, subgrade reaction, and degree of subgrade support can be computed for finite slabs subject to: (a) warping due to linear or non-linear temperature and/or moisture variations of sufficient magnitude to result in a partly supported slab; and (b) subgrade supports consisting of a Winkler foundation or a standard viscoelastic element.
2. Regardless of the type of subgrade support, thick slabs on weak subgrades develop significantly lower (30 to 80%) tensile stresses due to warping than do thin slabs on weak or strong subgrades, or thick slabs on strong subgrades. Thus, the combination of thick slabs and weak subgrades will combat the detrimental effects of warping most successfully.
3. Viscoelastic effects in the subgrade cause large reductions in the maximum tensile stress with time in the case of thick slabs on weak subgrades; for thin slabs, relaxation effects are relatively minor and may even result in an increase in the maximum tensile stress with time.
4. For a given temperature difference between slab surfaces, non-linear temperature (or moisture) distributions result in larger tensile stresses than linear temperature distributions if the gradients in the top half of the slab are larger than in the bottom half (for the case of upward warping). Since such non-linear temperature distributions are commonly encountered in practice, the non-linear case is critical from a design standpoint.
5. Although predictions based on the new theory are in qualitative agreement with performance records, field experiments are needed (including measurement of the significant parameters involved) to permit a full appraisal of its practical utility.

REFERENCES

1. Farrell, F.B., and Paterick, H.R., "The Capital Investment in Highways." HRB Proc. 32:1 (1953).
2. "Highway Statistics." U.S. Bureau of Public Roads, Washington (1960).
3. "The AASHO Road Test, Report 5, Pavement Research." HRB Special Report 61E (1962).
4. Harr, M.E., and Leonards, G.A., "Warping Stresses and Deflections in Concrete Pavements." HRB Proc. 38:286 (1959).
5. Goldbeck, A.T., "Thickness of Concrete Slabs." Public Roads, Vol. 1 (1919).
6. Older, C., "The Design of Rigid Pavements." Concrete, Vol. 18 (1921).
7. Westergaard, H.M., "Stresses in Concrete Pavements Computed by Theoretical Analyses." Public Roads (April 1926).
8. Westergaard, H.M., "Analysis of Stresses in Concrete Roads Caused by Variations of Temperature." Public Roads (May 1927).
9. Sparkes, F.N., "Stresses in Concrete Road Slabs." Structural Engineer, 17:II, 98-116 (1939).
10. Bradbury, R.D., "Reinforced Concrete Pavements." Wire Reinforcement Institute, Washington (1938).
11. "Concrete Pavement Design." Portland Cement Association, Chicago (1951).
12. Sparkes, F.N., and Smith, A.F., "Concrete Roads." Edward Arnold Co., London (1952).
13. Kelly, E.F., "Applications of the Results of Research to the Structural Design of Concrete Pavements." Public Roads, Vol. 20 (1939).

14. Spangler, M.G., "Stresses in the Corner Region of Concrete Pavements." Iowa Eng. Expt. Sta. Bull. 157 (1942).
15. Teller, L.W., and Sutherland, E.C., "The Structural Design of Concrete Pavements." Public Roads (Oct., Nov., Dec. 1935; Sept., Oct. 1936; Apr., May, June 1943).
16. Winkler, E., "Die Lehre von Elastizitat und Festigkeit." Prag (1867).
17. Terzaghi, K., "Evaluation of Coefficients of Subgrade Reaction." Geotechnique, 5:4:297 (Dec. 1955).
18. Gorbounov-Possadov, M.I., "Beams and Slabs on an Elastic Base." Mashstroyizdat, Moscow (1949). Also, "Tables for the Design of Thin Slabs on Elastic Foundations." Moscow (1959).
19. Hetenyi, M., "Beams on Elastic Foundation." Univ. of Michigan Press, Ann Arbor (1946).
20. Wiseman, J.F., Harr, M.E., and Leonards, G.A., "Warping Stresses and Deflections in Concrete Pavements: Part II." HRB Proc. 39:157 (1960).
21. Tan, T.K., "Secondary Time Effects and Consolidation of Clays." Academia Sinica, Inst. of Civil Eng. and Arch., Harbin, China (June 1957).
22. Lo, K.Y., "Secondary Compression of Clays." Jour., Soil Mech. and Fdn. Division, ASCE, 87:4:61 (Aug. 1961).
23. Freudenthal, A.M., "The Inelastic Behaviour of Engineering Materials and Structures." Wiley (1950).
24. Freudenthal, A.M., and Lorsch, H.G., "The Infinite Elastic Beam on a Linear Viscoelastic Foundation." Jour. of the Engineering Mech. Div., ASCE Proc. (Jan. 1957).
25. Hoskin, B.C., and Lee, E.H., "Flexible Surfaces on Viscoelastic Subgrades." Journ. of the Engineering Mech. Div., ASCE Proc. (Oct. 1959). "The Analysis of Loaded Flexible Surfaces over Subgrades with Viscoelastic Material." Tech. Rpt. No. 5 (Final), Division of Applied Mechanics, Brown Univ. (July 1958).
26. Pister, K.S., and Williams, M.L., "Bending of Plates on a Viscoelastic Foundation." Jour. of the Engineering Mech. Div., ASCE Proc. (Oct. 1960).
27. Reissner, E., "A Note on Deflections of Plates on a Viscoelastic Foundation." Jour. of Applied Mechanics, 25:1 (March 1958).
28. Kerr, A.D., "Viscoelastic Winkler Foundation with Shear Interactions." Jour. of the Engineering Mech. Div., ASCE Proc. (June 1961).
29. Lee, E.H., "Viscoelastic Stress Analysis." Proc. of the First Symposium on Naval Structural Mechanics, Pergamon Press (1960).
30. Boley, B.A., and Weiner, J.H., "Theory of Thermal Stresses." Wiley (1960).
31. Lang, F.C., "Investigational Concrete Pavement in Minnesota." HRB Proc., 20:348 (1940).
32. Corps of Engineers, U.S. Army, Ohio Division Laboratories, "Stresses in Thick Concrete Slabs Due to Curved Temperature Gradient." Lockborne No. 2 — 300,000 Pound Experimental Mat, August 1947.
33. Thomlinson, J., "Temperature Variations and Consequent Stresses Produced by Daily and Seasonal Temperature Cycles in Concrete Slabs." Conc. and Construction Engineering (1940).
34. Timoshenko, S., and Goodier, J.N., "Theory of Elasticity." McGraw-Hill (1951).
35. Timoshenko, S., and Woinowsky-Krieger, S., "Theory of Plates and Shells." McGraw-Hill (1959).
36. Colatz, L., "Numerische Behandlung Von Differentialgleichungen." Springer-Verlag, Berlin (1955).
37. Hildebrand, F.B., "Introduction to Numerical Analysis." McGraw-Hill (1956).
38. Reddy, A.S., "Time Dependent Warping Stresses and Deflections in Slabs on Ground." Ph.D. Thesis, Purdue Univ. (Jan. 1963).
39. McCracken, D.D., A Guide to FORTRAN Programming. Wiley (1961).
40. Leonards, G.A., and Harr, M.E., "Analysis of Concrete Slabs on Ground. Jour., Soil Mech. and Fdn. Division, ASCE, 87:4:35 (1959).
41. Bell, J.R., "A Study of the Dielectric Properties of Hardened Concrete with Respect to Their Utility as Moisture Indicators.", Ph. D. Thesis, Purdue Univ. (Jan. 1963).

Corrosion Resistance Study of Nickel-Coated Dowel Bars

L. E. WOOD and R. P. LAVOIE, respectively, Associate Professor and Graduate Research Assistant, School of Civil Engineering, Purdue University, Lafayette, Indiana

In order that a transverse expansion joint in a rigid pavement function properly, it is necessary that the load-transfer dowels offer little resistance to slab movements. Increased use of various salts for ice removal has caused dowel bar corrosion to be of some concern. The products of corrosion from ordinary steel dowel bars exhibit a large volume increase which causes a dowel to "freeze" so that it no longer functions properly. The use of rust-resistant metal coatings on steel dowel bars has shown promise in preventing the development of corrosion products.

This investigation consisted of subjecting ordinary steel dowel bars and varying thicknesses (3, 5, 7, and 10 mil) of nickel-coated dowel bars, embedded in concrete beams, to a soaking-in-brine and drying exposure. Periodically, the force necessary to cause movement of the dowel bars was measured.

Based on the present exposure period, it is evident that a very marked reduction in the force necessary to cause movement of the nickel-coated dowel bars was observed when compared to the uncoated dowel bars.

•CORROSION of load-transfer dowels has been one of the troublesome problems associated with transverse joints in concrete pavement. Dowel corrosion results in restraint to longitudinal movement of the slab followed by pavement failure. Van Breemen (1) concluded in his study of experimental dowel installations in New Jersey that "pavement failures have been due in large measure to deficiencies in joint design." He also found that at practically all of the joints with ordinary hot-rolled steel dowels, there was a progressive development of restraint to changes in dimension. In Van Breemen's study, all of the various dowel coatings, which included red lead, white lead, tar paint, graphite paint, transmission oil, cylinder stock grease, and asphaltic oils, deteriorated so much that they were practically worthless after a short time.

Robert Mitchell (2), in his study of corrosion of load-transfer dowels in Connecticut, found that the nickel-coated dowel appeared to hold considerable promise as a rust-free dowel. At the time when Mitchell released his report, no conclusive evidence of a superior rust-resisting quality between the various nickel coatings used had been noticed.

This report presents experimental laboratory results obtained from accelerated corrosion tests performed on nickel coatings of various thicknesses on 1 ¼-in. round steel dowels that were embedded in concrete blocks.

The metallurgical characteristics and manufacturing processes for the nickel-coated dowels used in this study are described by Sanborn (3).

EXPERIMENTAL PROCEDURE

It has been observed from previous studies that the corrosion of a dowel results in an increase in its size due to the fact that products of corrosion occupy a much greater

Paper sponsored by Committee on Rigid Pavement Design.

volume than the original metal. For example:

Sp. G. of iron = 7.87, Sp. G. of Fe_3O_4 (rust) = 5.18

1 cm^3 of iron weighs 7.87 gm

$$\begin{array}{ccc} 7.87 & & X \\ 3Fe + 2O_2 & \longrightarrow & Fe_3O_4 \\ 167.55 & & 231.55 \end{array} \qquad \text{or} \qquad 7.87\left(\frac{231.55}{167.55}\right) = 10.95 \text{ gm of } Fe_3O_4$$

$$\text{Volume of } Fe_3O_4 = \frac{10.95 \text{ gm}}{5.18 \text{ gm/cm}^3} = 2.1 \text{ cm}^3 \text{ or a volume increase of over 100\%}$$

This volume increase exerts tremendous pressure on the surrounding concrete and accounts for the development of restraint to longitudinal movement. With these observations in mind, the specimens for evaluating the various nickel coatings were formulated.

A specimen consisted of a 6- by 6- by 12-in. concrete block with the steel dowel bar running lengthwise through the center of the block. The dowel bar extends approximately 5 in. from one end and 1 in. from the other end of the concrete block. A total of 25 specimens were fabricated. Five contained dowel bars with a 3-mil nickel-coating thickness, five with a 5-, 7-, and 10-mil thickness, and five contained ordinary steel dowel bars.

The concrete used in making the specimens contained a well-graded Delphi dolomite, coarse, crushed aggregate with a maximum size of 1 in. and local western Indiana concrete sand. The 28-day compressive strength of the concrete was 4,185 psi. An air-entraining agent was used to improve the durability of the concrete, and its use resulted in a concrete with an air content of 4.5 percent.

A rectangular steel soaking tank containing a brine solution and a storage rack (Fig. 1), which stores 36 concrete specimens, were constructed for this project. The steel rack was used so the specimens could be easily raised and lowered into the brine solution. The soaking tank was constructed of ¼-in. steel plate, and the inside surfaces were coated with coal tar epoxy mastic to prevent corrosion of the tank. The tank is 2 by 6 ½ ft and is 3 ½ ft high.

A sodium chloride content of 27,000 ppm was established for the brine solution. This soultion remained at room temperature, which is approximately 80 F.

Two concrete specimens were made in each 6- by 30-in. mold (Fig. 2) with the center 6-in. section remaining empty. The dowel bars were lightly greased with Stanabar grease No. 2 before being placed in the concrete to prevent bonding with the concrete. The molds were stripped from the beams after a 24-hr period. The specimens were then placed in a standard moist room for 27 days. This moist room had a relative humidity of 100 percent and a

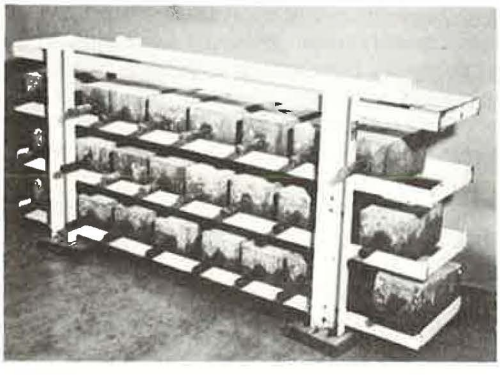

Figure 1. Storage rack.

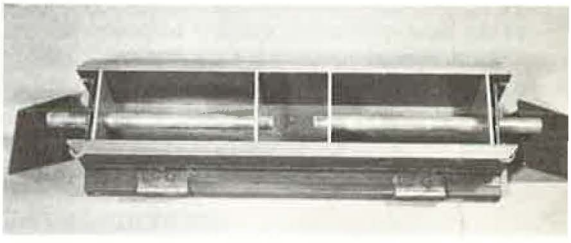

Figure 2. Mold used in making concrete blocks containing nickel-coated dowel specimens.

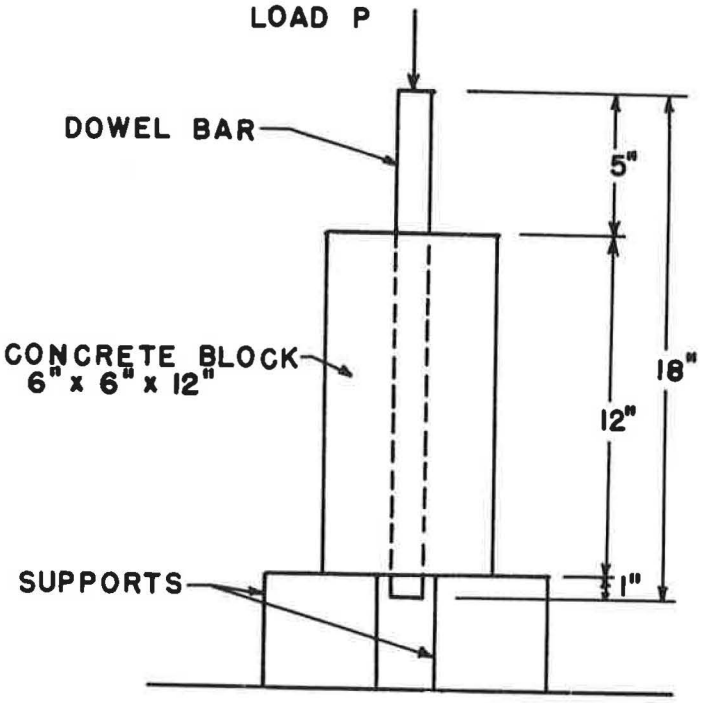

Figure 3. Loading arrangement of push-out test.

temperature of 75 F. At the end of 27 days, the specimens were removed from the moist room and placed on the rack in preparation for the brine exposure. This exposure consists of a 16-hr soaking and an 8-hr drying cycle. At the end of each 50-cycle period, a "push-out" test was performed. The push-out test consisted of applying a load to the protruding dowel in the concrete block and forcing the dowel through the concrete block (Fig. 3). The maximum load required to move the dowel was recorded as a measure of the amount of corrosion formed on the dowel. At the beginning of the test, or at "zero cycles," very little effort was necessary to move the dowels because they were not bonded to the concrete block and corrosion had not yet taken place.

STATISTICAL ANALYSIS

In order to find if there were any differences between dowel groups with different thicknesses of nickel coating, a statistical approach involving the "t" test was used because of the overlap of the results between groups. From statistics, a typical distribution of a normal population could be taken as the t-distribution (Fig. 4a). In this particular study, the populations are the maximum loads required to cause dowel bar movement in each specimen of the different groups. In other words, if a large number of dowel bar specimens with a certain nickel-coating thickness were tested, the resulting maximum loads required to cause dowel bar movement in the specimen would probably be distributed in the form of a t-distribution. Most specimens in the group would tend toward a certain average maximum load. Although there is always the possibility that certain maximum loads are much higher or lower than the average maximum load, this possibility gets smaller as the load differs from the average.

The maximum loads of each specimen group with different nickel-coating thicknesses may be represented by a t-distribution. In most cases these distributions overlap one another (Fig. 4b). Therefore, it is necessary to perform a statistical test to see if two specimen groups are truly different from one another. Since a

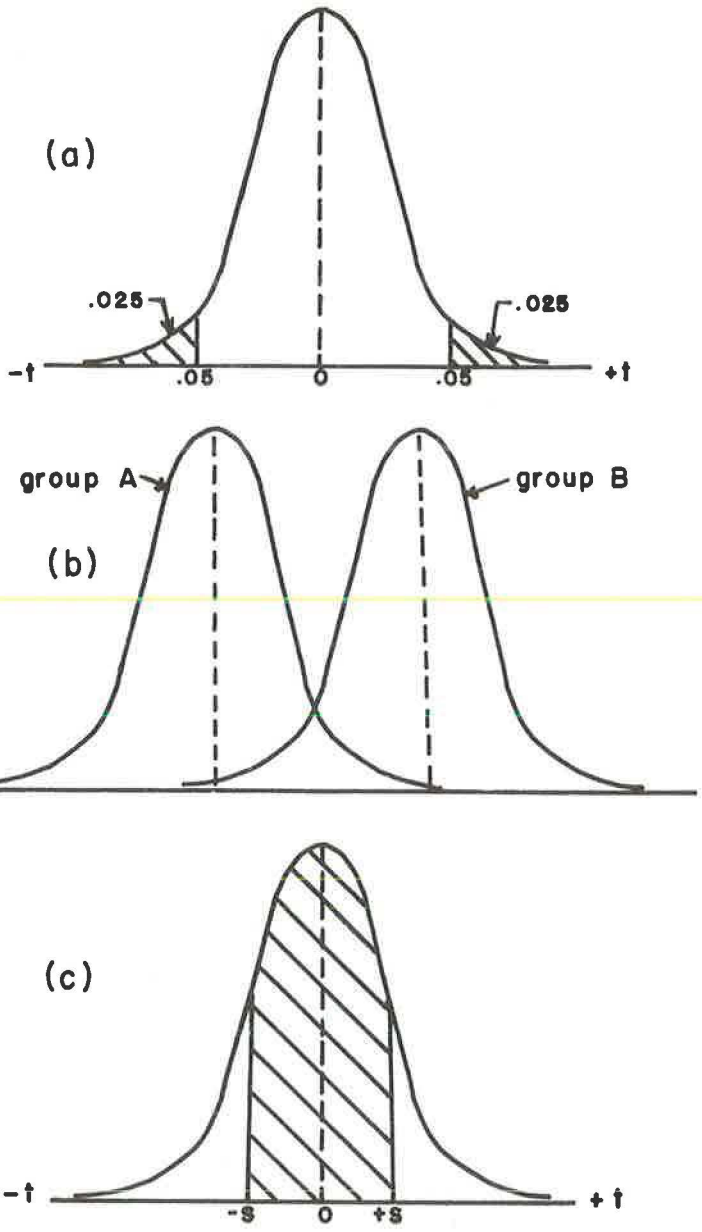

Figure 4. (a) t-distribution with (n - 1) degrees of freedom; (b) t-distribution of two overlapping groups; and (c) shaded area includes 68 percent of total area under t-distribution curve.

t-distribution has been assumed, the statistical test used in this case is called the t-test.

Essentially in performing the t-test, one tries to compare the true mean values of the two groups. The true mean value is not necessarily equal to the average of the maximum loads in each group. The average value of the group is located at the maximum ordinate of the t-distribution curve, but the location of the true mean value for the group on the t-distribution curve is not known at this moment.

If it is assumed that two random samples were obtained from two normal populations (t-distribution) and that the two populations have a common variance, it can be shown that Eq. 1 follows the t-distribution curve.

$$t = \frac{\bar{Y}_1 - \bar{Y}_2}{\sqrt{\frac{S^2}{N_1} + \frac{S^2}{N_2}}} \tag{1}$$

in which

$\bar{Y}_1$ = average maximum load of group 1;
$\bar{Y}_2$ = average maximum load of group 2;
N_1 = number of specimens in group 1;
N_2 = number of specimens in group 2;
S^2 = square of the pooled estimate of the common sample variance; that is,

$$S^2 = \frac{\sum_{i=1}^{N_1} (Y_{1i} - \bar{Y}_1)^2 + \sum_{j=1}^{N_2} (Y_{2j} - \bar{Y}_2)^2}{N_1 + N_2 - 2} \tag{2}$$

Y_{1i} = maximum load on each specimen of group 1;
Y_{2j} = maximum load on each specimen of group 2; and
$N_1 + N_2 - 2$ = degrees of freedom.

It should be noted that in this analysis the sample variances of the two groups are not equal as was assumed in arriving at Eqs. 1 and 2. However, these equations are still used because the statistical analysis is greatly simplified. The sample variance of each group may be calculated using Eq. 3.

$$S^2 = \frac{\sum_{i=1}^{N} (Y_1 - \bar{Y})^2}{N - 1} \tag{3}$$

The standard deviation s of the group is equal to the square root of the sample variance S^2 of the group (Eq. 3). The standard deviation may be used as a measure of the scatter of the data. An interval of plus and minus one standard deviation from the mean would include 68 percent of all the possible values of the maximum loads on the specimens in each group (Fig. 4c).

The calculated t gives an indication of the location of the mean values of the two groups. By use of a table of the percentage points of the t-distribution taken from any statistics book, it may be stated with what percentage certainty the true mean values of the two groups differ. For example, with a t-value of 2.306 and 8 degrees of freedom, a table of percentage points of the t-distribution would show a value of five percent.

This would mean that one would be 95 percent certain that the two groups are different.

RESULTS

The averages of the maximum loads necessary to cause slippage on the five identical specimens of each group for the various exposure periods are given in Table 1 and shown in Figure 5. Table 1 also contains the standard deviation for each set of data.

Table 2 summarizes the sample variances S^2 between groups that are needed in calculating the percentage points of the t-distribution between groups which are indicated in Table 3. All of the necessary calculations were performed as outlined in the preceding paragraphs, and sample calculations are in the Appendix.

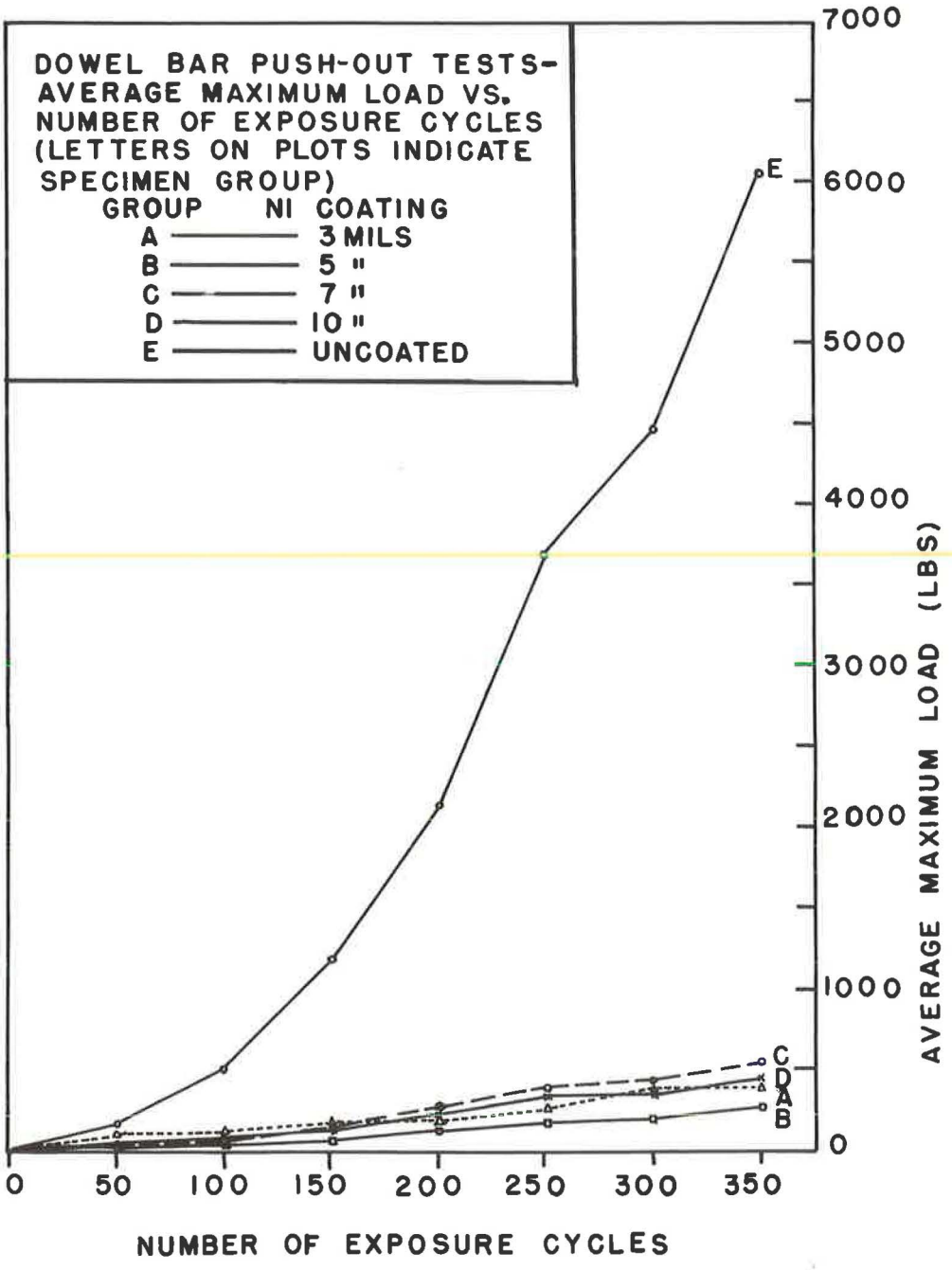

Figure 5.

Photographs of the different specimens were taken at the end of 50 and 350 exposure cycles (Fig. 6). The 3- and 5-mil nickel-coated dowels at the end of 50 exposure cycles appear to be rust-free, but the untreated dowels are obviously corroded. At the end of 350 exposure cycles, a rust spot was evident on the 3-mil nickel-coated dowel; no corrosion was evident on the 5-mil nickel-coated dowel; and considerable corrosion was evident on the untreated dowels.

TABLE 1

AVERAGE MAXIMUM LOAD (LB) NECESSARY TO FREE THE DOWEL BAR IN THE PUSH-OUT SPECIMENS, AND STANDARD DEVIATION OF EACH GROUP

No. of Cycles	Group A (3-mil Ni)		Group B (5-mil Ni)		Group C (7-mil Ni)		Group D (10-mil Ni)		Group E (untreated)	
	Avg.	s	Avg.	s	Avg.	s	Avg.	s	Avg.	s
50	76	33.6	23	7.8	37	10.8	42	21.3	186	51
100	115	37.0	40	9.3	72	11.6	88	32.4	506	134
150	168	52.0	71	26.0	150	40.5	156	36.6	1,184	365
200	200	56.9	114	31.1	250	106.0	217	20.8	2,139	854
250	260	87.8	185	31.0	373	135.5	320	23.8	3,680	1,458
300	365	157.5	208	49.8	416	197.0	349	51.3	4,446	1,444
350	400	181.0	271	49.2	570	243.0	432	42.4	6,042	2,700

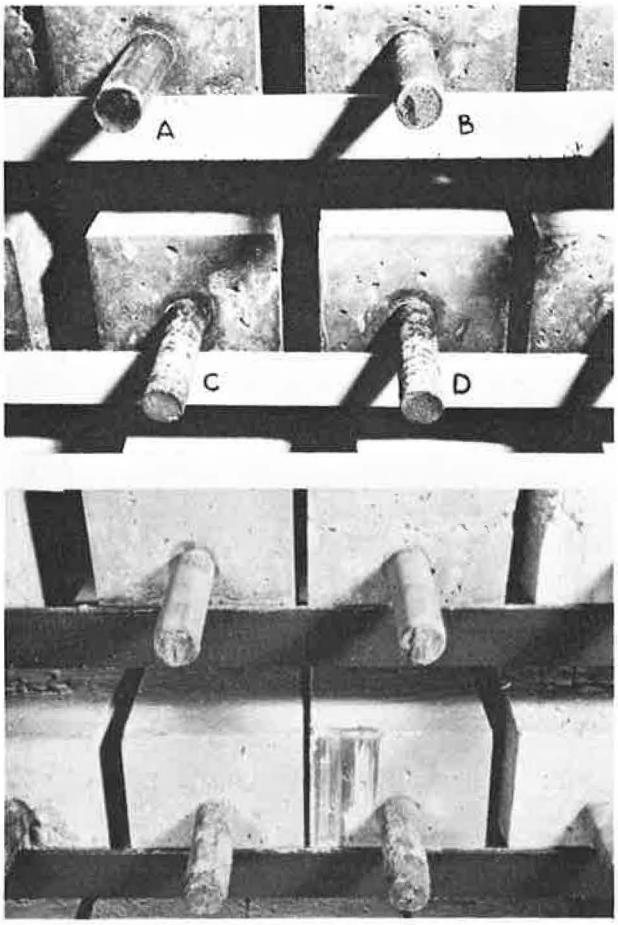

Figure 6. Dowel specimens (a) at end of 50 exposure cycles and (b) at end of 350 exposure cycles. Specimen A—5-mil nickel coating, B—3-mil coating, C and D—untreated.

TABLE 2

SAMPLE VARIANCE S^2
BETWEEN GROUPS OF TABLE 1

No. of Cycles	A & B	B & C	C & D	A & C	A & D
50	616	90	309	692	787
100	861	110	657	896	1,246
150	1,831	1,156	1,470	2,245	2,020
200	2,265	6,109	5,071	6,671	1,835
250	4,812	9,674	8,204	12,282	4,133
300	15,274	20,635	18,121	30,824	13,744
350	19,763	30,779	26,372	44,085	17,259

This is a continuing study and it will be carried on until no further useful purpose is served. Additional information will be reported as it is obtained and evaluated.

TABLE 3

STATISTICAL INFERENCES OF GROUP DIFFERENCES BASED ON PERCENTAGE POINTS OF THE t-DISTRIBUTION

No. of Cycles	A & B	B & C	C & D	A & C	A & D
50	2%	10	—	10	10
100	1	1	40	10	10
150	5	5	—	—	—
200	5	—	—	40	—
250	20	5	50	20	20
300	20	10	50	—	50
350	25	10	30	30	—

Discussion of Results

The conclusions reported herein are based on an accelerated, laboratory-controlled, exposure study. Nevertheless, it is believed that the same relative differences between the coated and the uncoated dowel groups should be obtained from long-time field exposures.

The various groups of dowels with the different thicknesses of nickel were very much alike throughout the study and the groups changed relative positions among themselves between exposure periods. Group E (Fig. 5), with no nickel coating, required the greatest effort by far to cause movement of the dowels. Even the thinnest nickel coating displayed greatly increased corrosion resistance and thereby appreciably reduced interference with freedom of movement of the dowel bars.

Results obtained to date on the nickel-coated dowels are within such a narrow scatter band that the relative merits of the coating thicknesses are not evident at this time.

REFERENCES

1. Van Breemen, W., "Experimental Dowel Installations in New Jersey." HRB Proc., Vol. 34 (1955).
2. Mitchell, R. G., "The Problem of Corrosion of Load Transfer Dowels." HRB Bull. 274, 57-69 (1960).
3. Sanborn, C., "Nickel-Coated Dowel Pins Exposed in Tidal Zone Harbor Island, North Carolina." Highway Research Record 31 (1963).

Appendix

SAMPLE CALCULATIONS

Data at the end of 50 exposure cycles
Maximum loads required to cause dowel bar movement:

Group A	Group D
86 lb	70 lb
44	18
117	43
39	53
94	24

Sum of 5 specimens in group A = 380
Average maximum load of group A = $\frac{380}{5}$ = 76 lb

Sum of 5 specimens in group D = 208
Average maximum load of group D = $\frac{208}{5}$ = 42 lb

Standard deviation s of group A

$$S^2 = \sum_{i=1}^{n} \frac{(Y_1 - \overline{Y})^2}{n - 1}$$

in which

n = number of specimens in group
n-1 = degrees of freedom
Y_1 = maximum load on specimen
$\overline{Y}$ = average maximum load for group

$$(86 - 76)^2 = 100$$
$$(44 - 76)^2 = 1,024$$
$$(117 - 76)^2 = 1,681$$
$$(39 - 76)^2 = 1,369$$
$$(94 - 76)^2 = 324$$

$$\sum_{i=1}^{n} (Y_1 - \overline{Y})^2 = 4,498$$

$$S^2 = \frac{4,498}{5 - 1} = 1,124.5$$

Standard deviation of group A = s = $\sqrt{1,124.5}$ = 33.6

Sample variance S^2 between groups A & D

$$S^2 = \frac{\sum_{i=1}^{n_1} (Y_{1i} - \overline{Y}_1)^2 + \sum_{j=1}^{n_2} (Y_{2j} - \overline{Y}_2)^2}{n_1 + n_2 - 2}$$

in which

n_1 = number of specimens in group A
n_2 = number of specimens in group D
$n_1 + n_2 - 2$ = degrees of freedom of system

For group A (see previous calculations):

$$\sum_{i=1}^{n} (Y_1 - \bar{Y})^2 = 4,498$$

For group D (similar to calculations for group A):

$$\sum_{j=1}^{n} (Y_j - \bar{Y})^2 = 1,806$$

Sample variance between groups A & D:

$$S^2 = \frac{4,498 - 1,806}{5 + 5 - 2} = 787$$

t-test

$$t = \frac{\bar{Y}_1 - \bar{Y}_2}{\sqrt{\frac{S^2}{n_1} + \frac{S^2}{n_2}}}$$

in which

$\bar{Y}_1$ = average maximum load of group A
$\bar{Y}_2$ = average maximum load of group D
S^2 = sample variance between groups A & D
n_1 = number of specimens in group A
n_2 = number of specimens in group B

All terms in the formula for t having been calculated previously:

$$t = \frac{76 - 42}{\sqrt{\frac{787}{5} + \frac{787}{5}}} = 1.93$$

From a table for the percentage points of the t-Distribution (reference: Ostle, "Statistics in Research")

For a system with 8 degrees of freedom ($n_1 + n_2 - 2$)
At a percentage point of 5%, t = 2.306
At a percentage point of 10%, t = 1.860

Therefore in this case where t = 1.93 the percentage point lies between 5% and 10%, or at a maximum of 10%.

Some Relationships of the AASHO Road Test To Concrete Pavement Design

PHIL FORDYCE and W. E. TESKE, Paving Bureau, Portland Cement Association.

•THIS IS a progress report on performance of concrete test sections at the AASHO Road Test. Study was limited to the main factorial and replicate (Design 1) test sections in truck loops 3, 4, 5 and 6.

In a previous study (1), end of test data from Design 1 sections in the four truck loops were related to three design concepts. This study showed:

1. No differences in performance between the 3-, 6- and 9-in. subbase depths.
2. Equal or slightly better performance on the plain slab design than on the reinforced slab design.
3. That the PCA slab thickness design procedure based on Pickett's stress equation is dependable (1, 2).

Constructed Serviceability of Design 1 Sections presents data on the initial serviceability of Design 1 concrete test sections in the four truck loops. From histograms of these data it was concluded that:

1. The as constructed serviceability index of Design 1 test sections in the four truck loops was 4.7.
2. There were slight but insignificant differences in as constructed serviceability between the three subbase depths, the two slab designs and the four truck loops.

Analysis of Concrete Performance presents end of test serviceability and data on cracking for each Design 1 concrete test section in the four truck loops. The data are shown in both table and chart form, and are summarized in charts under the two slab designs, the four thickness levels in each loop, and under single and tandem axles.

The two slab designs were plain pavement with doweled transverse joints spaced at 15 ft and reinforced pavement with doweled transverse joints spaced at 40 ft.

Slab depths increased at 1½-in. increments from 3½ in. to 12½ in. There were four slab thickness levels in each loop that also increased at 1½-in. increments.

Major conclusions from Analysis of Concrete Performance are:

1. End of test serviceability showed no significant differences in performance on the 3-, 6- and 9-in. subbases.
2. End of test serviceability of the plain and reinforced slab designs showed that:
   (A) At first slab thickness levels, the plain design performed better than the reinforced design under both single- and tandem-axle test traffic. Data presented in Subbase Pumping, Major Conclusions show that these differences in performance occurred after heavy subbase pumping started.
   (B) At second slab thicknesses, the plain design performed better than the reinforced design under single-axle test traffic. Data presented in Subbase Pumping, Major Conclusions show that these differences in performance occurred after heavy subbase pumping started. Performance was about equal under tandem axles.
   (C) At third and fourth slab thicknesses, performance was equal and excellent for both slab designs under both single and tandem axles.

Paper sponsored by Committee on Rigid Pavement Design.

3. End of test serviceability under single- and tandem-axle test traffic showed that:
   (A) At first and second slab thicknesses, performance was better under single-axle test traffic than under tandem-axle test traffic. These marked differences in performance under single and tandem axles are not shown by the Road Test performance equations (3). These equations show better performance under single axles at all thickness levels.
   (B) At the third and fourth slab thicknesses, performance was virtually identical under both single- and tandem-axle test traffic. These marked differences in performance under single and tandem axles are not shown by the Road Test performance equations (3). These equations show better performance under single axles at all thickness levels.
4. The Road Test environment had a major influence on the start of cracking in the reinforced test sections at all slab thickness levels. In some states environment does not cause visible cracks in reinforced pavements that have carried large volumes of trucks for 10 to 20 yr. In these states performance of reinforced pavements at the Road Test will have little or no application.
5. At the end of traffic testing, the plain slab design showed definite superiority over the reinforced design in regard to major cracking (Classes 3 and 4). Major cracks were used in computing serviceability indexes (3). However, at about equal serviceability, pavements free of the distress characteristic of major cracking should cost less to maintain.

Subbase Pumping presents data showing the extent and severity of subbase pumping and the relationships of subbase pumping to pavement serviceability. Data on trace, moderate and heavy subbase pumping are shown in table and chart form for all Design 1 test sections in the four truck loops. In the HRB data systems these three types of subbase pumping are combined into a pumping score. This score equals trace pumping, plus 10 times moderate pumping, plus 50 times heavy pumping. A detailed study was made on the second thickness 8-in. test sections in loop 5. Work on subbase pumping data is not complete. The following conclusions reflect work done so far:

1. Trace subbase pumping occurred on all Design 1 sections in the four truck loops.
2. Moderate subbase pumping occurred on all first and second slab thicknesses, on 95 percent of third slab thicknesses, and on 63 percent of fourth slab thicknesses.
3. Heavy subbase pumping occurred on all first slab thicknesses, on 89 percent of second slab thicknesses, on 34 percent of third slab thicknesses and on 21 percent of fourth slab thicknesses.
4. Neither trace nor moderate subbase pumping influenced serviceability at any slab thickness level.
5. Heavy subbase pumping was not extensive or severe at third and fourth thickness levels and did not influence serviceability.
6. On second level slab thicknesses, severity of heavy subbase pumping decreased as stress decreased and loss in serviceability was related to the severity of heavy subbase pumping.
7. On first level test sections, repetitions of test traffic from the start of heavy pumping to the first serviceability loss (when serviceability index fell below 4.0 and did not recover) varied considerably within and between loops. However, averaged data show that the effects of severe subbase pumping decreased as stress decreased.
8. Differences in serviceability under single and tandem axles on first and second thickness levels occurred only after heavy subbase pumping started.
9. Differences in serviceability between the plain and reinforced designs in the first and second thickness levels occurred only after heavy subbase pumping started.

The following conclusions relate only to the detailed study of the second thickness 8-in. test sections in loop 5.

1. Where the accumulated percentage of heavy subbase pumping was 60 or less and not severe. A measure of severity—it is the accumulated percentage of section length with heavy subbase pumping measured after each period of rainfall. For

example, if these percentages were 65, 80 and 70 after three periods of rainfall the accumulated percentage would be 215:

(A) End of test serviceability was about equal to the end of test serviceability on third and fourth slab thicknesses in loop 5.

(B) The relationship of serviceability to applied loads (single or tandem) can be adequately described by the following statement: At 100,000 repetitions the serviceability was 0.4 less than the as constructed serviceability, and there was no further loss in serviceability during the test period.

2. Where the accumulated percentage of heavy subbase pumping was 90 or more (severe), performance was as stated above until heavy subbase pumping approached severe intensity. Severe heavy subbase pumping was accompanied by a rapid serviceability loss with indexes usually reaching a value of 1.5 before the end of test.

3. With regard to the second level, 8-in. test sections in loop 5, the Road Test performance equations for concrete are deficient in the following respects:

(A) They do not describe concrete performance prior to the start of heavy pumping.

(B) They give incorrect values for end of test serviceability where the accumulated percentage of heavy subbase pumping was 60 or less (not severe).

(C) They fail to show that performance was equal under single and tandem axles where the accumulated percentage of heavy subbase pumping was 60 or less (not severe).

(D) They give incorrect values for end of test serviceability where the accumulated percentage of heavy subbase pumping was 90 or more (severe).

With regard to observations and records of subbase pumping made at the Road Test it is believed that:

1. Trace subbase pumping is uncommon on pavements in service.
2. Moderate subbase pumping is rare on pavements in service.
3. Heavy subbase pumping in more than very small amounts is probably unique to the Road Test.
4. Road Test performance measurements influenced by heavy subbase pumping of medium or severe intensity are not relevant to pavements in service.

At the outset, three conclusions were cited from a previous study (1). The results of the current study agree with all three conclusions and give additional support to the third one. In the previous study, summaries of pavement performance from all sections, including those affected by subbase pumping, showed that the PCA design procedure is dependable. The performance of second level pavements that had little or no heavy subbase pumping affords further evidence that this procedure is dependable and conservative.

At the Road Test, concrete pavement research was conducted on the south tangents of six loops. Most of the research on the six test loops had to do with three elements of concrete pavement design. These were slab thickness, subbase thickness and two slab designs: plain slabs with doweled transverse contraction joints spaced at 15 ft and reinforced slabs with doweled transverse contraction joints spaced at 40 ft. Dowels were the same for both slab designs. Dowel sizes, mesh weights and other jointing details are given in Ref. (3).

In all six loops these two slab designs were used in combination with each variation in slab and subbase depth to make a complete factorial design. Also, certain design combinations were repeated in each loop to check on experimental error. The structural design combinations were constructed 24 ft wide with a sawed longitudinal center joint between the 12-ft lanes. Each lane of each design combination was a test section. These test sections are the main factorial design (Design 1) at the Road Test. Loops 3 to 6 also had a limited number of sections for the study of paved shoulders and the presence or absence of subbase. This Design 3 study is not included in this report.

Loop 1 was restricted to various non-traffic tests. Slab depths were 2½, 5, 9½ and 12½ in. and subbase depths were 0 and 6 in. There were 32 factorial and 16 replicate test sections.

Loop 2, often called the passenger car loop, carried 2 kip single-axle loads in lane 1 and 6 kip single axles in lane 2. In all loops, lane 1 was the inside lane (next to the median) and lane 2 was the outside lane. Slab depths were 2½, 3½ and 5 in. and subbase depths were 0, 3 and 6 in. There were 36 factorial and 4 replicate test sections.

Loops 3, 4, 5 and 6, the truck loops, had similar factorial and replicate designs. In each of the loops, four levels of slab thickness were used in combination with the two slab designs and subbase depths of 3, 6 and 9 in., making 48 factorial sections per loop. There were eight replicate sections in each loop making a total of 56 test sections per loop. Both slab depths and thickness levels increased at a 1½-in. increment from 3½ in. in loop 3 to 12½ in. in loop 6.

TABLE 1

CONCRETE PAVEMENT THICKNESS, LEVELS AND LOADS

Item	Loop 3	Loop 4	Loop 5	Loop 6
Slab depth (in.):				
3½	1st			
5	2nd	1st		
6½	3rd	2nd	1st	
8	4th	3rd	2nd	1st
9½		4th	3rd	2nd
11			4th	3rd
12½				4th
Mean des. thickness (in.):	7.2	8.6	9.6	10.8
Axle load (kips):				
Single	12	18	22.4	30
Tandem	24	32	40	48

The four thickness levels in loops 3 to 6 were varied around the mean of designs submitted by four agencies during the planning stages of the Road Test. These mean designs, along with the slab depths tested, the thickness levels, and the axle loads in the four truck loops are shown in Table 1. This table shows that in loops 3, 4 and 5 the mean design depths are from 0.1 to 0.7 in. greater than the third thickness levels. In loop 6 the mean design is 0.2 in. less than the third thickness level.

In all four truck loops single-axle test traffic operated in lane 1 (inside lane) and tandem-axle traffic operated in lane 2 (outside lane). As a result each individual test section received repetitions of one single- or one tandem-axle load.

> Authors' Comment.—This procedure made it possible to get the performance on each test section for repetitions of a specific load. It also permits performance comparisons for repetitions of specific single- and tandem-axle loads on two test sections of the same design.
>
> However, pavements in service carry a wide variety of single- and tandem-axle loads. Since all test sections carried only one load (either single or tandem) the Road Test did not yield any experimental data on the effects of mixed traffic. This fact and its significance are expressed in the following unanswered question from the Road Test Report (3). "For example, at the Road Test a million axle loads of one weight were applied in two years to each section. What would have been the situation had these loads, accompanied by several million lighter loads, been applied in 20 years?" Because the question is unanswered, it is not wise to use extrapolations of Road Test performance equations for design of pavements in service.

At the Road Test performance was measured by means of two values—number of repetitions and serviceability index. Development of the serviceability index method for determining the ability of a pavement to serve traffic is described in detail in Appendix F of Ref. (3). On concrete test sections the serviceability index was determined by a formula that used the average of slope variance measured in the two wheel

paths and the amount of cracking and patching. In the charts presented, both the index and the number of load repetitions at the time that the index was measured are shown.

This paper is a progress report on study of concrete pavement performance on the Design 1 test sections in the truck loops—3, 4, 5 and 6. In a previous study (1) end of test serviceability data for these same test sections were studied in relation to 3 design concepts. Data were summarized by:

1. Computing average repetitions to 1.5 serviceability index for the first level thicknesses in loops 3, 4 and 5 where all sections dropped to this index during the test period.
2. Computing percent of sections that survived testing with an index of 1.5 or higher and the average index of these surviving sections for second level pavements in all four loops.
3. Computing the average end of test index for third and fourth thickness levels in all four loops where all sections survived testing with an index above 1.5.

Summaries of serviceability were not made for the individual loops, nor for single and tandem axles. In computing averages, data from both single- and tandem-axle test sections were used. The results of these computations showed:

1. About equal performance on the 3-, 6- and 9-in. subbase depths with slightly better performance on the 3- and 6-in. subbase depths.
2. About equal performance for the plain and reinforced slab designs with a slight advantage for the plain design.
3. That slab thicknesses determined by the PCA design procedure (1) were close to or slightly above the minimum needed for dependable performance at the Road Test.

Constructed Serviceability of Design One Sections includes information on the rates of load application at the Road Test. Analysis of Concrete Sections presents performance in the truck loops based on end of test serviceability indexes and data on minor and major cracking. Subbase Pumping presents data on subbase pumping in the truck loops and its relationship to pavement serviceability.

CONSTRUCTED SERVICEABILITY OF DESIGN 1 SECTIONS

Data on as constructed serviceability of Design 1 test sections in the truck loops were summarized for the two slab designs, the three subbase depths and the four loops.

Figure 1 shows histograms for as constructed serviceability on the two slab designs. From the summary in Table 2, these values show no significant difference in as constructed serviceability.

Figure 2 shows histograms for as constructed serviceability on the 3-, 6- and 9-in. subbase depths. The summary also shows no significant differences in as constructed serviceability.

Figure 3 shows histograms for as constructed serviceability on the four truck loops. Summary values show slightly higher initial serviceability on loops 3 and 4 than on loops 5 and 6. One crew paved loops 3 and 4, but another crew paved 5 and 6. The differences are not enough to be significant. The mean as constructed serviceability index for loops 3 to 6 is 4.7.

A study has been started on time-rates of loading at the Road Test. While there

TABLE 2

AS CONSTRUCTED SERVICEABILITY INDEX

Item	Min.	Mean	Max.
Slab design:			
Plain	4.3	4.69	5.0
Reinforced	4.4	4.73	5.0
Subbase depth (in.):			
3	4.3	4.68	4.9
6	4.3	4.72	5.0
9	4.3	4.72	5.0
Loop No.			
3	4.3	4.74	5.0
4	4.5	4.76	4.9
5	4.4	4.67	4.9
6	4.3	4.61	4.8

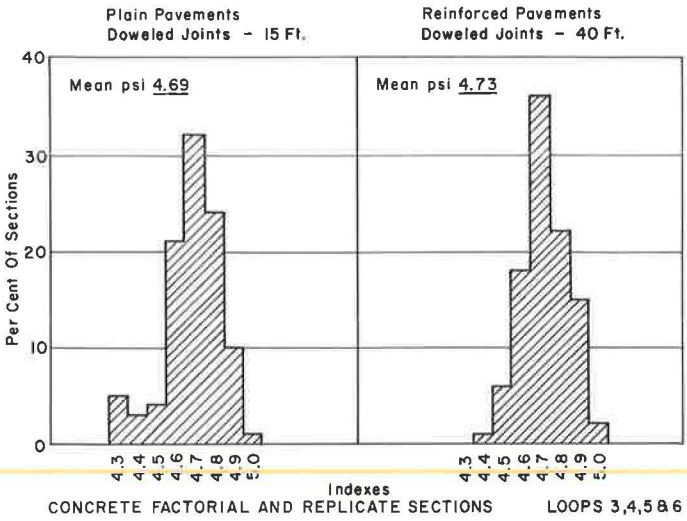

Figure 1. As constructed—serviceability indexes.

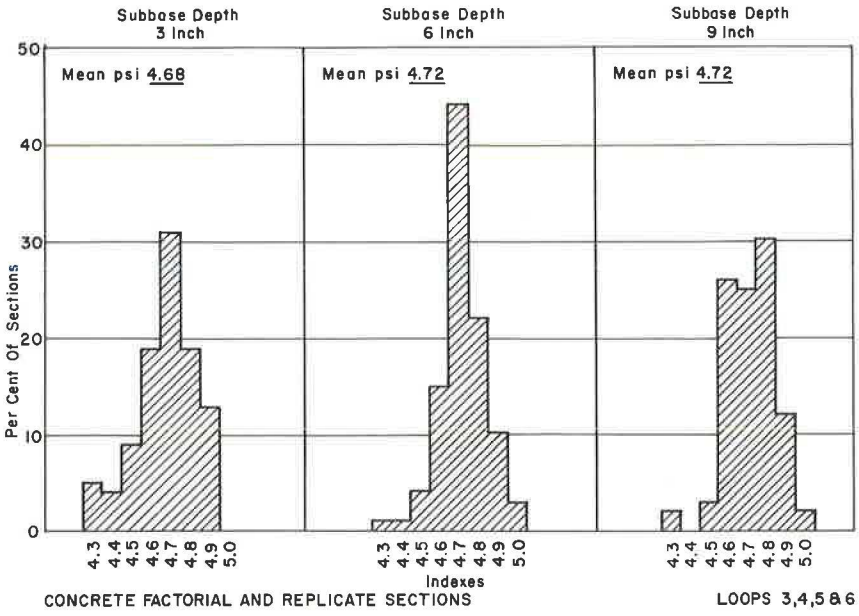

Figure 2. As constructed—serviceability indexes.

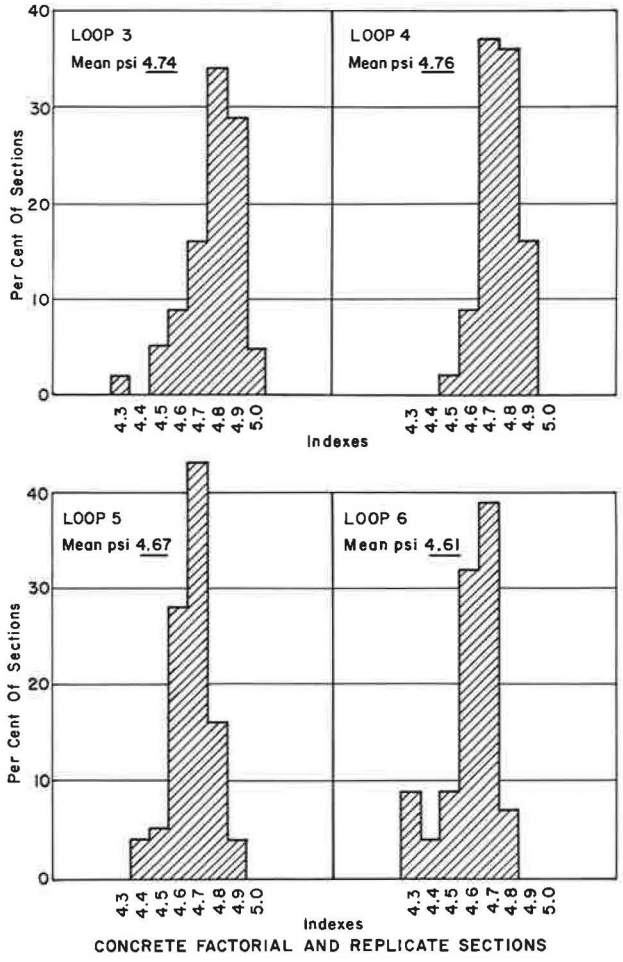

Figure 3. As constructed—serviceability indexes.

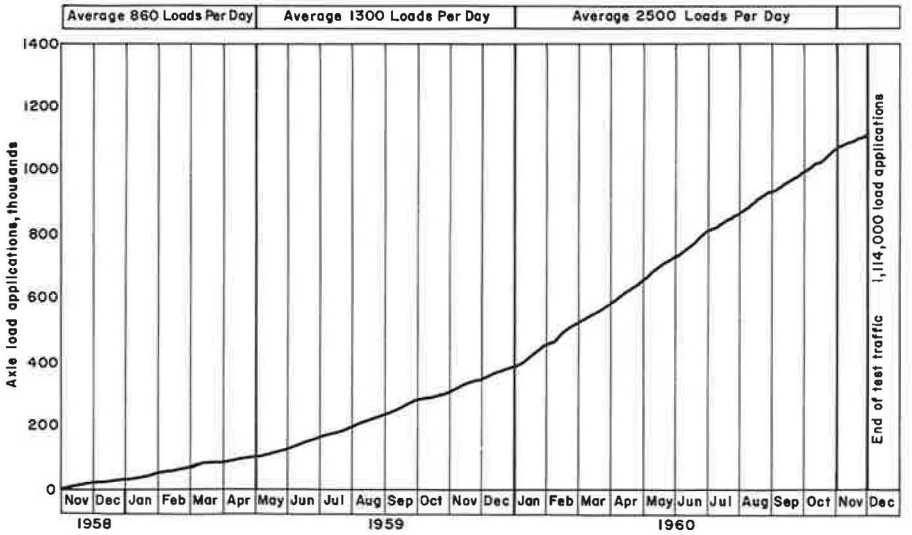

Figure 4. Rates of axle load applications per day at the AASHO Road Test.

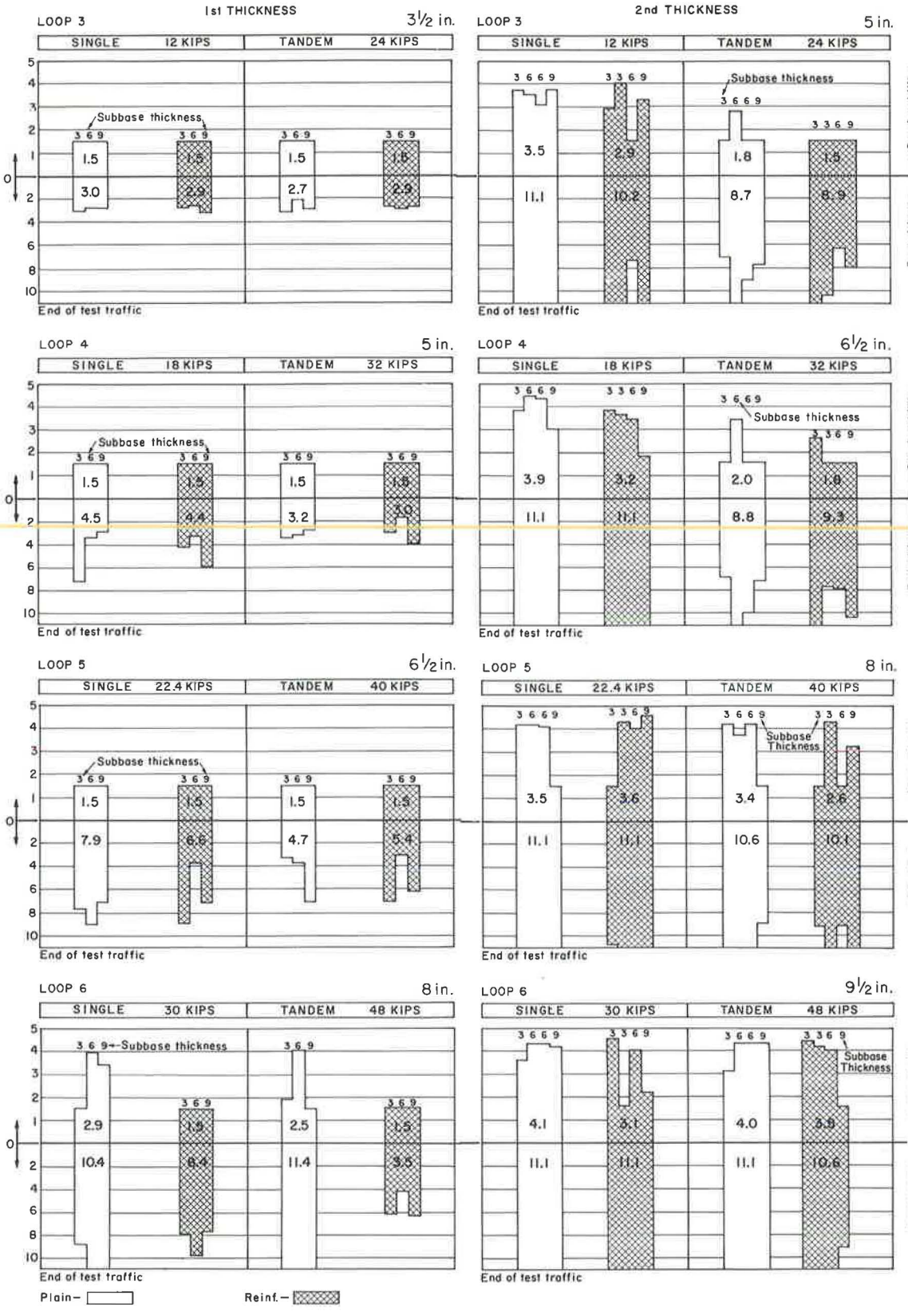
1st THICKNESS
2nd THICKNESS
LOOP 3
3½ in.
SINGLE 12 KIPS
TANDEM 24 KIPS
Subbase thickness
3 6 9
1.5
3.0
2.9
1.5
2.7
2.9
End of test traffic
LOOP 3
5 in.
SINGLE 12 KIPS
TANDEM 24 KIPS
3 6 6 9
3 3 6 9
3.5
11.1
2.9
10.2
Subbase thickness
1.8
8.7
1.5
8.9
End of test traffic
LOOP 4
5 in.
SINGLE 18 KIPS
TANDEM 32 KIPS
Subbase thickness
1.5
4.5
4.4
1.5
3.2
1.5
3.0
End of test traffic
LOOP 4
6½ in.
SINGLE 18 KIPS
TANDEM 32 KIPS
3.9
11.1
3.2
11.1
Subbase thickness
2.0
8.8
1.8
9.3
End of test traffic
LOOP 5
6½ in.
SINGLE 22.4 KIPS
TANDEM 40 KIPS
Subbase thickness
1.5
7.9
6.6
1.5
4.7
1.5
5.4
End of test traffic
LOOP 5
8 in.
SINGLE 22.4 KIPS
TANDEM 40 KIPS
3.5
11.1
3.6
11.1
Subbase Thickness
3.4
10.6
2.6
10.1
End of test traffic
LOOP 6
8 in.
SINGLE 30 KIPS
TANDEM 48 KIPS
3 6 9 Subbase thickness
2.9
10.4
1.5
8.4
2.5
11.4
1.5
3.5
End of test traffic
LOOP 6
9½ in.
SINGLE 30 KIPS
TANDEM 48 KIPS
4.1
11.1
3.1
11.1
Subbase Thickness
4.0
11.1
3.9
10.6
End of test traffic
Plain–
Reinf.–

Figu

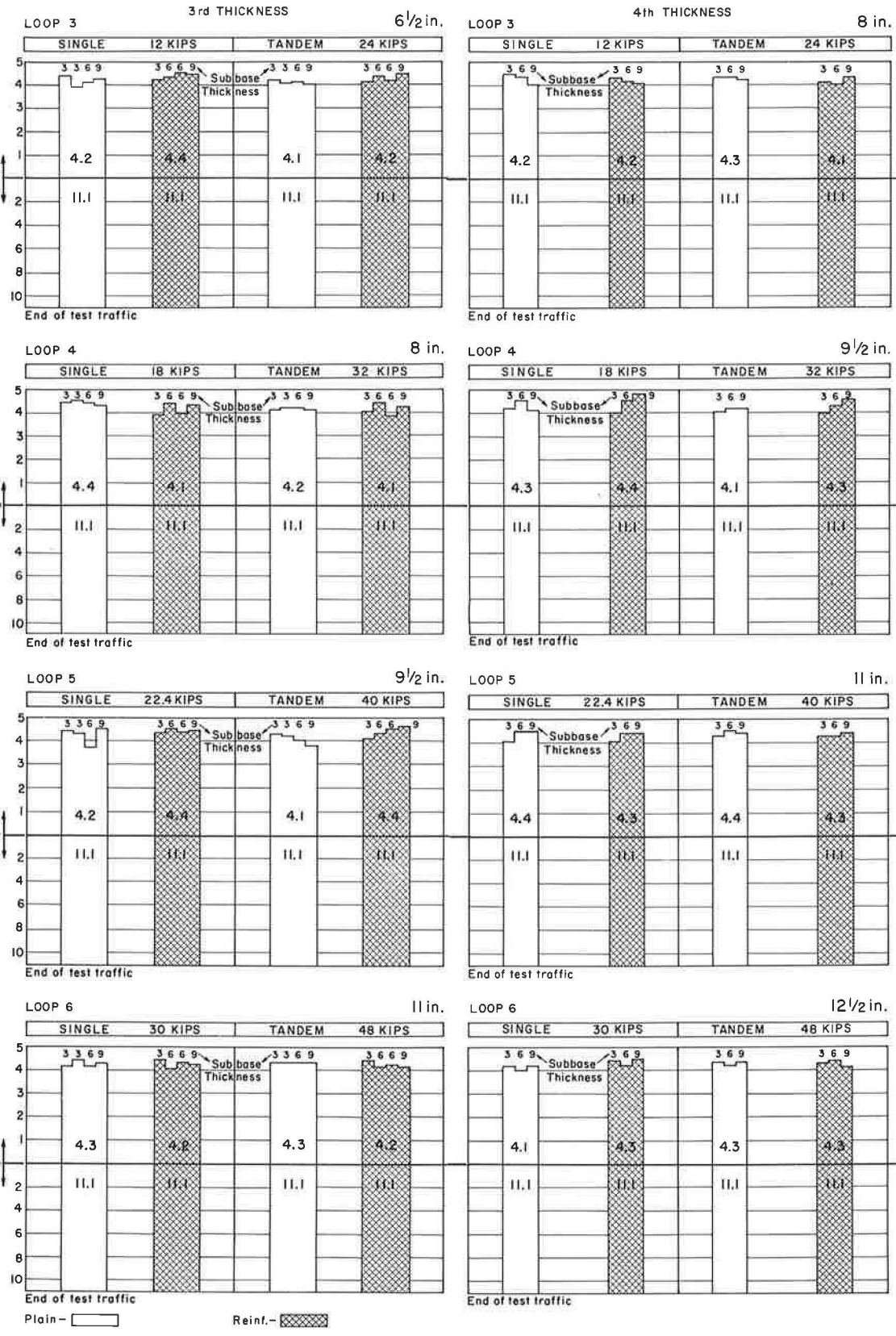

oncrete performance.

were minor variations between loops and between lanes in individual loops, averaged data show:

1. That there was essentially a single loading history for all traffic testing.
2. That the loading history had three distinct time-rates. These are shown in Figure 4 and are summarized in Table 3.

Authors' Comment.—The increases in time-rates are substantial. Road Test performance and the empirical equations based on this performance are dependent on one loading history with two major changes in time-rating of loading. Hence the performance and the equations do not have experimental application to any other loading history. This is another reason why it is believed to be unwise to use extrapolations of the Road Test equations for design of pavements in service.

TABLE 3

TIME-RATES OF LOADING

Repetitions	Time-Rates (loads per lane per day)
0— 101,000	860
101,000— 387,000	1,300
387,000—1,076,000[1]	2,500

(Ratios of time-rates are 1.0:1.5:2.9)

[1] From this point to the end of test, loading histories were varied slightly so that 1,114,000 applications could be applied to all surviving test sections.

ANALYSIS OF CONCRETE PERFORMANCE

This section deals with concrete behavior as shown by end of test serviceability and cracking. Table 4 gives the following information for all Design 1 test sections in loops 3 to 6:

1. Section number.
2. End of test serviceability index for sections that had values above 1.5.
3. Repetitions to 1.5 index for sections that fell to this value during the test.
4. Repetitions at which minor and major cracking started.

The serviceability data in Table 4 are shown in graph form in Figure 5. The charts are arranged under the four thickness levels. They show both repetitions and end of test serviceability for single and tandem axles, the three subbase depths and the two slab designs. The charts thus permit quick performance comparisons at any thickness level under single or tandem axles. Study of Figure 5 shows:

1. No significant differences in performance for the 3-, 6- and 9-in. subbase depths.
2. Wide variations in repetitions to a 1.5 serviceability index in the first thickness level, especially in loops 5 and 6. Note, for example, that two first thickness 8-in. test sections in loop 6 survived test traffic under both single and tandem axles with a serviceability index of about 4.0—only slightly below performance at third and fourth levels.
3. There were wide variations in performance at the second thickness level in all four loops.
4. At the second thickness level in loops 5 and 6, more than half the test sections performed as well as third and fourth level sections.
5. At the third and fourth level in all four loops, performance was very uniform and very good for both slab designs, all three subbase depths, and under both single and tandem axles.

Authors' Comments.—The previous study (1), this study, the Road Test Report (3), a subbase experiment under highway traffic (4), laboratory studies (5) and results of pavement performance surveys (6) all show that concrete highway pavements perform as well or better on 3- to 6-in. subbases as on subbases more than 6 in. thick. This evidence shows that subbases more than 6 in. thick are not required to insure the performance of concrete pavements.

TABLE 4
CONCRETE BEHAVIOR

LOOP 3

1st Thickness 3½ in.

Sec. No.	Design: Slab	Design: Subbase Depth, Inches	Axle Loads *, Kips	Performance: Serviceability: End Of Test Index	Performance: Serviceability: Rep. At 1.5 Index 1000-S	Performance: Repetitions at start of cracking 1000-S: Minor Class 1 & 2	Performance: Repetitions at start of cracking 1000-S: Major Class 3 & 4
195	Plain	3	12S	—	315	122	234
196			24T	—	318	120	282
239		6	12S	—	289	122	273
240	Doweled Joints 15 Ft.		24T	—	210	134	195
213		9	12S	—	289	135	200
214			24T	—	297	106	195
209	Reinf.	3	12S	—	278	122	273
210			24T	—	278	120	266
205		6	12S	—	273	98	135
206	Doweled Joints 40 Ft.		24T	—	295	79	180
231		9	12S	—	324	183	289
232			24T	—	294	120	266

LOOP 4

1st Thickness 5 in.

Sec. No.	Design: Slab	Design: Subbase Depth, Inches	Axle Loads *, Kips	Performance: Serviceability: End Of Test Index	Performance: Serviceability: Rep. At 1.5 Index 1000-S	Performance: Repetitions at start of cracking 1000-S: Minor Class 1 & 2	Performance: Repetitions at start of cracking 1000-S: Major Class 3 & 4
643	Plain	3	18S	—	716	274	325
644			32T	—	343	219	291
647		6	18S	—	353	235	292
648	Doweled Joints 15 Ft.		32T	—	328	201	236
677		9	18S	—	291	274	292
678			32T	—	289	201	273
681	Reinf.	3	18S	—	415	0	292
682			32T	—	304	168	291
661		6	18S	—	325	0	306
662	Doweled Joints 40 Ft.		32T	—	175	0	168
673		9	18S	—	592	136	338
674			32T	—	408	201	339

LOOP 5

1st Thickness 6½ in.

Sec. No.	Design: Slab	Design: Subbase Depth, Inches	Axle Loads *, Kips	Performance: Serviceability: End Of Test Index	Performance: Serviceability: Rep. At 1.5 Index 1000-S	Performance: Repetitions at start of cracking 1000-S: Minor Class 1 & 2	Performance: Repetitions at start of cracking 1000-S: Major Class 3 & 4
513	Plain	3	22.4S	—	760	69	702
514			40T	—	335	324	325
517		6	22.4S	—	898	668	668
518	Doweled Joints 15 Ft.		40T	—	369	337	337
505		9	22.4S	—	705	445	446
506			40T	—	698	291	337
523	Reinf.	3	22.4S	—	898	268	668
524			40T	—	705	273	635
491		6	22.4S	—	369	268	308
492	Doweled Joints 40 Ft.		40T	—	305	183	291
549		9	22.4S	—	708	11	339
550			40T	—	618	291	291

LOOP 6

1st Thickness 8 in.

Sec. No.	Design: Slab	Design: Subbase Depth, Inches	Axle Loads *, Kips	Performance: Serviceability: End Of Test Index	Performance: Serviceability: Rep. At 1.5 Index 1000-S	Performance: Repetitions at start of cracking 1000-S: Minor Class 1 & 2	Performance: Repetitions at start of cracking 1000-S: Major Class 3 & 4
353	Plain	3	30S	—	878	29	735
354			48T	1.8	—	814	997
393		6	30S	3.9	—	900	1100
394	Doweled Joints 15 Ft.		48T	4.1	—	NONE	NONE
369		9	30S	3.4	—	29	952
370			48T	—	1114	758	814
341	Reinf.	3	30S	—	782	292	635
342			48T	—	618	266	437
385		6	30S	—	974	635	807
386	Doweled Joints 40 Ft.		48T	—	415	266	353
347		9	30S	—	768	274	706
348			48T	—	624	86	385

*S = Single, T = Tandem, R = Replicate Section

TABLE 4

CONCRETE BEHAVIOR (Cont'd.)

LOOP 3 — 2nd Thickness 5 in.

Sec. No.	Design: Slab	Design: Subbase Depth, Inches	Axle Loads *, Kips	Performance: Serviceability: End Of Test Index	Performance: Serviceability: Rep. At 1.5 Index 1000-S	Performance: Repetitions at start of cracking 1000-S: Minor Class 1 & 2	Performance: Repetitions at start of cracking 1000-S: Major Class 3 & 4
225	Plain	3	12S	3.7	—	1021	1021
226			24T	—	705	266	299
245		6	12S	3.5	—	1021	988
221			R	3.1	—	775	810
246			24T	2.8	—	870	932
222			R	—	901	85	345
219		9	12S	3.7	—	273	324
220			24T	—	771	266	299
251	Reinf.	3	12S	2.8	—	11	337
203			R	4.0	—	289	870
252			24T	—	1100	266	668
204			R	—	1046	28	870
191		6	12S	—	725	273	385
192			24T	—	631	282	383
233		9	12S	3.3	—	200	836
234			24T	—	793	213	772

Doweled Joints 15 Ft. (Plain); Doweled Joints 40 Ft. (Reinf.)

LOOP 4 — 2nd Thickness 6½ in.

Sec. No.	Design: Slab	Design: Subbase Depth, Inches	Axle Loads *, Kips	Performance: Serviceability: End Of Test Index	Performance: Serviceability: Rep. At 1.5 Index 1000-S	Performance: Repetitions at start of cracking 1000-S: Minor Class 1 & 2	Performance: Repetitions at start of cracking 1000-S: Major Class 3 & 4
649	Plain	3	18S	3.8	—	NONE	988
650			32T	—	689	NONE	408
697		6	18S	4.4	—	NONE	NONE
655			R	4.3	—	NONE	NONE
698			32T	3.4	—	1021	1021
656			R	—	1000	836	836
703		9	18S	3.0	—	988	988
704			32T	—	722	86	671
641	Reinf.	3	18S	3.8	—	274	810
705			R	3.6	—	274	810
642			32T	2.6	—	273	810
706			R	—	793	273	707
685		6	18S	3.4	—	252	810
686			32T	—	796	273	774
653		9	18S	1.8	—	274	603
654			32T	—	1036	273	810

Doweled Joints 15 Ft. (Plain); Doweled Joints 40 Ft. (Reinf.)

LOOP 5 — 2nd Thickness 8 in.

Sec. No.	Design: Slab	Design: Subbase Depth, Inches	Axle Loads *, Kips	Performance: Serviceability: End Of Test Index	Performance: Serviceability: Rep. At 1.5 Index 1000-S	Performance: Repetitions at start of cracking 1000-S: Minor Class 1 & 2	Performance: Repetitions at start of cracking 1000-S: Major Class 3 & 4
547	Plain	3	22.4S	4.2	—	NONE	NONE
548			40T	4.2	—	409	NONE
539		6	22.4S	4.2	—	NONE	NONE
533			R	4.1	—	79	NONE
540			40T	3.7	—	808	809
534			R	4.2	—	982	NONE
507		9	22.4S	—	1111	902	903
508			40T	—	898	NONE	870
519	Reinf.	3	22.4S	—	1104	287	730
521			R	4.3	—	107	NONE
520			40T	—	915	273	736
522			R	4.3	—	107	NONE
501		6	22.4S	4.0	—	268	1052
502			40T	—	901	273	736
531		9	22.4S	4.6	—	69	NONE
532			40T	3.2	—	291	1074

Doweled Joints 15 Ft. (Plain); Doweled Joints 40 Ft. (Reinf.)

LOOP 6 — 2nd Thickness 9½ in.

Sec. No.	Design: Slab	Design: Subbase Depth, Inches	Axle Loads *, Kips	Performance: Serviceability: End Of Test Index	Performance: Serviceability: Rep. At 1.5 Index 1000-S	Performance: Repetitions at start of cracking 1000-S: Minor Class 1 & 2	Performance: Repetitions at start of cracking 1000-S: Major Class 3 & 4
351	Plain	3	30S	3.6	—	900	1049
352			48T	3.1	—	694	722
367		6	30S	4.3	—	983	NONE
389			R	4.3	—	80	NONE
368			48T	4.3	—	907	NONE
390			R	4.3	—	NONE	NONE
375		9	30S	4.2	—	NONE	NONE
376			48T	4.3	—	80	NONE
381	Reinf.	3	30S	4.5	—	928	NONE
371			R	1.6	—	325	774
382			48T	4.4	—	324	NONE
372			R	4.1	—	340	936
403		6	30S	4.0	—	200	900
404			48T	4.0	—	266	790
339		9	30S	2.2	—	274	774
340			48T	—	912	120	758

Doweled Joints 15 Ft. (Plain); Doweled Joints 40 Ft. (Reinf.)

*S = Single, T = Tandem, R = Replicate Section

TABLE 4

CONCRETE BEHAVIOR (Cont'd.)

LOOP 3

3rd Thickness 6½ in.

Sec. No.	Design: Slab	Design: Subbase Depth, Inches	Axle Loads * Kips	Performance: Serviceability: End Of Test Index	Performance: Serviceability: Rep. At 1.5 Index 1000-S	Performance: Repetitions at start of cracking 1000-S: Minor Class 1 & 2	Performance: Repetitions at start of cracking 1000-S: Major Class 3 & 4
217	Plain	3	12S	4.4	—	107	NONE
193			R	3.9	—	324	NONE
218			24T	4.2	—	NONE	NONE
194			R	4.0	—	NONE	NONE
249	Doweled Joints 15 Ft.	6	12S	4.1	—	70	NONE
250			24T	4.1	—	NONE	NONE
207		9	12S	4.2	—	NONE	NONE
208			24T	4.0	—	NONE	NONE
199	Reinf.	3	12S	4.2	—	289	NONE
200			24T	4.1	—	266	867
247	Doweled Joints 40 Ft.	6	12S	4.3	—	273	NONE
237			R	4.5	—	603	NONE
248			24T	4.3	—	600	890
238			R	4.1	—	735	772
241		9	12S	4.4	—	324	NONE
242			24T	4.4	—	332	901

LOOP 4

3rd Thickness 8 in.

Sec. No.	Design: Slab	Design: Subbase Depth, Inches	Axle Loads * Kips	Performance: Serviceability: End Of Test Index	Performance: Serviceability: Rep. At 1.5 Index 1000-S	Performance: Repetitions at start of cracking 1000-S: Minor Class 1 & 2	Performance: Repetitions at start of cracking 1000-S: Major Class 3 & 4
671	Plain	3	18S	4.4	—	80	NONE
687			R	4.5	—	NONE	NONE
672			32T	4.1	—	NONE	NONE
688			R	4.2	—	79	NONE
683	Doweled Joints 15 Ft.	6	18S	4.4	—	NONE	NONE
684			32T	4.2	—	5	NONE
651		9	18S	4.3	—	NONE	NONE
652			32T	4.1	—	NONE	NONE
691	Reinf.	3	18S	3.9	—	274	810
692			32T	4.0	—	273	989
669	Doweled Joints 40 Ft.	6	18S	4.4	—	274	1021
707			R	3.9	—	274	988
670			32T	4.4	—	273	1021
708			R	3.8	—	273	989
695		9	18S	4.3	—	274	988
696			32T	4.2	—	168	989

LOOP 5

3rd Thickness 9½ in.

Sec. No.	Design: Slab	Design: Subbase Depth, Inches	Axle Loads * Kips	Performance: Serviceability: End Of Test Index	Performance: Serviceability: Rep. At 1.5 Index 1000-S	Performance: Repetitions at start of cracking 1000-S: Minor Class 1 & 2	Performance: Repetitions at start of cracking 1000-S: Major Class 3 & 4
511	Plain	3	22.4S	4.4	—	NONE	NONE
541			R	4.3	—	NONE	NONE
512			40T	4.3	—	NONE	NONE
542			R	4.2	—	905	NONE
525	Doweled Joints 15 Ft.	6	22.4S	3.7	—	803	831
526			40T	4.0	—	771	808
535		9	22.4S	4.5	—	69	NONE
536			40T	3.8	—	951	982
553	Reinf.	3	22.4S	4.3	—	98	1052
554			40T	4.1	—	201	982
543	Doweled Joints 40 Ft.	6	22.4S	4.5	—	1052	NONE
503			R	4.3	—	268	NONE
544			40T	4.3	—	46	NONE
504			R	4.5	—	273	NONE
499		9	22.4S	4.4	—	268	1018
500			40T	4.6	—	273	NONE

LOOP 6

3rd Thickness 11 in.

Sec. No.	Design: Slab	Design: Subbase Depth, Inches	Axle Loads * Kips	Performance: Serviceability: End Of Test Index	Performance: Serviceability: Rep. At 1.5 Index 1000-S	Performance: Repetitions at start of cracking 1000-S: Minor Class 1 & 2	Performance: Repetitions at start of cracking 1000-S: Major Class 3 & 4
377	Plain	3	30S	4.2	—	NONE	NONE
363			R	4.4	—	NONE	NONE
378			48T	4.3	—	NONE	NONE
364			R	4.3	—	NONE	NONE
397	Doweled Joints 15 Ft.	6	30S	4.2	—	NONE	NONE
398			48T	4.3	—	NONE	NONE
365		9	30S	4.3	—	NONE	NONE
366			48T	4.3	—	NONE	NONE
391	Reinf.	3	30S	4.4	—	325	NONE
392			48T	4.4	—	340	NONE
337	Doweled Joints 40 Ft.	6	30S	4.0	—	292	807
345			R	4.3	—	292	NONE
338			48T	4.1	—	245	NONE
346			R	4.2	—	266	NONE
343		9	30S	4.2	—	341	NONE
344			48T	4.1	—	266	997

*S = Single, T = Tandem, R = Replicate Section

TABLE 4

CONCRETE BEHAVIOR (Cont'd.)

LOOP 3

4th Thickness 8 in.

Sec. No.	Design: Slab	Design: Subbase Depth, Inches	Axle Loads * Kips	Performance: Serviceability: End Of Test Index	Performance: Serviceability: Rep. At 1.5 Index 1000-S	Performance: Repetitions at start of cracking 1000-S: Minor Class 1 & 2	Performance: Repetitions at start of cracking 1000-S: Major Class 3 & 4
201	Plain	3	12S	4.4	—	NONE	NONE
202			24T	4.3	—	106	NONE
235	Doweled Joints 15 Ft.	6	12S	4.3	—	482	NONE
236			24T	4.3	—	NONE	NONE
185		9	12S	4.0	—	NONE	NONE
186			24T	4.2	—	NONE	NONE
211	Reinf.	3	12S	4.3	—	289	NONE
212			24T	4.1	—	600	NONE
215	Doweled Joints 40 Ft.	6	12S	4.2	—	273	1021
216			24T	4.0	—	244	1011
197		9	12S	4.1	—	289	1055
198			24T	4.3	—	953	NONE

LOOP 4

4th Thickness 9½ in.

Sec. No.	Design: Slab	Design: Subbase Depth, Inches	Axle Loads * Kips	Performance: Serviceability: End Of Test Index	Performance: Serviceability: Rep. At 1.5 Index 1000-S	Performance: Repetitions at start of cracking 1000-S: Minor Class 1 & 2	Performance: Repetitions at start of cracking 1000-S: Major Class 3 & 4
675	Plain	3	18S	4.2	—	29	NONE
676			32T	4.0	—	NONE	NONE
701	Doweled Joints 15 Ft.	6	18S	4.5	—	169	NONE
702			32T	4.2	—	86	NONE
689		9	18S	4.1	—	70	NONE
690			32T	4.2	—	NONE	NONE
645	Reinf.	3	18S	4.0	—	274	810
646			32T	4.0	—	273	810
665	Doweled Joints 40 Ft.	6	18S	4.5	—	274	NONE
666			32T	4.3	—	273	1021
667		9	18S	4.8	—	274	NONE
668			32T	4.6	—	273	1085

LOOP 5

4th Thickness 11 in.

Sec. No.	Design: Slab	Design: Subbase Depth, Inches	Axle Loads * Kips	Performance: Serviceability: End Of Test Index	Performance: Serviceability: Rep. At 1.5 Index 1000-S	Performance: Repetitions at start of cracking 1000-S: Minor Class 1 & 2	Performance: Repetitions at start of cracking 1000-S: Major Class 3 & 4
529	Plain	3	22.4S	4.1	—	702	986
530			40T	4.3	—	905	NONE
497	Doweled Joints 15 Ft.	6	22.4S	4.5	—	NONE	NONE
498			40T	4.5	—	NONE	NONE
509		9	22.4S	4.5	—	NONE	NONE
510			40T	4.4	—	NONE	NONE
515	Reinf.	3	22.4S	4.1	—	287	1018
516			40T	4.3	—	291	NONE
545	Doweled Joints 40 Ft.	6	22.4S	4.4	—	1052	NONE
546			40T	4.3	—	273	NONE
495		9	22.4S	4.4	—	NONE	NONE
496			40T	4.4	—	707	NONE

LOOP 6

4th Thickness 12½ in.

Sec. No.	Design: Slab	Design: Subbase Depth, Inches	Axle Loads * Kips	Performance: Serviceability: End Of Test Index	Performance: Serviceability: Rep. At 1.5 Index 1000-S	Performance: Repetitions at start of cracking 1000-S: Minor Class 1 & 2	Performance: Repetitions at start of cracking 1000-S: Major Class 3 & 4
395	Plain	3	30S	4.2	—	834	NONE
396			48T	4.3	—	658	NONE
349	Doweled Joints 15 Ft.	6	30S	4.0	—	NONE	1081
350			48T	4.2	—	790	NONE
379		9	30S	4.2	—	NONE	NONE
380			48T	4.4	—	NONE	NONE
359	Reinf.	3	30S	4.4	—	1016	NONE
360			48T	4.3	—	790	NONE
355	Doweled Joints 40 Ft.	6	30S	4.2	—	635	NONE
356			48T	4.4	—	472	NONE
357		9	30S	4.5	—	NONE	NONE
358			48T	4.2	—	623	1029

*S = Single, T = Tandem, R = Replicate Section

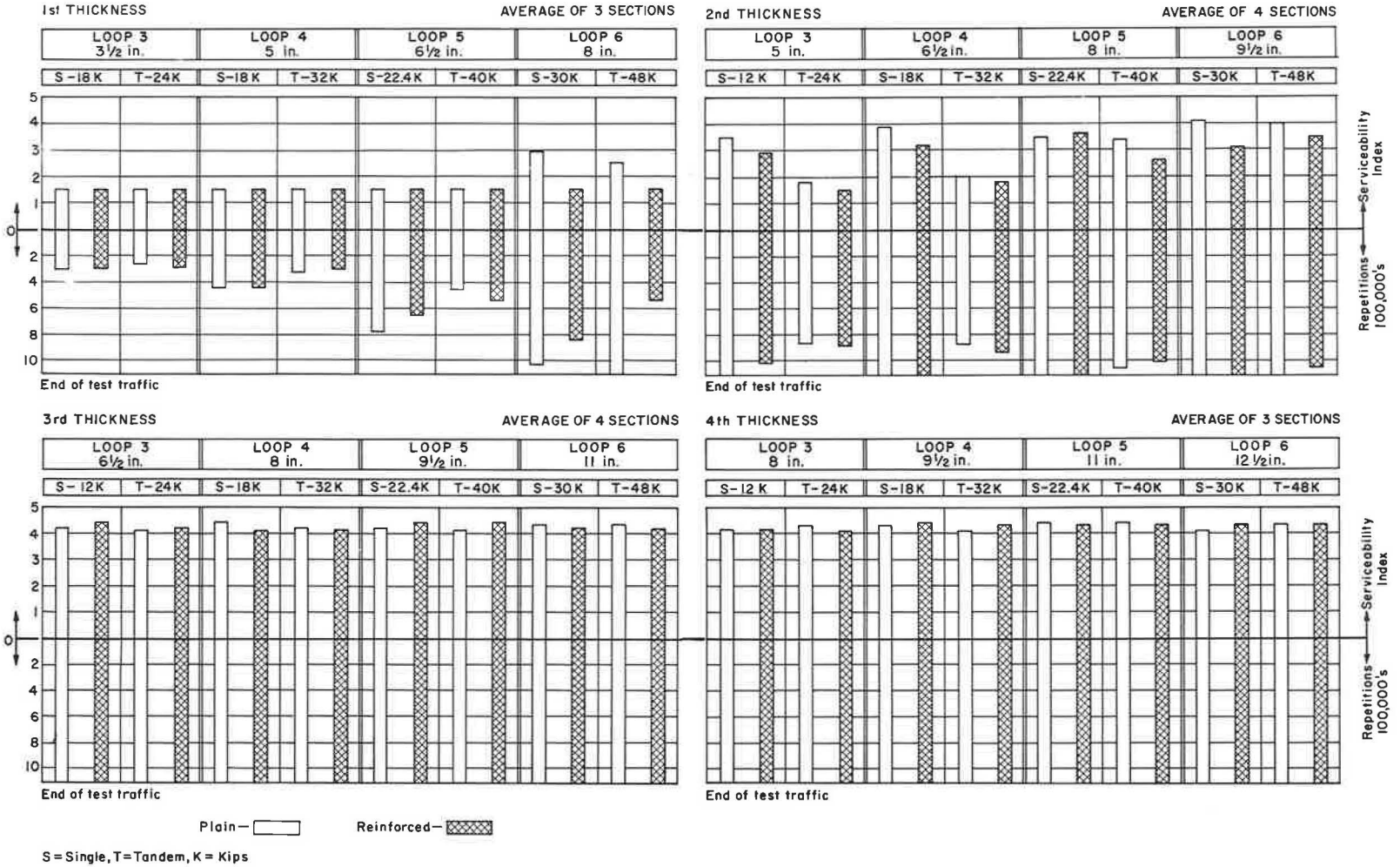

Figure 6. Summary of serviceability and repetitions, concrete test sections (factorial and replicate).

In Figure 6, data on serviceability and repetitions are averaged for the three subbase depths. Bar graphs of these averages are shown for the two slab designs under single and tandem axles for the four thickness levels in the four truck loops. In this case, and in all other data summaries, averages include values from both factorial and replicate sections.

At the first thickness level the graph records:

1. About equal performance on plain and reinforced designs in loops 3, 4 and 5.
2. In loop 6, the 8-in. plain design performed better than the 8-in. reinforced design.
3. In all four loops, performance was better under single-axle traffic than under tandem-axle traffic.

At the second thickness level the graph shows wide differences in performance:

1. Under single-axle test traffic, the plain slab design performed better than the reinforced slab design in loops 3, 4 and 6. In loop 5 the reinforced design was slightly better than the plain design under single-axle traffic.
2. Under tandem-axle traffic, the plain slabs performed better than the reinforced slabs in loops 5 and 6. In loops 3 and 4 there were only slight differences between the two slab designs under tandem-axle traffic.
3. Performance was better under single-axle traffic than under tandem-axle traffic in loops 3, 4 and 5. In loop 6, performance was about equal under single and tandem axles.

At the third and fourth thickness levels in all four truck loops, performance was equal and very good (serviceability indexes above 4.0) for both slab designs under both single- and tandem-axle test traffic.

In Figure 7, data on serviceability and repetitions have been summarized by computing average values from all four loops for each thickness level. The bar graphs show mean values for both slab designs under single- and tandem-axle test traffic. Figure 7 shows:

1. At the first thickness level the plain design performed better than the reinforced design under both single- and tandem-axle truck traffic.
2. At the second thickness level the plain design performed better than the reinforced design under single-axle test traffic. Under tandem-axle traffic, performance was equal for the two slab designs. Here average values tend to mask the differences in performance shown in Figures 5 and 6.

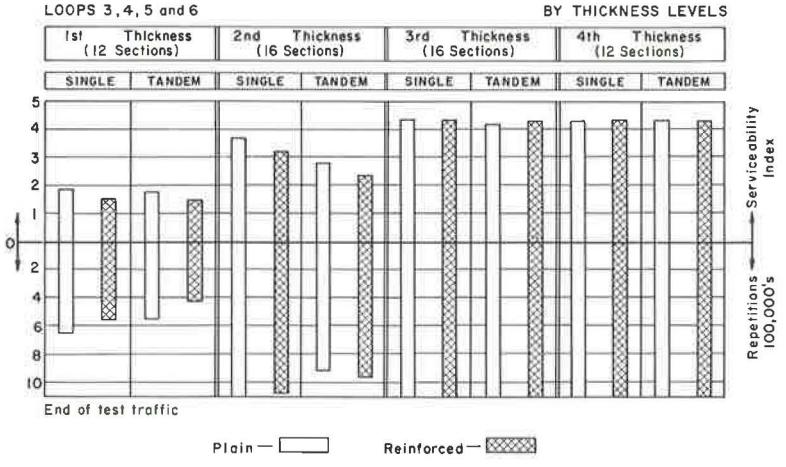

Figure 7. Summary of serviceability and repetitions, concrete test sections (factorial and replicate).

3. At the third and fourth thickness levels, performance was equal and very good (serviceability indexes above 4.0) for both slab designs under both single- and tandem-axle truck traffic.
4. At first and second thickness levels, performance was better under single-axle test traffic than under tandem-axle test traffic.
5. At the third and fourth thickness levels, performance was virtually identical under both single and tandem axles.

The data presented in Analysis of Concrete Performance on end of test serviceability can be summed up in three conclusions:

1. At first and second thickness levels the plain slab design performed slightly better than the reinforced design. However, at the third and fourth thickness levels both slab designs showed equal performance.
2. At first and second thickness levels performance was consistently better under single-axle test traffic than under tandem-axle test traffic. However, at third and fourth thickness levels, performance is equal under both single- and tandem-axle test traffic.
3. Performance is the same at the third and fourth thickness levels.

Authors' Comment.— These conclusions are in conflict with the Road Test performance equation for concrete (3). This equation shows:

1. Equal performance for the two slab designs, regardless of thickness level.
2. Better performance under single axles than under tandem axles, regardless of slab thickness-load relationships.
3. Increasingly better performance as slab thickness is increased, regardless of thickness level.

CRACKING

Table 4 gives the number of repetitions at which minor and major cracking started for all Design 1 test sections in the four truck loops. Minor cracking (classes 1 and 2) includes cracks not visible at 15 ft under dry surface conditions and cracks that could be seen at 15 ft but showed only minor spalling or crack widths less than ¼ in. Major cracking (classes 3 and 4) included cracks that had opened more than ¼ in., and had spalled or had been sealed. Examples of minor and major cracking are shown on page 124 (3).

The data show that cracking started in many reinforced sections during the early fall of 1959. Cracking was first observed at 273,000 or 274,000 repetitions in 31 of the 112 reinforced sections in loops 3 to 6. The data also show that cracking started in 57 percent of the reinforced sections between 250,000 and 300,000 repetitions. Data from the first thickness in loop 3 were excluded because five of six sections dropped to a 1.5 index before 300,000 repetitions of test traffic. Values for thickness levels are first thickness level, 56 percent; second thickness level, 59 percent; third thickness level, 59 percent; and fourth thickness level, 50 percent. It was concluded that the road test environment had a major influence on the start of cracking in the reinforced test sections at all four thickness levels.

Authors' Comment.— The cracking started in an environment similar to one that is believed to have caused high stresses due to restrained warping on another experimental project—the Arlington Test Track (7). In both cases:

1. There was a period of relatively low precipitation likely to produce a firm subgrade.
2. There were fairly low minimum night temperatures likely to keep the subgrade and the bottom of the concrete cool.

3. There were fairly warm sunshiny days likely to cause rapid increases in temperature on the top surface of the concrete and a much higher temperature in the top of concrete than in the bottom.

When these conditions prevail, the top of the slab tends to expand and warp the slab downward along the slab edges and at joints. The expansion and downward warping are resisted by the subgrade, producing tensile stresses in the bottom of the slab. These stresses tend to reach a maximum value at about 15 to 20 ft from a joint or edge (8).

It is not known whether stresses due to restrained warping (in combination with loads) caused the start of cracking in the reinforced sections at the Road Test. However, the crack pattern that did develop is an integral part of the experimental test results. This means that the experimental data show the performance of a group of reinforced test sections, 50 percent or more of which started cracking during a brief fall period—in spite of wide differences in the ratios of loads to slab thicknesses.

In some states, reinforced pavements do not develop a crack pattern like the one that occurred at the Road Test. This is true of reinforced pavements 8 to 10 in. thick on 4- to 12-in. subbases after 10 to 20 years of service on projects carrying large volumes of heavy truck traffic. These pavements do not have visible cracks. The very few cracks that do occur are isolated between long sections without cracks and are usually associated with abrupt changes in subgrade support, rather than climatic environment. In states where reinforced pavements do not exhibit cracking, except at isolated locations, Road Test performance on the reinforced sections will have little or no application.

The data on major cracking in Table 4 have been summarized on bar graphs in Figure 8. The bars show the percent of sections without major cracking and average repetitions at the start of major cracking for the two slab designs by thickness levels and loops. With regard to major cracking, Figure 8 shows:

1. About equal performance on first thickness levels except that the plain design showed slightly better performance than the reinforced design on the first level 8-in. test sections in loop 6.
2. At the second thickness level, performance was about equal in loop 3. In loops 4, 5 and 6 performance was better on the plain design than on the reinforced design.
3. At the third thickness level, performance was better on the plain slab design than on the reinforced design in loops 3, 4 and 6. In these loops no major cracking occurred on the plain design, but 62 to 100 percent of the reinforced test sections had major cracks. In loop 5 the percent of slabs with major cracking was equal, but the average number of repetitions to the start of cracking showed a slight superiority for the reinforced slab design.
4. At the fourth thickness level, performance was better on the plain slab design in loops 3 and 4 and about equal in loops 5 and 6.
5. Overall performance showed about equal performance on 7 of 16 load-thickness combinations. In one case (the third thickness in loop 5) performance was slightly better on the reinforced slab design. In the other eight load-thickness combinations, performance was superior on the plain design, with five of these eight combinations showing no major cracking.

It was concluded that the plain slab design showed definite overall superiority to the reinforced design with regard to major cracking.

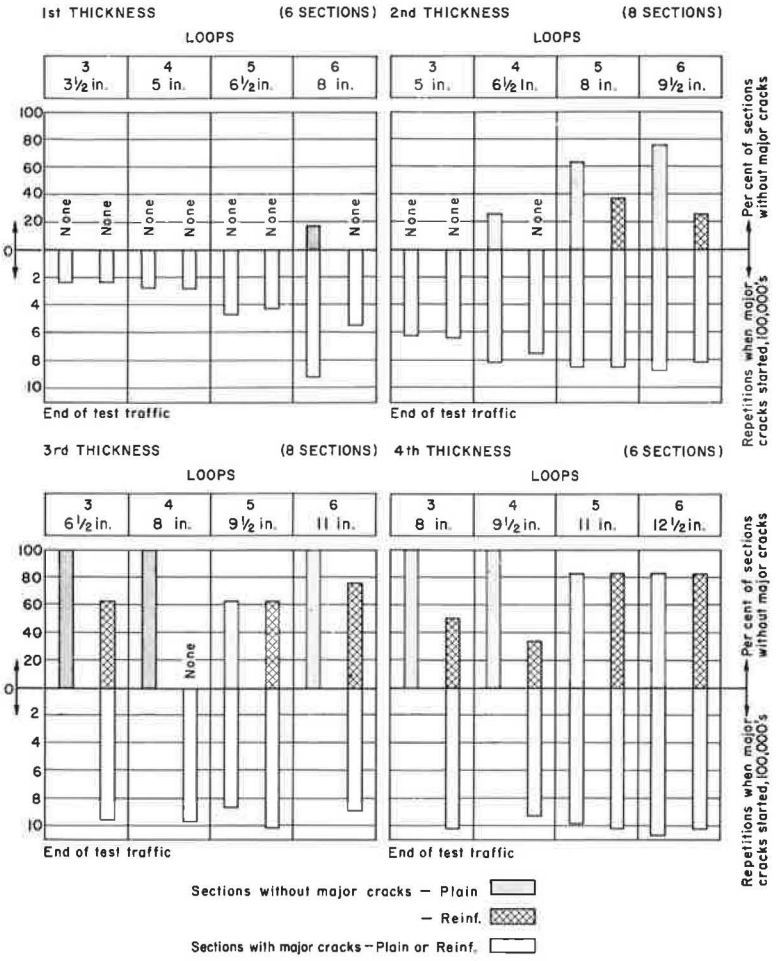

Figure 8. Major cracking — class 3 and 4—concrete test sections (factorial and replicate).

Authors' Comment[1]. — Major (class 3 and 4) cracking was used in computing serviceability indexes. However, where the serviceability is about equal, a pavement without major cracking should be a better maintenance risk than a pavement with these cracks. It is true that there are more joints to maintain with a plain slab design. However, with a short joint spacing there is less movement at the joints and this tends to reduce the amount and frequency of maintenance required. Also, maintenance costs are usually higher for spalled or otherwise defective cracks than they are for joints.

SUBBASE PUMPING

This section deals with the extent and severity of subbase pumping at the Road Test and the relationships of subbase pumping to serviceability and performance. The data and analyses are on trace, moderate and heavy subbase pumping. (In the HRB data systems, trace, moderate and heavy subbase pumping are combined into a pumping

[1] The limitations set forth in the comments on start of cracking in reinforced sections also apply here.

score. This score equals trace pumping, plus 10 times moderate pumping, plus 50 times heavy pumping. In the Road Test Report the Pumping Index equals the Pumping Score divided by 100.) These types (or intensities) of subbase pumping are not defined in the Road Test Report (3) or in the Data System on pumping (R4243). However, examples of subbase pumping are shown in Figure 9.

Table 5 gives the data for all Design 1 concrete test sections in loops 3 to 6. These data are arranged across the table to make abridged section histories referenced to subbase pumping.

With regard to the extent of subbase pumping in loops 3 to 6, Table 5 shows the following:

Trace subbase pumping: (1) occurred on all Design 1 test sections.

Moderate subbase pumping: (1) occurred on all first and second level test sections, (2) occurred on 95 percent of the third level test sections, and (3) occurred on 63 percent of the fourth level test sections.

Heavy subbase pumping: (1) occurred on all first level test sections, and (2) occurred on 89 percent of the second level test sections, (3) occurred on 34 percent of the third level test sections (heavy subbase pumping was not severe on third and fourth level test sections), and (4) occurred on 21 percent of the fourth level test sections.

A major part of the data in Table 5 is shown in Figure 10. The bar graphs are performance histories showing Road Test performance in the truck loops up to the point heavy subbase pumping started. Serviceability and repetitions are plotted in the following order: (1) as constructed values, (2) at the start of trace subbase pumping, (3) at the start of moderate subbase pumping, and (4) at the start of heavy subbase pumping.

When moderate or heavy subbase pumping did not occur during the test period, end of test repetitions and serviceability indexes were used.

Bar graph histories are shown for the plain and reinforced slab designs, under single and tandem axles and by thickness levels and loops. The bar graph values are averages for the three subbase thicknesses.

Study of the bar graph histories in Figure 10 shows that:

1. Prior to the start of heavy subbase pumping there were no significant differences in serviceability on the plain and reinforced slab designs at any thickness level.
2. Prior to the start of heavy subbase pumping there were no significant differences in serviceability under single- and tandem-axle test traffic at any thickness level.
3. There was an initial loss in serviceability of about 0.4 prior to, or at the start of, trace subbase pumping. On most sections, trace subbase pumping started at 101,000 repetitions. Further study of performance histories showed that on most sections the initial loss in serviceability reached its low point at about 100,000 repetitions regardless of number of repetitions at which trace subbase pumping started. The initial serviceability loss occurred during the first period of spring weather after traffic testing started. Concrete pavements in service often exhibit lower serviceability during the first spring period than during subsequent spring periods or during other periods in the yearly weather cycle.
4. Prior to the start of heavy subbase pumping there were no further significant losses in serviceability at any thickness level.

To further check these conclusions, changes in serviceability between the start of trace subbase pumping and the start of heavy subbase pumping were computed. Where heavy subbase pumping did not occur during the test period, the end of test serviceability values was used. These computations are given in Table 6.

These mean changes (Table 6) do not show a significant loss in serviceability and hence support the conclusion that no losses occurred prior to the start of heavy subbase pumping.

Figure 9. (a) Test section where subbase pumping had not occurred; (b)trace subbase pumping along full length of test section; (c) initial stages of moderate subbase pumping; (d) initial stages of heavy subbase pumping; and (e) severe stage of heavy subbase pumping.

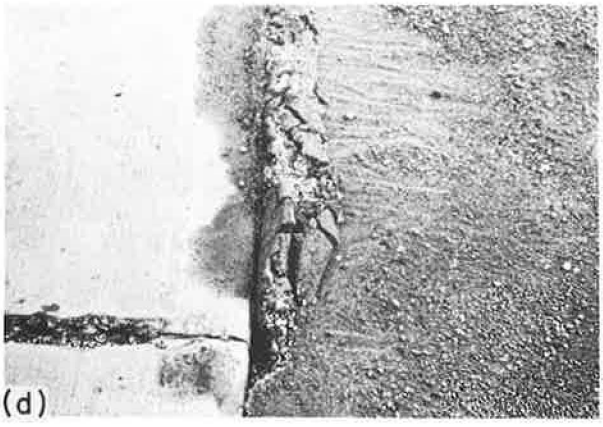

TABLE 5

SUBBASE PUMPING AND CONCRETE SERVICE

1st Thickness — LOOP 3 — 3½ in.

Sec. No.	Design: Slab	Design: Subbase Depth In.	Axle Loads kips*	Serviceability Indexes: At Start Of Test	At Start Of Subbase Pumping: Trace	Mod.	Heavy	At End Of Test	Repetitions (1000-S): At Start Of Subbase Pumping: Trace	Mod.	Heavy	At First Loss **	At End Of Test
195	Plain	3	12S	4.3	4.1	4.1	3.7	1.5	77	101	274	250	315
196	Doweled Joints 15 Ft.		24T	4.5	4.1	4.1	4.0	1.5	101	143	267	265	318
239		6	12S	4.6	4.2	4.2	4.2	1.5	101	101	101	250	289
240			24T	4.6	4.2	4.2	4.2	1.5	101	101	101	170	210
213		9	12S	5.0	4.7	4.7	4.7	1.5	101	101	101	170	289
214			24T	4.9	4.7	4.7	4.7	1.5	101	101	101	180	297
209	Reinf.	3	12S	4.6	4.6	4.6	4.6	1.5	101	101	101	235	278
210	Doweled Joints 40 Ft.		24T	4.8	4.6	4.6	4.6	1.5	101	101	101	245	278
205		6	12S	4.8	4.4	4.4	4.4	1.5	101	101	101	135	273
206			24T	4.9	4.7	4.7	4.6	1.5	101	101	131	180	295
231		9	12S	4.7	4.5	4.5	4.5	1.5	101	101	101	275	324
232			24T	4.8	4.5	4.5	4.5	1.5	101	101	101	265	294

1st Thickness — LOOP 4 — 5 in.

Sec. No.	Design: Slab	Design: Subbase Depth In.	Axle Loads kips*	Serviceability Indexes: At Start Of Test	At Start Of Subbase Pumping: Trace	Mod.	Heavy	At End Of Test	Repetitions (1000-S): At Start Of Subbase Pumping: Trace	Mod.	Heavy	At First Loss **	At End Of Test
643	Plain	3	18S	4.8	4.4	4.4	4.4	1.5	101	101	145	315	716
644	Doweled Joints 15 Ft.		32T	4.8	4.3	4.3	4.4	1.5	101	101	145	295	343
647		6	18S	4.8	4.3	4.4	4.4	1.5	101	145	145	280	353
648			32T	4.7	4.4	4.4	4.4	1.5	101	101	101	220	328
677		9	18S	4.6	4.2	4.2	4.2	1.5	101	101	101	275	291
678			32T	4.8	4.3	4.2	4.3	1.5	101	120	145	275	289
681	Reinf.	3	18S	4.6	4.3	4.3	4.3	1.5	101	101	101	315	415
682	Doweled Joints 40 Ft.		32T	4.7	4.4	4.4	4.4	1.5	101	101	101	225	304
661		6	18S	4.7	4.3	4.3	4.3	1.5	101	101	101	300	325
662			32T	4.6	4.2	4.2	4.2	1.5	101	101	101	150	175
673		9	18S	4.7	4.3	4.3	4.2	1.5	101	101	145	400	592
674			32T	4.7	4.2	4.2	4.2	1.5	101	101	101	360	408

1st Thickness — LOOP 5 — 6½ in.

Sec. No.	Design: Slab	Design: Subbase Depth In.	Axle Loads kips*	Serviceability Indexes: At Start Of Test	At Start Of Subbase Pumping: Trace	Mod.	Heavy	At End Of Test	Repetitions (1000-S): At Start Of Subbase Pumping: Trace	Mod.	Heavy	At First Loss **	At End Of Test
513	Plain	3	22.4S	4.7	4.3	4.3	4.2	1.5	101	101	142	700	760
514	Doweled Joints 15 Ft.		40T	4.7	4.4	4.4	4.4	1.5	101	101	101	310	335
517		6	22.4S	4.7	4.2	4.2	4.3	1.5	101	101	287	665	898
518			40T	4.7	4.2	4.2	4.3	1.5	101	101	123	325	369
505		9	22.4S	4.5	4.2	4.2	4.2	1.5	101	101	270	410	705
506			40T	4.6	4.2	4.2	4.1	1.5	101	101	123	350	698
523	Reinf.	3	22.4S	4.6	4.2	4.2	4.4	1.5	101	101	649	700	898
524	Doweled Joints 40 Ft.		40T	4.7	4.2	4.2	4.4	1.5	101	101	586	620	705
491		6	22.4S	4.6	4.2	4.2	4.2	1.5	101	101	190	285	369
492			40T	4.7	4.2	4.2	4.2	1.5	101	101	143	275	305
549		9	22.4S	4.6	4.0	4.0	4.0	1.5	101	101	101	575	708
550			40T	4.7	4.2	4.2	4.2	1.5	101	101	101	275	618

1st Thickness — LOOP 6 — 8 in.

Sec. No.	Design: Slab	Design: Subbase Depth In.	Axle Loads kips*	Serviceability Indexes: At Start Of Test	At Start Of Subbase Pumping: Trace	Mod.	Heavy	At End Of Test	Repetitions (1000-S): At Start Of Subbase Pumping: Trace	Mod.	Heavy	At First Loss **	At End Of Test
353	Plain	3	30S	4.3	3.9	4.0	3.9	1.5	101	143	332	710	878
354	Doweled Joints 15 Ft.		48T	4.2	4.0	3.8	3.9	1.8	101	121	331	850	1114
393		6	30S	4.8	4.4	4.3	4.2	3.9	101	143	332	1100	1114
394			48T	4.7	4.4	4.3	4.3	4.1	101	245	284	—	1114
369		9	30S	4.5	4.2	4.1	4.0	3.4	101	130	349	880	1114
370			48T	4.3	4.0	4.0	4.1	1.5	101	331	672	755	1114
341	Reinf.	3	30S	4.7	4.3	4.2	4.1	1.5	101	143	292	710	782
342	Doweled Joints 40 Ft.		48T	4.7	4.2	4.2	4.2	1.5	101	101	101	410	618
385		6	30S	4.6	4.2	4.2	4.2	1.5	101	292	332	745	974
386			48T	4.6	4.3	4.3	4.3	1.5	101	101	101	345	415
347		9	30S	4.7	4.3	4.3	4.4	1.5	101	101	206	670	768
348			48T	4.8	4.4	4.4	4.4	1.5	101	101	145	570	624

*S = Single, T = Tandem

**When serviceability index fell below 4.0 and did not recover

LOOP 3 — 2nd Thickness 5 in.

Sec. No.	Design: Slab	Design: Subbase Depth in.	Axle Loads kips*	Serviceability Indexes: At Start Of Test	At Start Of Subbase Pumping: Trace	Mod.	Heavy	At End Of Test	Repetitions (1000-S): At Start Of Subbase Pumping: Trace	Mod.	Heavy	At First Loss **	At End Of Test
225	Plain	3	12S	4.6	4.4	4.0	4.1	3.7	101	172	890	970	1114
226			24T	4.8	4.5	4.2	4.2	1.5	101	169	273	320	705
245	Doweled Joints 15 Ft.	6	12S	4.7	4.3	4.2	4.2	3.5	101	274	704	950	1114
221			R	4.9	4.6	4.2	4.0	3.1	101	172	749	750	1114
246			24T	4.8	4.5	4.3	4.3	2.8	101	598	772	905	1114
222			R	4.9	4.2	4.2	4.0	1.5	101	143	338	445	901
219		9	12S	4.9	4.4	4.2	4.1	3.9	144	176	629	970	1114
220			24T	4.8	4.5	4.3	4.3	1.5	101	169	282	570	771
251	Reinf.	3	12S	4.5	4.0	4.0	4.0	2.8	101	101	329	810	1114
203			R	4.7	4.4	4.4	4.4	4.0	101	101	280	—	1114
252	Doweled Joints 40 Ft.		24T	4.5	4.1	4.1	4.0	1.5	101	101	169	735	1100
204			R	4.7	4.4	4.4	4.3	1.5	101	273	413	885	1046
191		6	12S	4.7	4.4	4.4	4.3	1.5	101	101	172	670	725
192			24T	4.7	4.2	4.2	4.3	1.5	101	101	202	440	631
233		9	12S	4.8	4.6	4.3	4.0	3.3	101	176	868	960	1114
234			24T	4.9	4.5	4.5	4.2	1.5	101	101	273	635	793

LOOP 4 — 2nd Thickness 6½ in.

Sec. No.	Design: Slab	Design: Subbase Depth in.	Axle Loads kips*	Serviceability Indexes: At Start Of Test	At Start Of Subbase Pumping: Trace	Mod.	Heavy	At End Of Test	Repetitions (1000-S): At Start Of Subbase Pumping: Trace	Mod.	Heavy	At First Loss **	At End Of Test
649	Plain	3	18S	4.8	4.3	4.4	—	3.8	101	346	NONE	990	1114
650			32T	4.6	4.3	4.4	4.0	1.5	101	131	413	410	689
697	Doweled Joints 15 Ft.	6	18S	4.9	4.3	4.3	—	4.4	101	730	NONE	—	1114
655			R	4.8	4.4	4.3	4.6	4.3	101	345	730	—	1114
698			32T	4.7	4.3	4.5	4.6	3.4	101	295	598	1000	1114
656			R	4.8	4.4	4.5	4.5	1.5	101	346	346	825	1000
703		9	18S	4.8	4.3	4.3	4.5	3.0	101	346	774	940	1114
704			32T	4.8	4.4	4.4	4.4	1.5	101	196	196	640	772
641	Reinf.	3	18S	4.9	4.4	4.5	4.6	3.8	101	276	685	965	1114
705			R	4.8	4.3	4.5	4.5	3.6	101	195	774	945	1114
642	Doweled Joints 40 Ft.		32T	4.7	4.4	4.4	4.4	2.6	101	101	196	780	1114
706			R	4.8	4.5	4.5	4.5	1.5	101	101	196	715	793
685		6	18S	4.8	4.5	4.5	4.6	3.4	101	276	774	925	1114
686			32T	4.8	4.3	4.3	4.4	1.5	101	101	346	750	796
653		9	18S	4.9	4.4	4.5	4.5	1.8	101	282	331	945	1114
654			32T	4.8	4.4	4.4	4.4	1.5	101	101	101	880	1036

LOOP 5 — 2nd Thickness 8 in.

Sec. No.	Design: Slab	Design: Subbase Depth in.	Axle Loads kips*	Serviceability Indexes: At Start Of Test	At Start Of Subbase Pumping: Trace	Mod.	Heavy	At End Of Test	Repetitions (1000-S): At Start Of Subbase Pumping: Trace	Mod.	Heavy	At First Loss **	At End Of Test
547	Plain	3	22.4S	4.4	4.0	4.2	—	4.2	101	316	NONE	—	1114
548			40T	4.7	4.0	4.2	—	4.2	101	586	NONE	—	1114
539	Doweled Joints 15 Ft.	6	22.4S	4.7	4.2	4.3	4.3	4.2	101	628	710	—	1114
533			R	4.7	4.2	4.2	4.3	4.1	101	316	601	—	1114
540			40T	4.7	4.2	4.4	4.3	3.7	202	586	771	1045	1114
534			R	4.7	4.1	4.3	4.2	4.2	101	586	1087	—	1114
507		9	22.4S	4.7	4.3	4.6	4.6	1.5	103	710	710	900	1111
508			40T	4.8	4.5	4.7	4.6	1.5	101	586	727	850	898
519	Reinf.	3	22.4S	4.6	4.2	4.2	4.1	1.5	101	270	331	715	1104
521			R	4.5	4.2	4.2	4.3	4.3	101	270	310	—	1114
520	Doweled Joints 40 Ft.		40T	4.7	4.2	4.2	4.4	1.5	101	101	686	715	915
522			R	4.6	4.2	4.2	4.3	4.3	101	101	716	—	1114
501		6	22.4S	4.6	4.2	4.2	4.2	4.0	101	270	270	—	1114
502			40T	4.8	4.3	4.3	4.4	1.5	101	101	275	785	901
531		9	22.4S	4.9	4.4	4.4	4.6	4.6	101	101	331	—	1114
532			40T	4.8	4.2	4.2	4.6	3.2	101	101	600	1085	1114

LOOP 6 — 2nd Thickness 9½ in.

Sec. No.	Design: Slab	Design: Subbase Depth in.	Axle Loads kips*	Serviceability Indexes: At Start Of Test	At Start Of Subbase Pumping: Trace	Mod.	Heavy	At End Of Test	Repetitions (1000-S): At Start Of Subbase Pumping: Trace	Mod.	Heavy	At First Loss **	At End Of Test
351	Plain	3	30S	4.4	4.1	4.1	4.0	3.6	101	101	795	1050	1114
352			48T	4.3	4.1	3.9	3.8	3.1	101	122	145	695	1114
367	Doweled Joints 15 Ft.	6	30S	4.7	4.3	4.3	—	4.3	101	143	NONE	—	1114
389			R	4.6	4.2	4.2	4.2	4.3	101	130	898	—	1114
368			48T	4.7	4.2	4.2	—	4.3	101	575	NONE	—	1114
390			R	4.7	4.2	4.2	4.3	4.3	101	130	408	—	1114
375		9	30S	4.6	4.2	4.2	4.2	4.2	101	588	728	—	1114
376			48T	4.6	4.2	4.2	4.3	4.3	101	368	715	—	1114
381	Reinf.	3	30S	4.5	4.3	4.4	—	4.5	101	703	NONE	—	1114
371			R	4.6	4.3	4.3	4.4	1.6	101	130	703	760	1114
382	Doweled Joints 40 Ft.		48T	4.7	4.3	4.3	4.3	4.4	101	122	331	—	1114
372			R	4.7	4.3	4.3	4.2	4.1	101	284	348	—	1114
403		6	30S	4.4	4.2	4.2	4.4	4.0	101	171	629	—	1114
404			48T	4.7	4.2	4.1	4.3	4.0	101	202	575	—	1114
339(1)		9	30S	4.7	4.3	4.4	4.5	2.2	101	122	686	775	1114
340			48T	4.8	4.4	4.4	4.4	1.5	101	101	169	755	912

* S = Single, T = Tandem, R = Replicate
** When serviceability index fell below 4.0 and did not recover
(1) Section history shown page 148 HRB Special Report 61-E

TABLE 5

SUBBASE PUMPING AND CONCRETE SERVICE (Cont'd.)

3rd Thickness — LOOP 3 — 6½ in.

Sec. No.	Design: Slab	Design: Subbase Depth In.	Axle Loads kips*	Serviceability Indexes: At Start Of Test	At Start Of Subbase Pumping: Trace	Mod.	Heavy	At End Of Test	Repetitions (1000-S): At Start Of Subbase Pumping: Trace	Mod.	Heavy	At First Loss **	At End Of Test
217	Plain	3	12S	4.9	4.7	4.6	—	4.4	131	274	NONE	—	1114
193			R	4.6	4.2	—	—	3.9	131	NONE	NONE	1114	1114
218			24T	4.8	4.7	4.7	—	4.2	101	703	NONE	—	1114
194			R	4.6	4.3	4.2	—	4.0	131	267	NONE	—	1114
249	Doweled Joints 15 Ft.	6	12S	4.7	4.5	4.2	—	4.1	172	974	NONE	—	1114
250			24T	4.8	4.3	4.3	—	4.1	169	647	NONE	—	1114
207		9	12S	4.9	4.4	4.3	—	4.2	172	974	NONE	—	1114
208			24T	4.8	4.2	4.4	—	4.0	169	647	NONE	—	1114
199	Reinf.	3	12S	4.7	4.6	4.4	—	4.2	101	728	NONE	—	1114
200			24T	4.9	4.5	4.4	4.5	4.1	101	267	867	—	1114
247	Doweled Joints 40 Ft.	6	12S	4.8	4.6	4.5	—	4.3	101	790	NONE	—	1114
237			R	5.0	4.7	4.2	—	4.5	171	715	NONE	—	1114
248			24T	4.8	4.6	4.4	4.6	4.3	101	714	890	—	1114
238			R	5.0	4.7	4.1	4.1	4.1	101	361	772	—	1114
241		9	12S	4.9	4.4	4.4	—	4.4	172	715	NONE	—	1114
242			24T	4.9	4.6	4.5	4.6	4.4	101	169	901	—	1114

3rd Thickness — LOOP 4 — 8 in.

Sec. No.	Design: Slab	Design: Subbase Depth In.	Axle Loads kips*	Serviceability Indexes: At Start Of Test	At Start Of Subbase Pumping: Trace	Mod.	Heavy	At End Of Test	Repetitions (1000-S): At Start Of Subbase Pumping: Trace	Mod.	Heavy	At First Loss **	At End Of Test
671	Plain	3	18S	4.9	4.3	4.3	—	4.4	101	346	NONE	—	1114
687			R	4.8	4.4	—	—	4.5	101	NONE	NONE	—	1114
672			32T	4.6	4.4	4.2	—	4.1	101	586	NONE	—	1114
688			R	4.7	4.3	4.5	—	4.2	101	346	NONE	—	1114
683	Doweled Joints 15 Ft.	6	18S	4.9	4.7	4.7	—	4.4	101	716	NONE	—	1114
684			32T	4.8	4.6	4.5	4.2	4.2	101	716	983	—	1114
651		9	18S	4.8	4.5	4.5	—	4.3	282	716	NONE	—	1114
652			32T	4.7	4.2	4.3	—	4.1	101	585	NONE	—	1114
691	Reinf.	3	18S	4.8	4.4	4.3	4.3	3.9	101	716	716	1100	1114
692			32T	4.9	4.3	4.3	4.3	4.0	101	101	101	—	1114
669	Doweled Joints 40 Ft.	6	18S	4.9	4.6	4.8	4.8	4.4	101	716	716	—	1114
707			R	4.7	4.3	4.2	4.2	3.9	101	132	132	1110	1114
670			32T	4.8	4.4	4.7	4.7	4.4	101	585	585	—	1114
708			R	4.7	4.3	4.3	4.3	3.8	101	101	101	1055	1114
695		9	18S	4.8	4.6	—	—	4.3	101	NONE	NONE	—	1114
696			32T	4.8	4.4	4.6	4.6	4.2	101	585	585	—	1114

3rd Thickness — LOOP 5 — 9½ in.

Sec. No.	Design: Slab	Design: Subbase Depth In.	Axle Loads kips*	Serviceability Indexes: At Start Of Test	At Start Of Subbase Pumping: Trace	Mod.	Heavy	At End Of Test	Repetitions (1000-S): At Start Of Subbase Pumping: Trace	Mod.	Heavy	At First Loss **	At End Of Test
511	Plain	3	22.4S	4.7	4.3	4.6	—	4.4	168	768	NONE	—	1114
541			R	4.4	4.3	4.3	4.3	4.3	101	744	768	—	1114
512			40T	4.8	4.3	4.4	—	4.3	101	586	NONE	—	1114
542			R	4.6	4.0	4.0	—	4.2	101	123	NONE	—	1114
525	Doweled Joints 15 Ft.	6	22.4S	4.7	4.2	4.4	4.3	3.7	101	628	784	830	1114
526			40T	4.8	4.2	4.7	4.5	4.0	101	586	686	—	1114
535		9	22.4S	4.7	4.2	4.4	—	4.5	101	601	NONE	—	1114
536			40T	4.6	4.0	4.2	4.3	3.8	101	586	727	1010	1114
553	Reinf.	3	22.4S	4.7	4.2	4.2	—	4.3	101	122	NONE	—	1114
554			40T	4.9	4.1	4.1	—	4.1	101	101	NONE	—	1114
543	Doweled Joints 40 Ft.	6	22.4S	4.7	4.1	4.4	—	4.5	101	710	NONE	—	1114
503			R	4.7	4.2	4.2	—	4.3	101	101	NONE	—	1114
544			40T	4.7	4.0	4.0	4.3	4.3	101	101	727	—	1114
504			R	4.8	4.3	4.3	4.4	4.5	101	101	750(1)	—	1114
499		9	22.4S	4.6	4.4	4.4	—	4.4	101	101	NONE	—	1114
500			40T	4.8	4.4	4.4	—	4.6	101	101	NONE	—	1114

3rd Thickness — LOOP 6 — 11 in.

Sec. No.	Design: Slab	Design: Subbase Depth In.	Axle Loads kips*	Serviceability Indexes: At Start Of Test	At Start Of Subbase Pumping: Trace	Mod.	Heavy	At End Of Test	Repetitions (1000-S): At Start Of Subbase Pumping: Trace	Mod.	Heavy	At First Loss **	At End Of Test
377	Plain	3	30S	4.6	4.0	4.3	—	4.2	369	749	NONE	—	1114
363			R	4.7	4.2	4.2	—	4.4	101	143	NONE	—	1114
378			48T	4.6	4.3	4.4	—	4.3	284	615	NONE	—	1114
364			R	4.8	4.3	4.4	—	4.3	101	570	NONE	—	1114
397	Doweled Joints 15 Ft.	6	30S	4.7	4.2	4.4	—	4.2	101	1042	NONE	—	1114
398			48T	4.6	4.3	4.3	—	4.3	101	615	NONE	—	1114
365		9	30S	4.6	4.2	4.2	—	4.3	101	749	NONE	—	1114
366			48T	4.7	4.2	4.2	—	4.3	101	779	NONE	—	1114
391	Reinf.	3	30S	4.6	4.2	4.2	—	4.4	101	281	NONE	—	1114
392			48T	4.6	4.3	4.4	4.4	4.4	101	284	1022	—	1114
337	Doweled Joints 40 Ft.	6	30S	4.6	4.3	4.2	—	4.0	101	130	NONE	—	1114
345			R	4.7	4.2	4.3	4.3	4.3	101	369	795	—	1114
338			48T	4.5	4.3	4.3	4.2	4.1	101	101	408	—	1114
346			R	4.7	4.4	4.4	—	4.2	101	368	NONE	—	1114
343		9	30S	4.6	4.2	4.2	—	4.2	101	582	NONE	—	1114
344			48T	4.7	4.3	4.2	4.3	4.1	101	130	331	—	1114

*S = Single, T = Tandem, R = Replicate

**When serviceability index fell below 4.0 and did not recover

TABLE 5

SUBBASE PUMPING AND CONCRETE SERVICE (Cont'd.)

LOOP 3 — 4th Thickness 8 in.

Sec. No.	Design: Slab	Design: Subbase Depth In.	Axle Loads kips*	Serviceability Indexes: At Start Of Test	At Start Of Subbase Pumping: Trace	Mod.	Heavy	At End Of Test	Repetitions (1000-S): At Start Of Subbase Pumping: Trace	Mod.	Heavy	At First Loss **	At End Of Test
201	Plain	3	12S	4.8	4.4	—	—	4.4	206	NONE	NONE	—	1114
202			24T	4.8	4.3	4.3	—	4.3	206	727	NONE	—	1114
235	Doweled Joints 15 Ft.	6	12S	4.8	4.5	4.7	—	4.3	172	652	NONE	—	1114
236			24T	4.9	4.5	4.6	4.3	4.3	169	582	772	—	1114
185		9	12S	4.6	4.2	—	—	4.0	144	NONE	NONE	—	1114
186			24T	4.7	4.3	4.2	—	4.2	131	647	NONE	—	
211	Reinf.	3	12S	4.9	4.6	—	—	4.3	274	NONE	NONE	—	1114
212			24T	4.9	4.4	4.2	—	4.1	101	772	NONE	—	1114
215	Doweled Joints 40 Ft.	6	12S	4.9	4.5	4.6	—	4.2	172	890	NONE	—	1114
216			24T	4.8	4.3	4.2	—	4.0	101	647	NONE	—	1114
197		9	12S	4.8	4.3	4.2	—	4.1	172	974	NONE	—	1114
198			24T	4.8	4.4	4.3	4.3	4.3	101	647	901	—	1114

LOOP 4 — 4th Thickness 9½ in.

Sec. No.	Design: Slab	Design: Subbase Depth In.	Axle Loads kips*	Serviceability Indexes: At Start Of Test	At Start Of Subbase Pumping: Trace	Mod.	Heavy	At End Of Test	Repetitions (1000-S): At Start Of Subbase Pumping: Trace	Mod.	Heavy	At First Loss **	At End Of Test
675	Plain	3	18S	4.7	4.2	4.2	—	4.2	145	171	NONE	—	1114
676			32T	4.5	4.1	4.2	4.1	4.0	101	585	730	—	1114
701	Doweled Joints 15 Ft.	6	18S	4.9	4.4	—	—	4.5	132	NONE	NONE	—	1114
702			32T	4.7	4.4	—	—	4.2	101	NONE	NONE	—	1114
689		9	18S	4.7	4.2	—	—	4.1	282	NONE	NONE	—	1114
690			32T	4.7	4.3	4.4	—	4.2	101	585	NONE	—	1114
645	Reinf.	3	18S	4.9	4.3	4.3	4.3	4.0	171	730	730	—	1114
646			32T	4.7	4.3	4.3	4.3	4.0	101	274	274	—	1114
665	Doweled Joints 40 Ft.	6	18S	4.7	4.4	—	—	4.5	171	NONE	NONE	—	1114
666			32T	4.7	4.3	4.6	—	4.3	101	774	NONE	—	1114
667		9	18S	4.8	4.8	—	—	4.8	282	NONE	NONE	—	1114
668			32T	4.8	4.7	4.8	—	4.6	101	585	NONE	—	1114

LOOP 5 — 4th Thickness 11 in.

Sec. No.	Design: Slab	Design: Subbase Depth In.	Axle Loads kips*	Serviceability Indexes: At Start Of Test	At Start Of Subbase Pumping: Trace	Mod.	Heavy	At End Of Test	Repetitions (1000-S): At Start Of Subbase Pumping: Trace	Mod.	Heavy	At First Loss **	At End Of Test
529	Plain	3	22.4S	4.7	4.2	—	—	4.1	130	NONE	NONE	—	1114
530			40T	4.6	4.1	4.3	—	4.3	101	649	NONE	—	1114
497	Doweled Joints 15 Ft.	6	22.4S	4.7	4.4	—	—	4.5	720	NONE	NONE	—	1114
498			40T	4.8	4.2	—	—	4.5	101	NONE	NONE	—	1114
509		9	22.4S	4.6	4.3	—	—	4.5	681	NONE	NONE	—	1114
510			40T	4.7	4.3	—	—	4.4	314	NONE	NONE	—	1114
515	Reinf.	3	22.4S	4.7	4.3	4.3	—	4.1	168	270	NONE	—	1114
516			40T	4.8	4.3	4.3	—	4.3	101	275	NONE	—	1114
545	Doweled Joints 40 Ft.	6	22.4S	4.6	4.0	4.5	4.3	4.4	101	768	768	—	1114
546			40T	4.6	4.0	4.0	—	4.3	101	101	NONE	—	1114
495		9	22.4S	4.6	4.2	4.2	—	4.4	101	203	NONE	—	1114
496			40T	4.6	4.2	4.2	4.2	4.4	101	101	207	—	1114

LOOP 6 — 4th Thickness 12½ in.

Sec. No.	Design: Slab	Design: Subbase Depth In.	Axle Loads kips*	Serviceability Indexes: At Start Of Test	At Start Of Subbase Pumping: Trace	Mod.	Heavy	At End Of Test	Repetitions (1000-S): At Start Of Subbase Pumping: Trace	Mod.	Heavy	At First Loss **	At End Of Test
395	Plain	3	30S	4.7	4.3	4.3	4.4	4.2	686	686	897	—	1114
396			48T	4.7	4.2	4.2	4.2	4.3	101	331	331	—	1114
349	Doweled Joints 15 Ft.	6	30S	4.3	4.0	4.0	—	4.0	193	281	NONE	—	1114
350			48T	4.5	4.0	4.1	4.1	4.2	145	169	315	—	1114
379		9	30S	4.6	4.2	—	—	4.2	774	NONE	NONE	—	1114
380			48T	4.6	4.2	4.3	—	4.4	315	1022	NONE	—	1114
359	Reinf.	3	30S	4.7	4.2	—	—	4.4	101	NONE	NONE	—	1114
360			48T	4.5	4.2	—	—	4.3	101	NONE	NONE	—	1114
355	Doweled Joints 40 Ft.	6	30S	4.7	4.3	4.3	—	4.2	101	292	NONE	—	1114
356			48T	4.7	4.5	4.6	4.6	4.4	101	575	575	—	1114
357		9	30S	4.7	4.3	—	—	4.5	292	NONE	NONE	—	1114
358			48T	4.6	4.2	—	—	4.2	101	NONE	NONE	—	1114

*S = Single, T = Tandem

**When serviceability index fell below 4.0 and did not recover

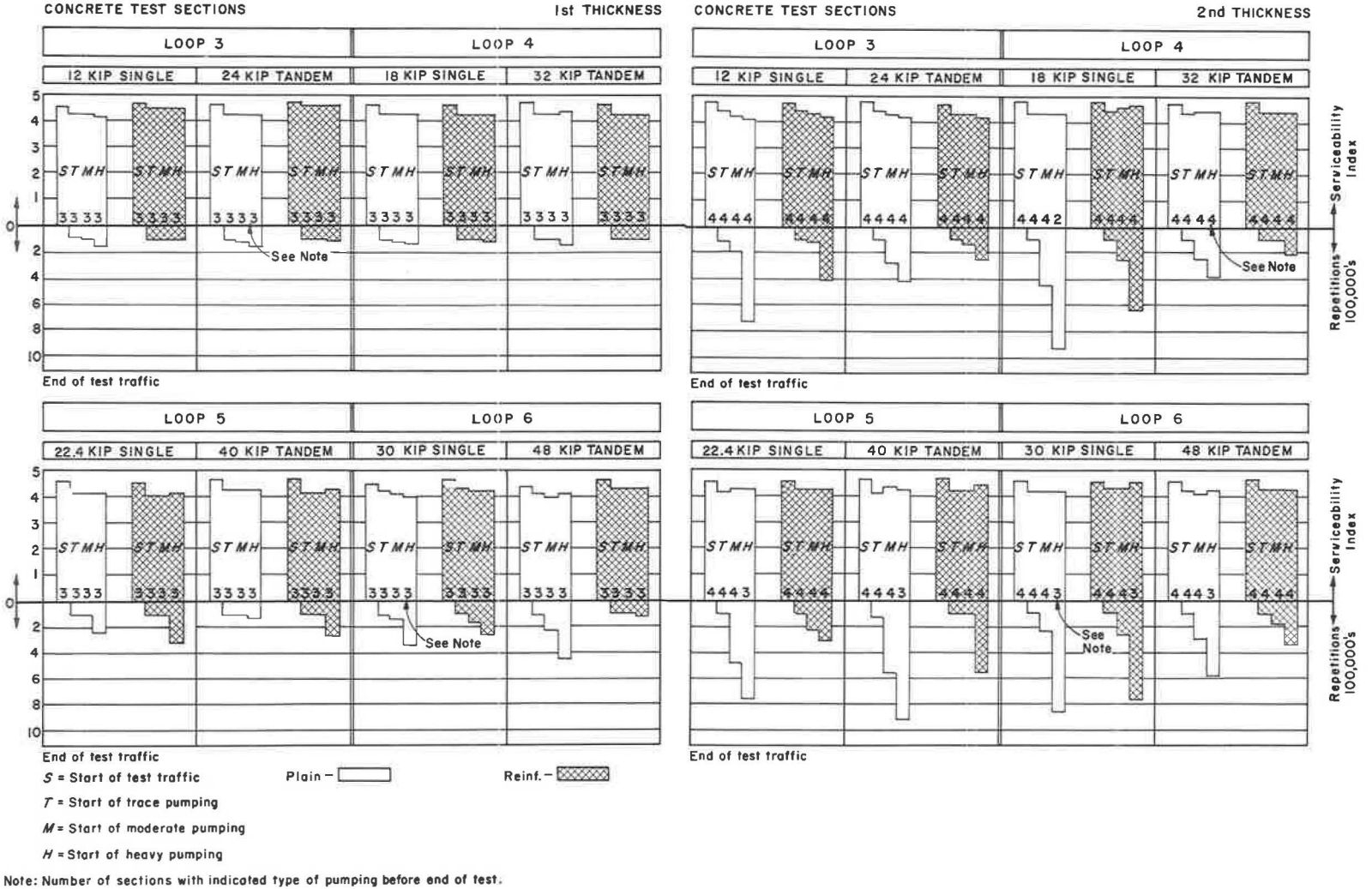

Note: Number of sections with indicated type of pumping before end of test.

Figure 10. Summary of serviceability and repetitions as related to subbase pumping.

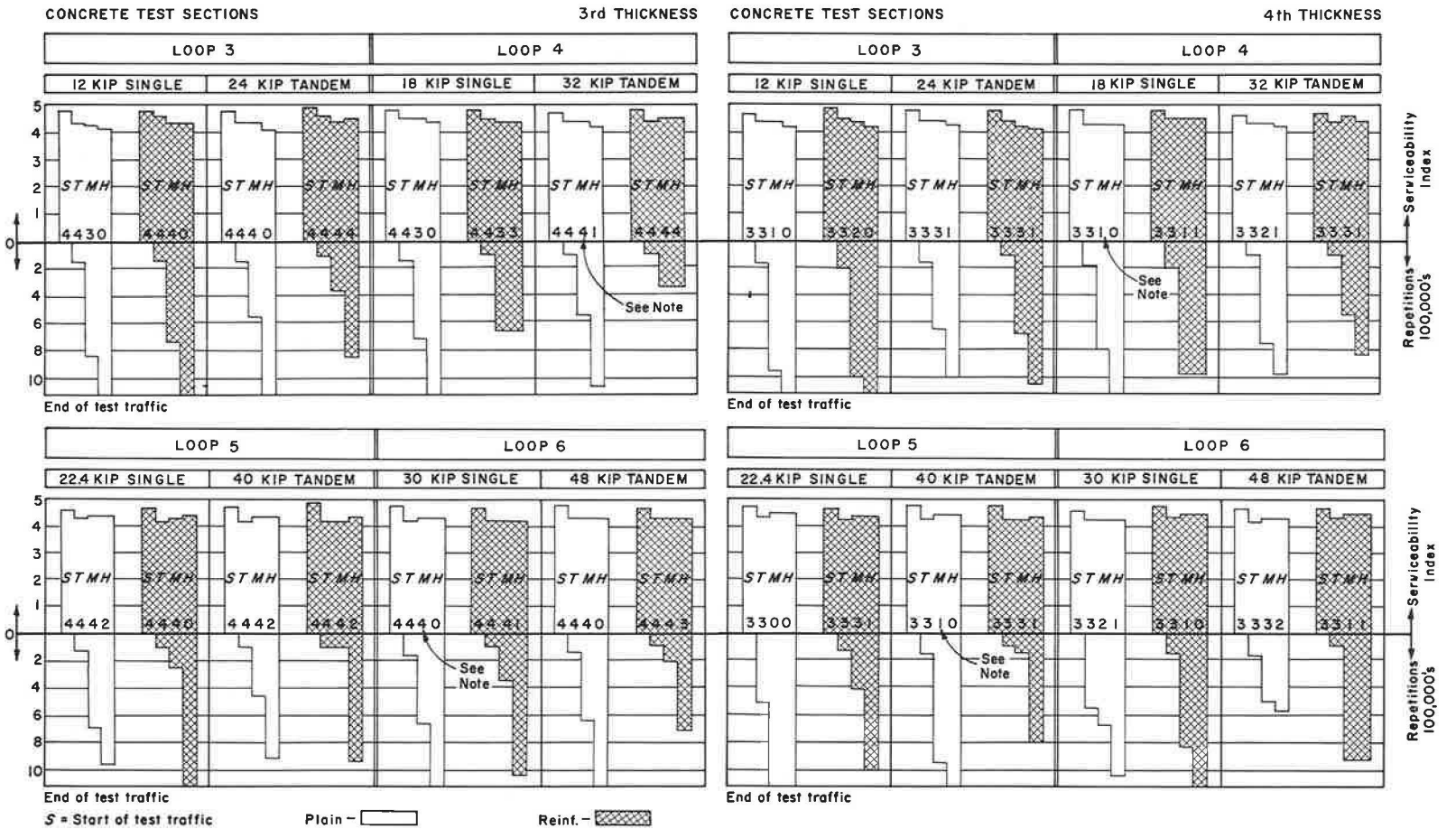

Figure 10. (continued)

As a further check on the conclusions, the mean losses in serviceability were first computed between the as constructed values and at the start of trace subbase pumping. Mean values for the four thickness levels are shown in Table 6. It is significant that these initial serviceability losses changed very little between thickness levels and did not decrease as slab thickness increased relative to load.

The next step was to check the validity of the following statement:

> On all Design 1 concrete test sections in loops 3 to 6 there was an initial 0.4 serviceability loss up to the start of trace subbase pumping, and there was no further loss in serviceability prior to the start of heavy subbase pumping—or during the test period on sections where no heavy pumping occurred.

TABLE 6

CHANGE IN SERVICEABILITY BETWEEN THE START OF TRACE AND HEAVY SUBBASE PUMPING

Thickness Level	Change	Mean
1	-0.10	-0.37
2	+0.08	-0.43
3	-0.20	-0.41
4	-0.01	-0.42
All 4	-0.02	-0.41

To check this statement 0.4 was subtracted from the as constructed serviceability index of each test section and the standard deviation was computed between this value and the serviceability index at the start of heavy subbase pumping—or the end of test serviceability index where no heavy subbase pumping occurred. Values were computed for the two slab designs and the two axle loads at each thickness level. Results of these computations are given in Table 7. These values show quite uniform concrete performance and no significant differences between the variables of load and design. The values support both the statement and the other conclusions.

The mean replicate difference in serviceability was 0.14 at the start of trace subbase pumping and 0.18 at the start of heavy subbase pumping, or at the end of the test where no heavy subbase pumping occurred. These replicate differences also show that concrete performance was quite uniform and that the deviation values are reliable.

> Authors' Comment.—The data and conclusions on subbase pumping thus far presented are at variance with the Road Test performance equations in the following respects:
>
> 1. The equations fail to show the initial loss in serviceability up to the start of trace subbase pumping.

TABLE 7

STANDARD DEVIATION IN SERVICEABILITY

Thickness Level	Mean	Plain		Reinf.	
		Single	Tandem	Single	Tandem
1*	0.12	0.10	0.10	0.14	0.14
2	0.20	0.27	0.20	0.22	0.10
3	0.20	0.17	0.17	0.14	0.22
4	0.20	0.17	0.14	0.24	0.24

*Data from the first level in loop 3 were omitted because all three types of subbase pumping started at the same number of repetitions on nine of twelve sections.

2. The equations fail to show that there were no further significant losses in serviceability prior to the start of heavy subbase pumping—or to the end of test where no heavy subbase pumping occurred.

3. The equations fail to show the equality of performance on Design 1 test sections at all thickness levels prior to the start of heavy subbase pumping—or to the end of test where no heavy subbase pumping occurred.

4. The equations fail to show equality of performance under single- and tandem-axle test traffic prior to the start of heavy subbase pumping—or to the end of test where heavy subbase pumping did not occur.

Table 5 shows repetitions to the first loss in serviceability—the point at which the serviceability index fell below 4.0 and did not recover. (The performance history of Section 339 is shown on page 148 (3, Fig. 115). The first loss in serviceability occurred at 775,000 repetitions.) This is approximately the point at which concrete test sections began to suffer damage from the effects of heavy subbase pumping (probably from non-uniform subbase support). The work on repetitions to the first loss in serviceability has thus far been limited to the first level test sections in the four truck loops. In Figure 11, the number of repetitions between the start of heavy subbase pumping and the first serviceability loss are related to computed stresses. These stresses (and others shown later) were computed for the maximum loop wheel load with a 20 percent load safety factor using the procedure described in the previous study (1, 2). Figure 11 shows:

1. Wide variations in the number of repetitions between the start of heavy subbase pumping and the first loss in serviceability.

2. That average values varied at a nearly constant rate where the stress was between 513 and 845 psi (loops 3, 4 and 5).

3. That there was a sharp increase in average repetitions to the first loss in serviceability where the stress was less than 513 psi (between loops 5 and 6).

Performance of the second level test sections are of special interest because of the wide variations in their performance, particularly in loops 4, 5 and 6. The following is a summary of major differences in end of test serviceability in these three loops:

Loop 4, Second Level, 6½ In., Stress: 424 Psi

Four sections survived test traffic with a mean serviceability index of 4.1, only slightly below end of test averages for the third and fourth levels.

However, six sections dropped to a 1.5 index at repetitions varying from 689,000 to 1,036,000.

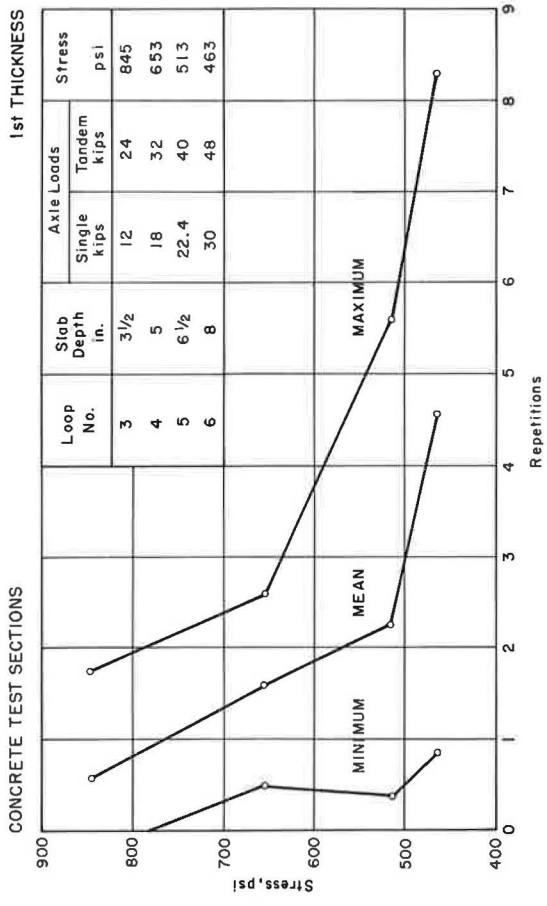

Figure 11. Repetitions from start of heavy pumping to first loss in serviceability (when serviceability fell below 4.0 and did not recover) as related to computed stresses.

Loop 5, Second Level, 8 In., Stress: 370 Psi

Eight sections survived test traffic with a mean serviceability index of 4.2—about equal to end of test values for third and fourth levels.

However, five sections dropped to a 1.5 index at repetitions varying from 898,000 to 1,104,000 repetitions.

Loop 6, Second Level, 9½ In., Stress: 346 Psi

Twelve sections survived with a mean serviceability index of 4.2—again equal to terminal values at the third and fourth thickness levels.

However, one section ended the test with an index of 1.6 and another dropped to 1.5 at 912,000 repetitions.

It is evident from this summary that concrete performance improved consistently as computed stresses dropped to values that are often used for design of pavements in service. (For concrete with an anticipated 28-day flexural strength of 700 psi, a stress of 350 psi affords a fatigue safety factor of 2.0, the value used for more than 100,000 load repetitions in the PCA design procedure.) But why the extremes of performance in these second level test sections? It was found that the differences in performance were related to the amount, or severity, of heavy subbase pumping and computed stresses. These relationships are shown in Table 8. The second level test sections were divided into five groups. The first group had no heavy subbase pumping and the other four groups had increasing amounts (or intensities) of heavy subbase pumping. In Table 8 the amount of heavy subbase pumping is the accumulated percentage of section length with heavy subbase pumping. The percent of section length with heavy subbase pumping was measured after each period of rainfall. The accumulated percentage is the sum of these values. For example, if on a given section these percentages were 10, 14 and 21 after three periods of rainfall, the accumulated percentage would be 45 (these values are illustrative only, not taken from Road Test data). If, on another section, these percentages were 80, 45 and 60 after three periods of rainfall, the accumulated percentage would be 190. Table 8 shows that as stress decreased the test sections were able to withstand increasing amounts of heavy subbase pumping without significant loss in serviceability. Mean values to the left of and below the heavy line in Table 8 are:

Loop	No. of Sections	Mean Serviceability Index
3	None	---
4	4	4.1
5	8	4.2
6	12	4.2

Table 8 also shows that sections with a serviceability index of 1.5 before the end of test had suffered the effects of severe subbase pumping. On 19 of 20 sections in this category, the accumulated percentage of heavy subbase pumping was 60 or more. Eighty percent of the 20 sections with a 1.5 index before the end of test had accumulated percentages of 90 or more.

Eight-inch concrete pavements are widely used on routes carrying heavy traffic. This led to preparation of detail performance history graphs for the 8-in., second thickness test sections in loop 5. These graphs are shown in Figure 12. The test sections are grouped together to illustrate the effects of heavy subbase pumping. Curves for the Road Test performance equations are also shown. Conclusions from Figure 12 are:

1. Where the accumulated percentage of heavy subbase pumping was 60 or less, the 8-in. second level pavements performed about as well as the third and fourth thickness levels.

TABLE 8

TERMINAL SERVICEABILITY AS RELATED TO HEAVY SUBBASE PUMPING AND COMPUTED STRESSES

CONCRETE TEST SECTIONS — 2nd THICKNESS

Loop & Slab	Axle Loads Kips	Stress psi	AMOUNT OF HEAVY SUBBASE PUMPING**																	
			NONE				0–30				30–60				60–90				90 +			
			Plain		Reinf.		Plain		Reinf.		Plain		Reinf.		Plain		Reinf.		Plain		Reinf.	
			S*	T*	S	T	S	T	S	T	S	T	S	T	S	T	S	T	S	T	S	T
Loop 3 5"	12 S* 24 T*	473					3.7 3.1	2.8	3.3		3.7 3.5		4.0			1.5	2.8	1.5		1.5 1.5	1.5	1.5 1.5 1.5
Loop 4 6½"	18 S 32 T	424	4.4 3.8	***			4.3		3.8			1.5	3.6			3.4 1.5	3.4	2.6	3.0	1.5	1.8	1.5 1.5 1.5
Loop 5 8"	22.4S 40 T	370	4.2	4.2			4.2	4.2	4.3 4.0	4.3			4.6		4.1	3.7			1.5	1.5	1.5	3.2 1.5 1.5
Loop 6 9½"	30 S 48 T	346	4.3	4.3	4.5		4.3 4.2 3.6	4.3	4.0	4.4 4.1 4.0						4.3				3.1	2.2 1.6	1.5

*S = Single, T = Tandem

** Amounts shown are accumulated percentages of section length with heavy pumping, measured after each period of rainfall.

*** Terminal Serviceability Indexes

LOOP 5 – 22.4 KIP SINGLE AXLE LOADS

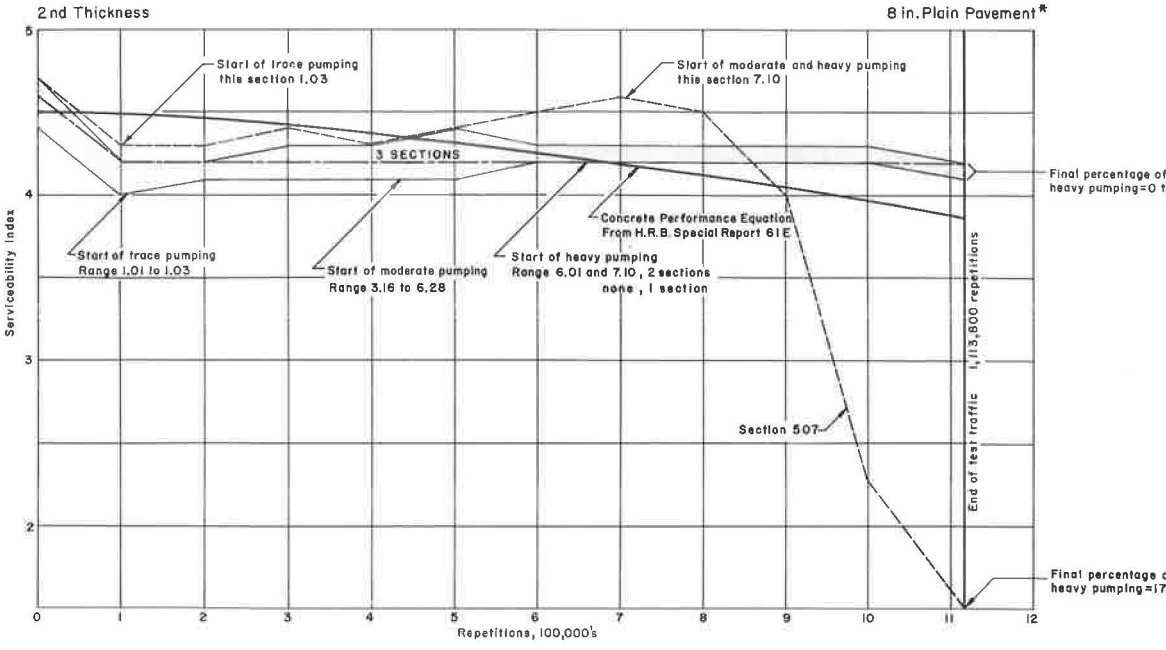

*With doweled transverse joints at 15 ft.

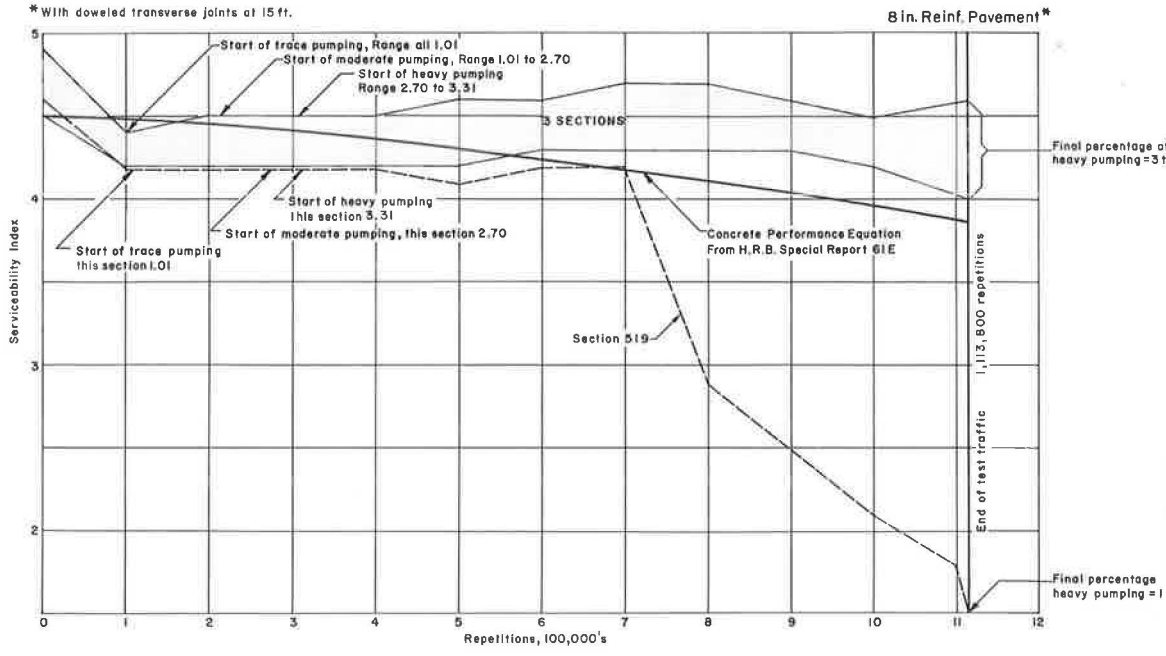

*With doweled transverse joints at 40 ft.

LOOP 5 – 40 KIP TANDEM AXLE LOADS

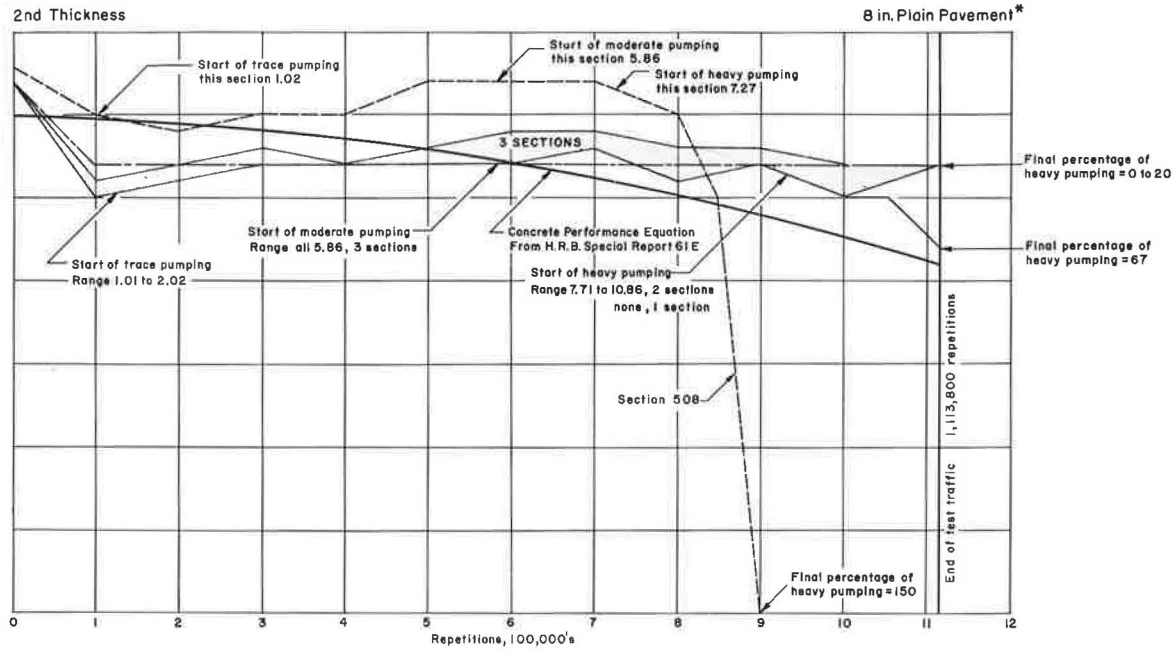

*With doweled transverse joints at 15 ft.

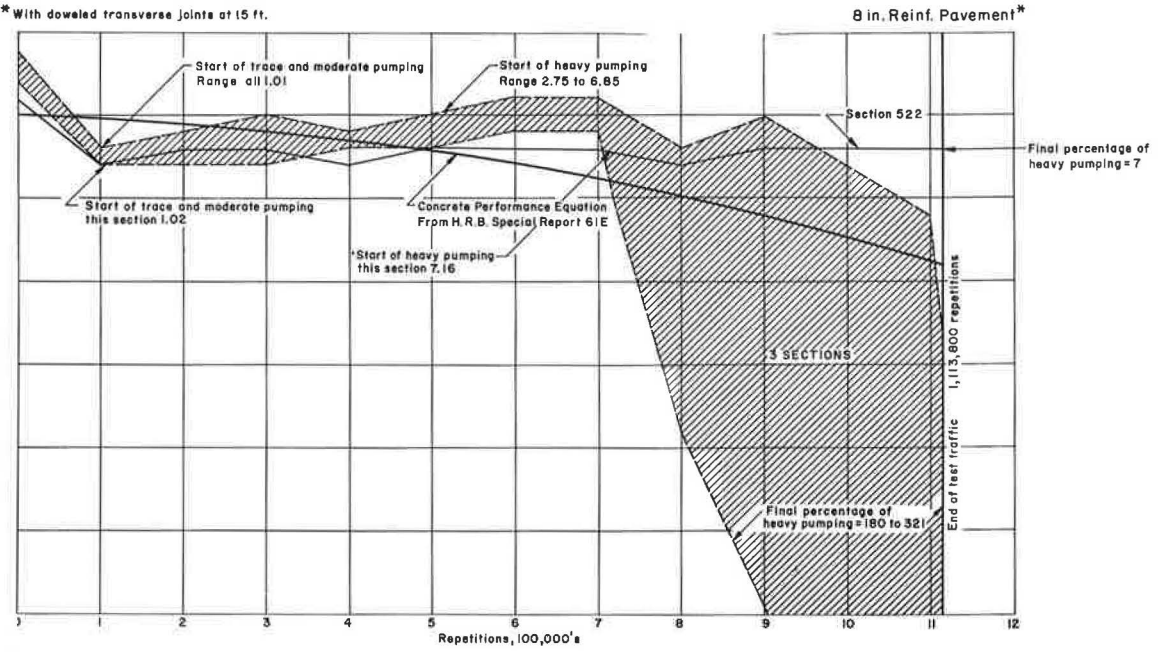

With doweled transverse joints at 40 ft.

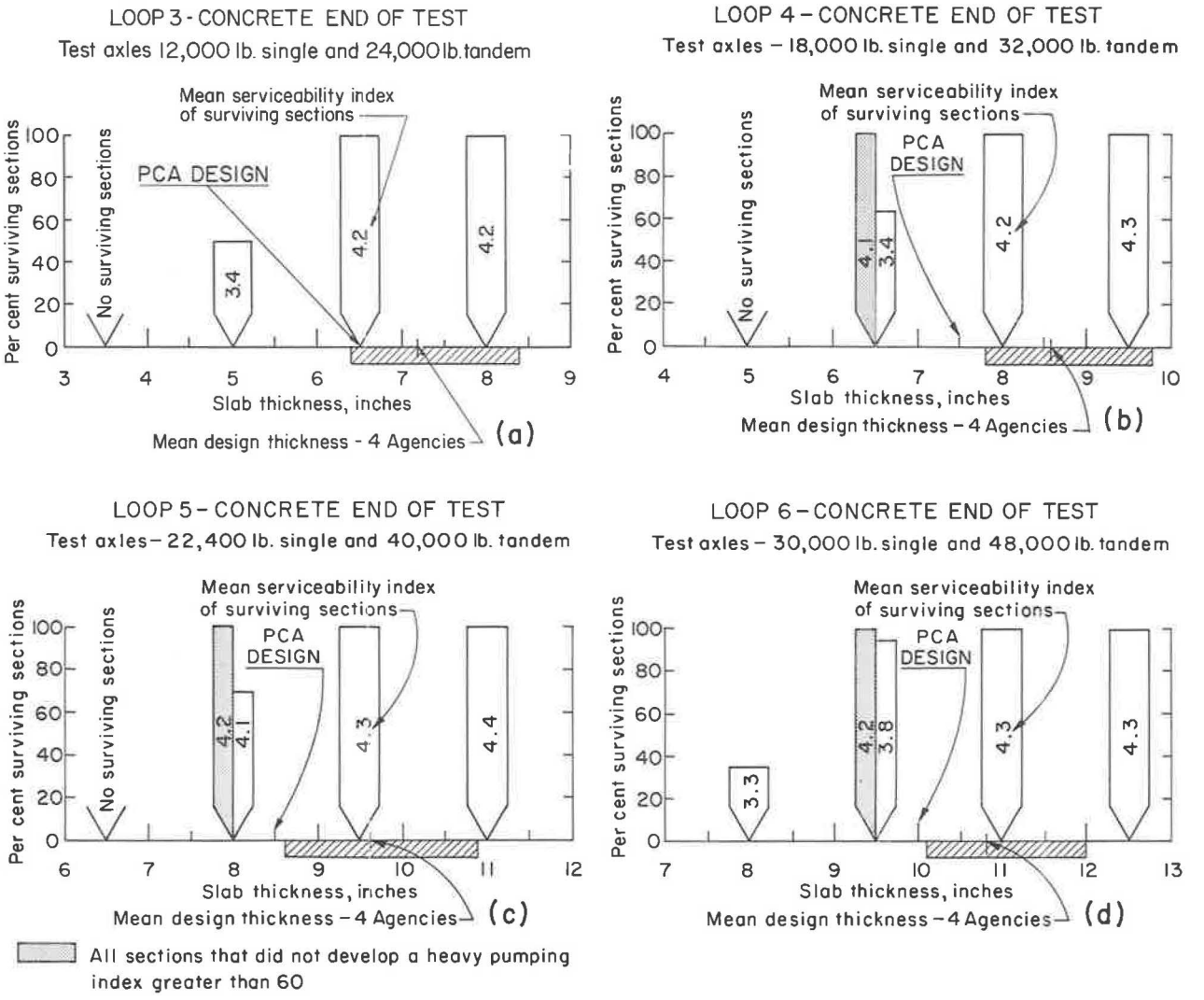
LOOP 3 - CONCRETE END OF TEST
Test axles 12,000 lb. single and 24,000 lb. tandem
Mean serviceability index of surviving sections
PCA DESIGN
No surviving sections
3.4
4.2
4.2
Per cent surviving sections
Slab thickness, inches
Mean design thickness - 4 Agencies
(a)
LOOP 4 - CONCRETE END OF TEST
Test axles - 18,000 lb. single and 32,000 lb. tandem
Mean serviceability index of surviving sections
PCA DESIGN
No surviving sections
4.1
3.4
4.2
4.3
Per cent surviving sections
Slab thickness, inches
Mean design thickness - 4 Agencies
(b)
LOOP 5 - CONCRETE END OF TEST
Test axles - 22,400 lb. single and 40,000 lb. tandem
Mean serviceability index of surviving sections
PCA DESIGN
No surviving sections
4.2
4.1
4.3
4.4
Per cent surviving sections
Slab thickness, inches
Mean design thickness - 4 Agencies
(c)
LOOP 6 - CONCRETE END OF TEST
Test axles - 30,000 lb. single and 48,000 lb. tandem
Mean serviceability index of surviving sections
PCA DESIGN
3.3
4.2
3.8
4.3
4.3
Per cent surviving sections
Slab thickness, inches
Mean design thickness - 4 Agencies
(d)
All sections that did not develop a heavy pumping index greater than 60

Figure 13.

2. Where the accumulated percentage of heavy subbase pumping was 60 or less, performance of the 8-in. test sections could be described by the following statement: At 100,000 repetitions of either single- or tandem-axle loads the serviceability index was 0.4 less than the as constructed values, and there were no further losses in serviceability during the test period.

3. Where the accumulated percentage of heavy subbase pumping was 90 or more, performance was as previously stated until heavy subbase pumping approached severe intensity. Severe heavy subbase pumping was accompanied by a rapid serviceability loss with indexes usually reaching a value of 1.5 before the end of test.

4. The performance shown in Figure 12 is at variance with the Road Test performance equations in the following respects:

(A) They do not describe concrete performance prior to the start of heavy subbase pumping.

(B) They give incorrect values for end of test serviceability where the accumulated percentage of heavy pumping was 60 or less (not severe).

(C) They fail to show that performance was equal under single and tandem axles where the accumulated percentage of heavy subbase pumping was 60 or less (not severe).

(D) They give incorrect values for end of test serviceability where the accumulated percentage of heavy subbase pumping was 90 or more (severe).

In the previous study (1) the relationships of design depths to end of test serviceability are shown in chart form for the four truck loops. These charts (Figs. 18, 19, 20 and 21 in Ref. 1) have been reproduced and revised to show end of test serviceability for second level test sections that were not affected by heavy subbase pumping (sections to the left of and below the heavy line in Table 8 of this report). These revisions are shown in Figure 13.

Figure 13a shows the relationships of design depths to the four thickness levels in loop 3. The PCA design depth and both the mean and range of design depths submitted by four agencies during the planning stage of the Road Test are shown on the slab thickness scale. In loop 3 all second level test sections were affected by heavy subbase pumping. As a result, no revision is shown.

Figure 13b shows the relationships of performance to design depth in loop 4. The right half of the second level bar graph ($6\frac{1}{2}$ in.) shows the performance of all second level test sections in loop 4. The left half shows performance of second level sections not influenced by heavy subbase pumping (accumulated percentage: 30 or less). These sections have a mean serviceability index of 4.1 and show that both the PCA and four agency designs have a wide margin of safety.

Figure 13c shows revised relationships of performance to design depth in loop 5. Here the eight test sections that were not affected by heavy subbase pumping (accumulated percentage of not more than 60) have a mean serviceability index of 4.2—only slightly below values for the third and fourth levels. This performance again shows that both PCA and the four agency designs are conservative and reliable.

Figure 13d shows performance design relationships for loop 6. In this loop the twelve sections not affected by heavy subbase pumping (accumulated percentage of less than 90) had a mean serviceability index of 4.2, almost equal to the third and fourth thickness values. Again this performance shows that both the PCA and four agency designs are adequate and reliable.

The final conclusion is that the PCA design procedure is somewhat more dependable than was indicated by the previous study (1).

REFERENCES

1. Teske, W. E., and Fordyce, P., "A Discussion of Established Design Concepts as Related to Road Test Performance." HRB Sp. Rpt. 73, pp. 259-267 (1962).
2. "Concrete Pavement Design." 2nd Ed., Portland Cement Association, Chicago, Ill.

3. "The AASHO Road Test Report 5—Pavement Research." HRB Sp. Rpt. 61E (1962).
4. Spencer, W. T., Allen, H., and Smith, P. C., "Report on Pavement Research Project in Indiana." HRB Bull. 116, 1-56 (1956).
5. Colley, B. E., and Nowlen, W. J., "Performance of Concrete Pavements Under Repetitive Loading." Bull. D23, Res. and Dev. Lab., Portland Cement Association, Chicago, Ill.
6. "Subgrades, Subbases and Shoulders for Concrete Pavements." Portland Cement Association, Chicago, Ill.
7. Teller, L. W., and Sutherland, E. C., "The Structural Design of Concrete Pavements." Public Roads, 16:8, 9 and 10; 17:7 and 8; 23:8.
8. ACI Subcommittee II, ACI Committee 325, "Considerations in the Selection of Slab Dimensions." Jour. ACI, 28:5.

Nickel-Coated Dowel Pins Exposed in Tidal Zone Harbor Island, North Carolina

CHARLES B. SANBORN, Supervisor, Coated Products Development, International Nickel Co.

•THE International Nickel Co. has been engaged in developing nickel coatings for the surfaces of various steel mill products to provide corrosion resistant protection of carbon steel. Prior to the early stages of this development, the problems associated with the corrosion of dowels in highway load-transfer devices had been brought to the company's attention. The studies of Van Breemen (1) were reviewed and, in addition, the various methods employed and proposed to provide corrosion resistant dowels were investigated. Development effort was then directed toward determining the utility of a hot-rolled, nickel-coated dowel bar; and for this purpose approximately 5 tons of nickel-coated bar stock were produced experimentally. The product was fabricated into load-transfer devices and placed in six highway test projects (Table 1).

In addition to the highway performance tests which have been in progress up to 5 years, an accelerated corrosion test was conducted in tidal sea water at the company's corrosion test station at Harbor Island, N. C. Similar accelerated exposure tests were conducted in tidal waters at Old Saybrook, Connecticut and reported by Mitchell (2). Accelerated corrosion tests under controlled laboratory conditions were set up at Purdue University (3). This study investigated various types of nickel coatings and stainless steel sheathing on carbon steel bars and showed their influence on reducing the restraining action of dowels cast in concrete.

Also, marine and industrial atmospheric exposure tests of a qualitative nature have been made and are continuing at Kure Beach, N. C., and Bayonne, N. J., respectively.

This report is concerned primarily with the pull-out tests of plain uncoated, hot-rolled carbon steel dowels and hot-rolled nickel-coated steel dowels after exposure in the tidal zone at Harbor Island, N. C.

TABLE 1

HIGHWAY TEST PROJECTS

State	Nickel-Coated Dowels		Location of Installation
	No.	Size (in.)	
Conn.	288	1 diam. × 18	US 9, Middleton
Kan.	240	1¼ diam. × 18	US 36, between Seneca and Maysville
Mich.[a]	240	1¼ diam. × 18	US 16, Proj. 34044, Portland
N. J.	240	1¼ diam. × 18	US 202, north of Flemington
N. Y.	240	1¼ diam. × 18	Interstate 502, Colonie
D. C.	240	1¼ diam. × 18	Eastern Ave.

[a] Also, 132 each steel dowels sheathed with types 430, 304 and 316 stainless steel and Monel; same size.

Paper sponsored by Committee on Rigid Pavement Design.

EXPERIMENTAL MATERIAL

In producing the nickel-coated bars, a typical industrial type, heavy nickel coating was electrodeposited by standard methods on commercial grade carbon steel billets. The nickel-plated billets were then heated to rolling mill temperatures, approximately 2,100 F, and hot-rolled to the final round bar size.

Figure 1 shows a typical 3- by 3-in. plated carbon steel billet cross-section with corresponding nickel-coated bar section and longitudinal piece of $1\frac{1}{4}$-in. diameter nickel-coated bar stock after hot rolling.

The nominal nickel thickness on the finished hot-rolled bars used in the highway performance tests and the tidal zone exposure ranged from 0.007 in. to 0.010 in. Figure 2 shows cross-sections of three typical bars which have been polished and acid etched. The steel was blackened to reveal the nickel coating.

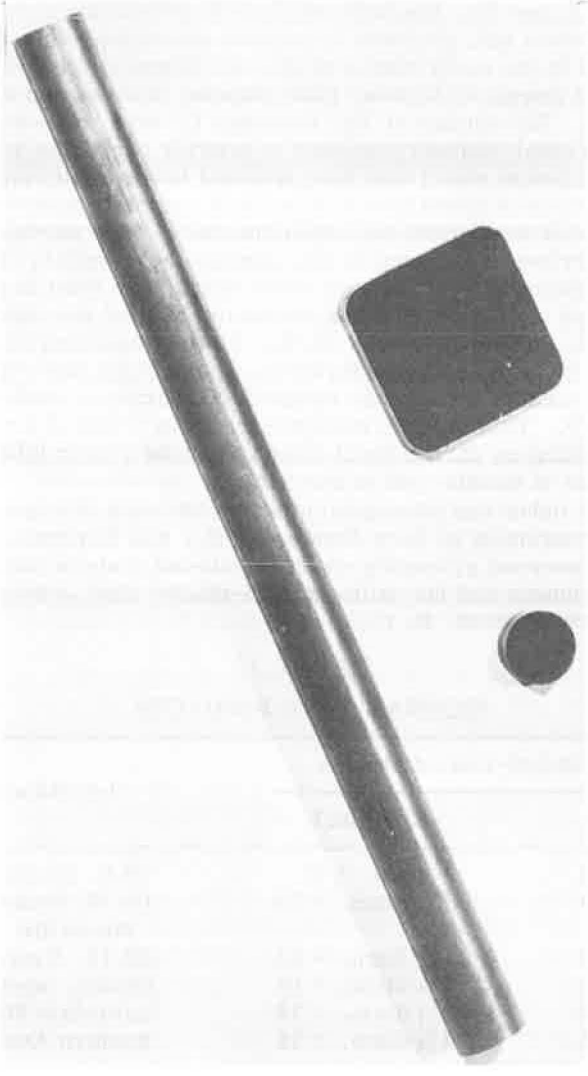

Figure 1. Nickel-plated steel billet section (3 x 3 in.) and $1\frac{1}{4}$-in. hot-rolled nickel-coated bar.

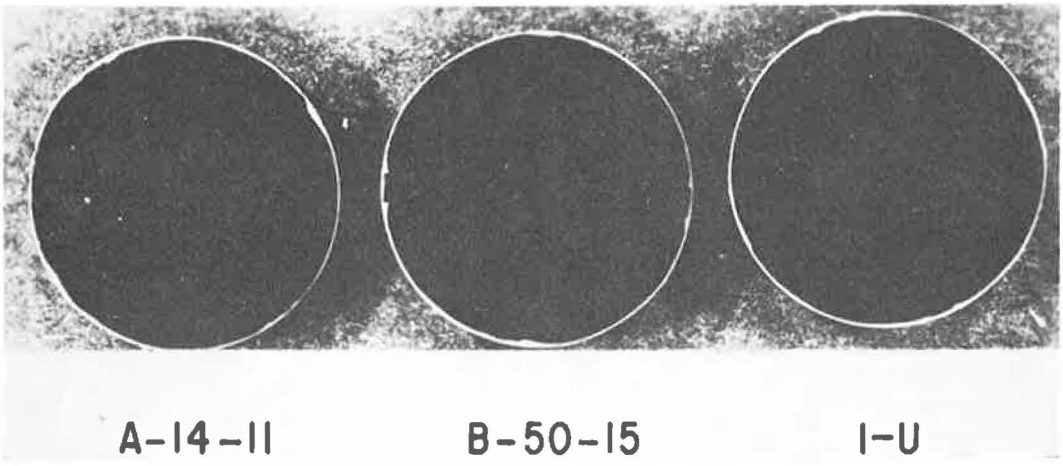

Figure 2. Nickel-coated dowel pins (1.25-in. diameter).

In the process of heating and rolling the plated billet, the typical cast-like columnar structure of the electrodeposited nickel is converted to a wrought type nickel structure (Fig. 3). Also, during heating, diffusion occurs at the nickel-iron interface which improves the original metallurgical bond of the nickel to the basis metal. Thus, by the method of manufacture the nickel becomes an integral part of the bar without changing the mechanical properties of the steel. This type of dowel, along with the more familiar plain, hot-rolled carbon steel dowels, was employed in the exposure and pull-out tests.

TIDAL ZONE EXPOSURE SPECIMENS

On June 23, 1959, sixteen dowel pins were exposed on the Harbor Island bulkhead in the upper part of the tidal zone (Fig. 4). They were immersed 2 to 3 hours a day in sea water. Six inches of each end of a dowel pin had been cast in a concrete cylindrical form, $7\frac{1}{2}$ in. long by 6 in. in diameter. From 5 to 6 in. of the middle portion of the dowel was not covered by concrete, thus providing a dumbbell like configuration. The concrete consisted of about $2\frac{3}{8}$-in. cover of a Class "A" air mixture of the following composition: 94 lb cement, 156 lb sand, 363 lb gravel, 5 gal water, and $\frac{3}{4}$ oz Darex admixture.

Before casting, six inches of one end of each dowel was thinly coated with Esso Nebula EP-1 multi-use industrial grease, to prevent bonding of one end of the dowels to the concrete in a way similar to the practice employed in highway, doweled joint construction to provide a sliding member. This portion of the dowel will be referred to as the "greased end." The other end of the dowel cast in concrete was not greased so that the concrete would adhere to this portion of the dowel to simulate the fixed end of a doweled pavement joint. This end of the dowel will be referred to as the "fixed end."

Four of the specimens contained plain hot-rolled carbon steel dowels and 12 contained hot-rolled nickel-coated steel dowels. All specimens were subjected to frequently agitated and generally highly aerated sea water during the immersion periods. The agitation and aeration were caused by high velocity pumps operating nearby and discharging large volumes of sea water at several feet above the surface. This also subjected the specimens to considerable splashing before and after each tidal immersion cycle.

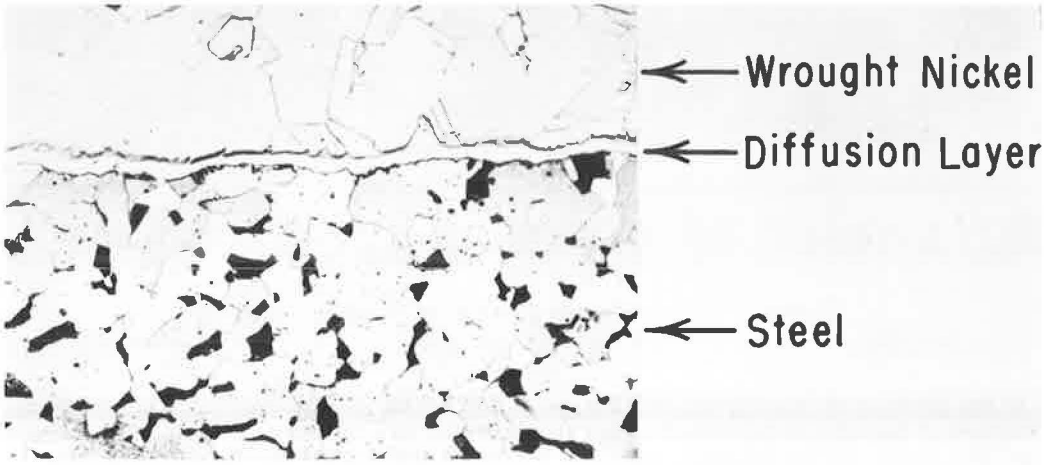

HOT ROLLED NICKEL
ON STEEL

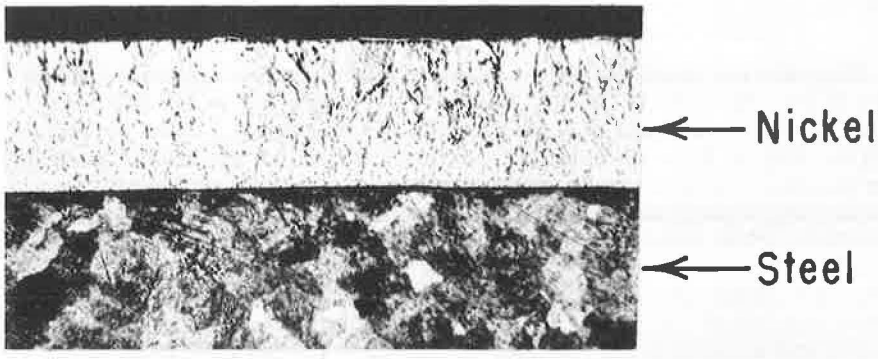

NICKEL ELECTRODEPOSITED
FROM WATTS TYPE BATH

Figure 3.

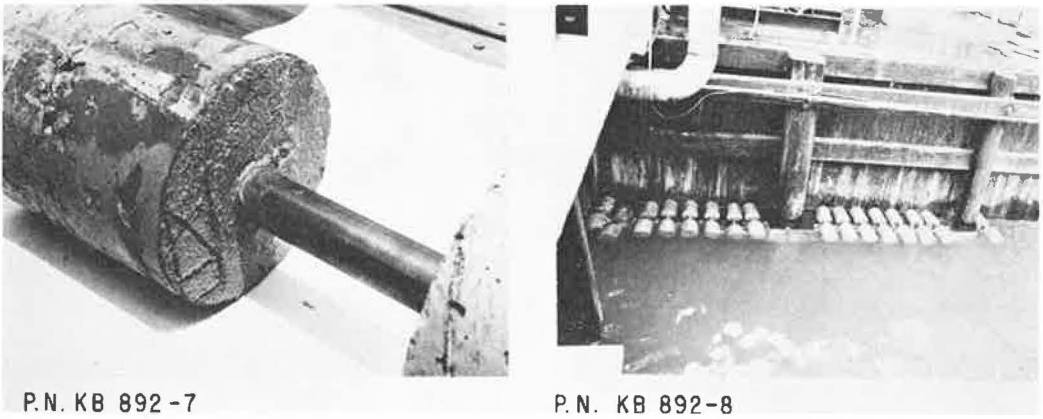

Figure 4. Dowel pin specimens at time of tidal zone exposure: (left) pin cast into concrete, specimen XII; (right) specimens in exposure location—tide four-fifths high.

PULL-OUT TESTS

After $1\frac{3}{4}$ years continuous exposure to tidal action, 10 specimens containing nickel-coated hot-rolled dowels and 3 specimens containing plain, hot-rolled carbon steel dowels were removed from exposure and prepared for the pull-out tests. This was done by cutting the dowel pin midway between the cement blocks and drilling and tapping the cut end to accommodate a pull rod (Fig. 5). Irregularities of the cement blocks were rectified through the use of capping material. The possibility of misalignment in the actual test was minimized by using a universal alignment head. As the dowels were pulled, only the initial ultimate loads that caused movement were recorded as these were considered the loads necessary to free the dowel bar from the concrete. The area of the dowel pin actually in the concrete was then used to calculate the apparent shear stress.

$$S = \frac{L}{A}$$

in which

S = apparent shear stress;
L = ultimate load measured; and
A = measured area of the dowel in concrete.

TEST RESULTS

The pull-out test data (Table 2) have been plotted in Figure 6. From the average apparent shear stress data, the plain carbon steel dowels required 7.5 times the force to initiate movement as compared to the nickel-coated steel dowels. Also, there is very little difference between the shear stress of the plain carbon steel dowels that had been greased and the same dowels without grease.

Following the pull-out tests all dowels were removed from the concrete specimens and the hole in the concrete was inspected and evaluated for residual corrosion products, smoothness of surface, and pitting (Table 2). Figure 7 compares the conditions of the plain dowel pins with the nickel-coated dowel pins at the greased and fixed ends. The nickel-coated dowels retained their original finish although those that were initially greased were slightly tarnished. It is believed that the grease was eventually washed away thus permitting the corrosive medium to come in contact with the metal surfaces within the concrete.

The plain hot-rolled carbon steel dowels were cleaned to remove all corrosion products without disturbing sound steel. The segment of these dowels between the concrete blocks where the pins were exposed to sea water was measured and found to

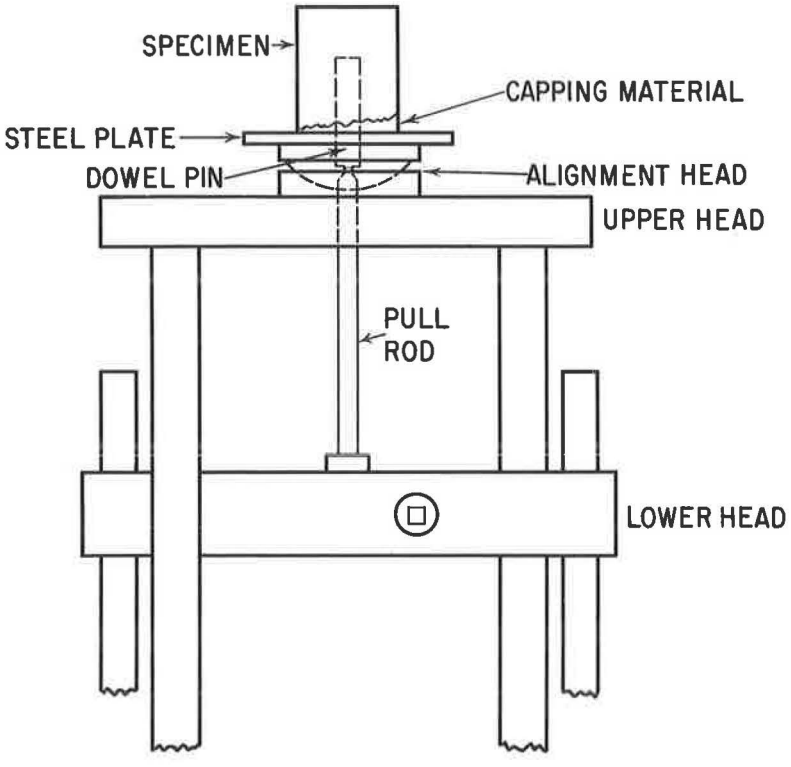

Figure 5. Pull-out test apparatus.

TABLE 2

PULL-OUT TEST DATA

Specimen No.	Nickel Coated	Bond Breaker Greased	Ultimate Load (lb)	Apparent Shear Stress (psi)	Condition of Hole in Concrete Block[a]
I	Yes	No	9,600	348.2	S-C, no CP
I	Yes	Yes	2,900	124.6	S-C, no CP
II	Yes	No	9,500	356.6	S-C, no CP
II	Yes	Yes	2,300	97.5	R-C, no CP
III	Yes	No	9,100	345.7	S-C, no CP
III	Yes	Yes	2,850	122.5	R-C, no CP
IV	Yes	No	4,500	184.8	S-C, no CP
IV	Yes	Yes	2,900	120.7	S-C, no CP
V	Yes	No	5,500	211.6	S-C, no CP
V	Yes	Yes	3,150	137.0	S-C, no CP
VI	Yes	No	14,000	558.3	S-C, no CP
VI	Yes	Yes	3,250	144.7	S-C, no CP
VII	Yes	No	8,100	342.6	S-C, no CP
VII	Yes	Yes	2,500	169.8	S-C, no CP
VIII	Yes	No	5,600	207.2	S-C, no CP
VIII	Yes	Yes	2,300	83.3	S-C, no CP
XI	Yes	No	9,550	386.7	R-C, no CP
XI	Yes	Yes	2,400	102.4	S-C, no CP
XII	Yes	No	7,300	290.1	S-C, no CP
XII	Yes	Yes	2,350	99.7	S-C, no CP
XIII	No	No	24,300	924.3	S, some CP
XIII	No	Yes	18,800	784.3	R-P, some CP
XIV	No	No	27,050	1,064.9	R, some CP
XIV	No	Yes	23,900	995.1	S, some CP
XVI	No	No	23,500	852.2	R, some CP
XVI	No	Yes	24,600	1,026.6	R-P, some CP

[a] S = smooth, R = rough, C = clean, P = pitted, and CP = corrosion products.

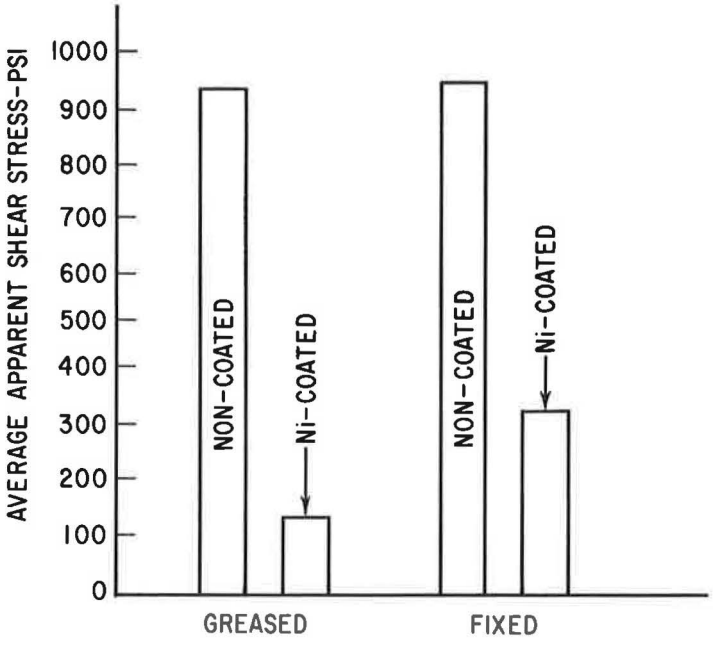

Figure 6. Average apparent shear stress for nickel-coated and plain carbon steel.

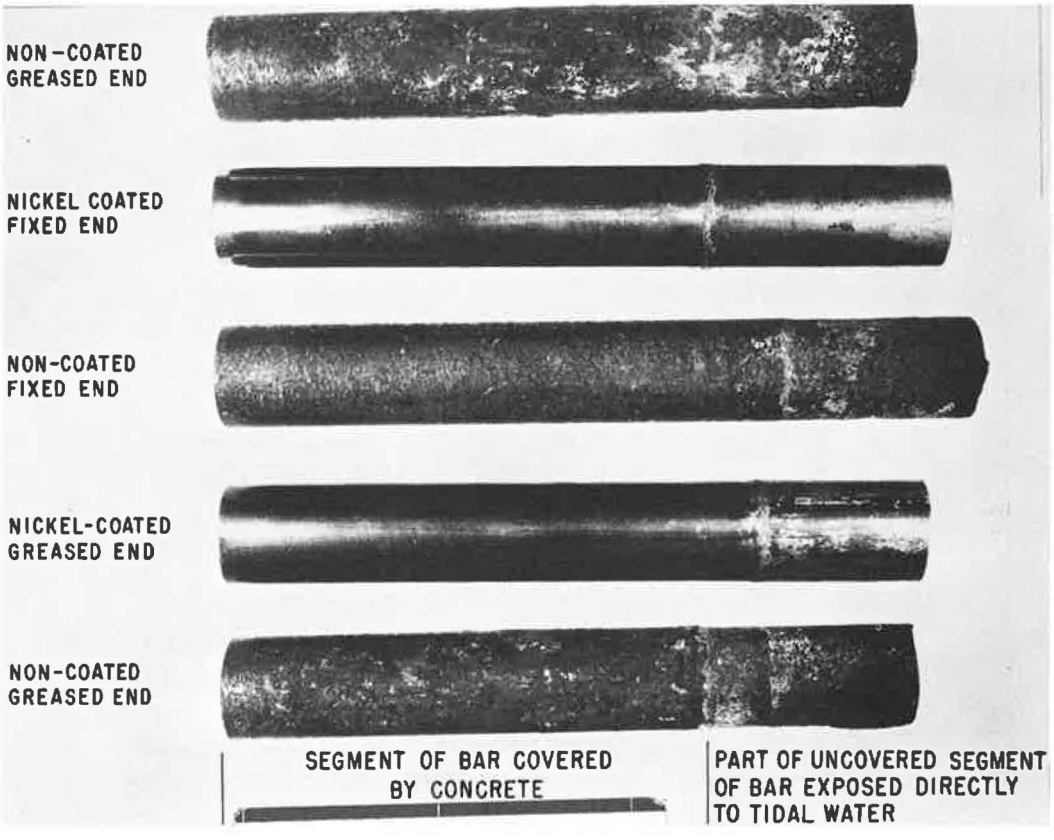

Figure 7. Dowel bars after 21 months' tidal zone exposure.

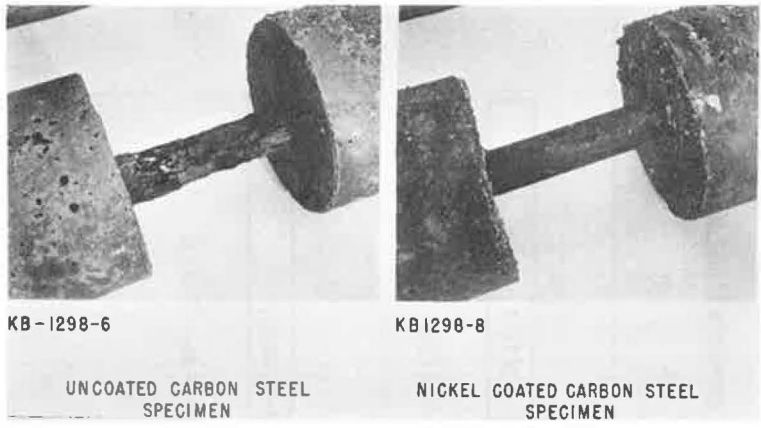

Figure 8. Dowel pin specimens after 3 years and 4 months of exposure in tidal zone.

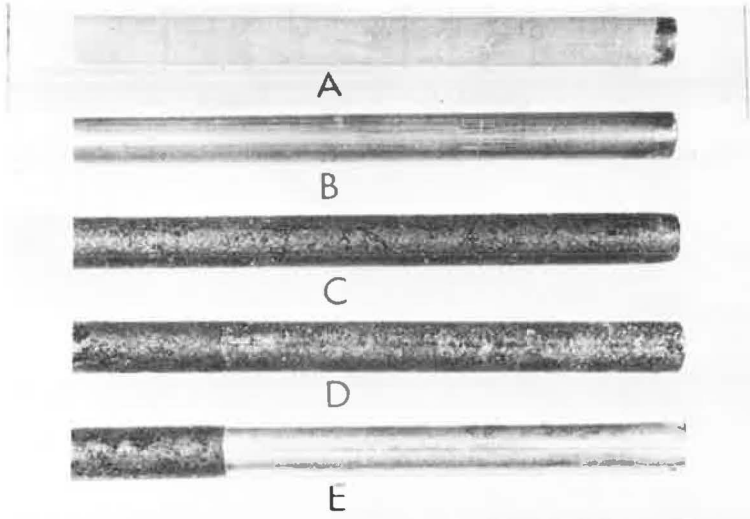

A. NICKEL COATED DOWEL 3-1/4 YEARS EXPOSURE. WETTED ONCE A WEEK WITH 5% SALT SOLUTION.

B. NICKEL COATED DOWEL 1-1/2 YEARS EXPOSURE. WETTED TWICE WEEKLY WITH 5% SALT SOLUTION.

C. UNCOATED CARBON STEEL DOWEL. SAME EXPOSURE CONDITION AS B.

D. TYPE 410 STAINLESS STEEL SEAM WELDED SHEATH ON CARBON STEEL DOWEL - SAME EXPOSURE AS B&C.

E. TYPE 302 STAINLESS STEEL SEAM WELDED ON CARBON STEEL DOWEL - SAME EXPOSURE AS B, C & D.

Figure 9. Atmospheric exposure of dowels at Bayonne, N. J.

have been reduced in cross-sectional area by approximately 6.5 percent. The nickel-coated dowels had no measurable reduction in cross-sectional area.

Of the original 16 specimens, two containing nickel-coated dowels and one containing plain carbon steel dowels have remained on the tidal zone rack. The comparative condition of these dowels after 3 years and 4 months of exposure is shown in Figure 8.

It is evident that during the tidal zone exposure the corrosive media had reached the surface of the greased or free end of the dowels. Judging from appearance, corrosive media had also reached the fixed end but to a somewhat less degree. The plain, hot-rolled carbon steel dowels were restrained from movement at the greased end of the concrete specimen to nearly the same extent that the fixed end was restrained. Thus, the possible utility of nickel-coated dowels for highway use in concrete road joints is indicated by the low degree of restraint offered when compared with the plain carbon steel dowels.

Two types of stainless steel-sheathed dowels, nickel-coated dowels and a plain carbon steel dowel from the atmospheric exposure test are shown in Figure 9.

CONCLUSIONS

1. Sufficient time has not elapsed to provide conclusive results from the several state highway department performance tests. All types of corrosion-resistant dowels appear to be functioning properly as nearly as can be determined from seasonal measurements of joint opening and closing.

2. The tidal zone exposure and accompanying pull-out data confirm Mitchell's (2) conclusion that a nickel-coated dowel is promising.

REFERENCES

1. Van Breemen, William, "Experimental Dowel Installations in New Jersey." HRB Proc. 34: 8-33 (1955).
2. Mitchell, R. G., "The Problem of Load Transfer Dowels." HRB Bull. 274, 57-69 (1960).
3. Wood, L. E., and Lavoie, R. P., "Corrosion Resistance Study of Nickel-Coated Dowel Bars." HRB Research Record 32, 25-34 (1963).

Study of Stresses in Prestressed Concrete Pavements at Maison-Blanche Airport

J. G. CLAUDON, Engineer of Bridges and Highways, French Ministry of Public Works, Paris, France*

Both runways of the Algiers airport are of prestressed concrete. The first one was built in 1953-4, and the second in 1960-1. The pavements are posttensioned by cables in the transverse direction and poststressed in the longitudinal direction by means of elastic abutments.

These pavements were continuously surveyed and tested during and since their construction. After seven years of service certain conclusions can be drawn.

The paper briefly describes the design and construction of the runways and explains the reasoning followed in selecting this particular design. An appraisal is provided of the results of the observations concerning the displacements of the extremities of the pavements and the variations of stresses in the concrete.

The principal results of the field experiments concern (a) the friction of the pavement on the friction reducing layer, (b) the variations of temperature in the slab, and (c) the variations of hygrometry. The variation of the stresses in a pavement more than two years old is studied by correlation with friction, variations of temperature and hygrometry, and also by studying the eventual variations of Young's modulus, and the eventual variations of the thermal coefficient with temperature, stresses, and hygrometry.

For a pavement of this age (one in which the most important part of the creep has occurred) the study makes evident the very important effect of the hygrometry on the thermal coefficient.

The variation of stresses for the same variation of temperature can be in the ratio of 3.5 to 2.35 for certain conditions of hygrometry. These great variations are at least partially due, in this particular case, to the fact that limestone aggregates were used.

•BOTH RUNWAYS and one taxiway of the Maison-Blanche Airport in Algiers are of prestressed concrete. The first runway and the taxiway were built in 1953-4 and the second runway in 1960-1, by the "Service de l'Infrastructure Aeronautique de l'Algerie," under the direction of M. Pousse, Director of this service. These airfield pavements were not built specifically for experimentation; however, they provided an excellent opportunity to experiment in the laboratory and in the field and to observe pavement performance during and since construction.

Paper sponsored by Committee on Rigid Pavement Design.
*Formerly Chief, First District, Algerian Airports.

Since the first runway and the taxiway were put into operation more than seven years ago they have been continuously observed and a great amount of data is now available. The pavements are presently in excellent condition, with no indication of spalling or cracking, even though the volume of traffic at Maison-Blanche is only slightly less than at Paris-Orly. Therefore, the method of prestressing used can be considered as practical and successful, and the interpretation of the results is in good agreement with the behavior of the pavements.

Notations

The following notations are used in this paper:

- T = temperature, in °C;
- t = time;
- n = stress;
- e = strain;
- E = Young's modulus; and
- μ = Poisson's ratio.

All other notations are specified in the text. The subscript "a" is used for steel; concrete is denoted by the subscript "b" or no subscript at all.

GENERAL CHARACTERISTICS

Subgrade

The existing soil is a homogeneous silty clay with a reaction modulus of 165 psi per in. (4.5 kg per sq cm per cm) (1) and Atterberg limits as follows: Liquid limit, 50 to 55; Plastic limit, 18 to 23; Plasticity index, 32 to 37; Shrinkage limit 10. When compacted to standard density this soil, upon soaking, will swell more than 5 percent and develop swell pressures as high as 18 psi (1.3 kg per sq cm).

Subbase

The concrete slab was placed on a 12-in. (30-cm) thick subbase made up of three layers each 4 in. (10 cm) thick (Fig. 1). The bottom layer consists of river gravel (0 to 2 in.) and is used to prevent intrusion of the subgrade soil into the subbase. The middle layer consists of washed river gravel (0 to 2 in.) and is used for drainage. The top layer consists of an asphalt-impregnated waterbound macadam made of crushed chalk stone. The macadam was impregnated with cutback asphalt, sealed with an asphalt emulsion, and sanded. The resulting surface was very stable.

This type of subbase design has several advantages. In this particular case, the reaction modulus on the total thickness was increased to about 252 psi per in. (7 kg per sq cm per cm). The bottom layer assures at least 8 in. (20 cm) of well-drained uncontaminated material beneath the concrete slab. The 12-in. (30-cm) thickness of subbase also acts as a surcharge to restrict eventual swelling of the subgrade. This is particularly important where non-uniform moisture contents exist, such as at the edges and middle of the wide runway pavement. The most important use of the subbase was to provide a stable working surface for construction equipment and traffic.

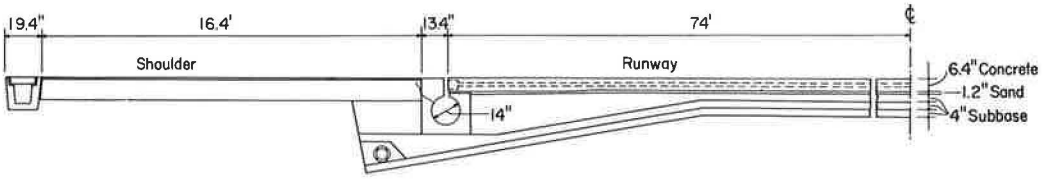

Figure 1. Typical half-section of second runway.

Friction-Reducing Layer

A layer of sea sand 1 in. (2.5 cm) thick was placed on the subbase and covered with impervious paper to (a) permit accurate grade adjustment, thus assuring that the proper thickness of concrete slab would be obtained, and (b) reduce friction under the slab and thereby permit greater intervals between jacking joints. For the first pavement the jacking interval was 329 ft (100 m) and for the second, 645 ft (197 m).

Concrete Slab

The first runway is 8,000 ft (2,430 m) long and 197 ft (60 m) wide; the second is 7,700 ft (2,350 m) long and 148 ft (45 m) wide.

Thickness and Prestress Rates.—The first pavement slabs are 7.2 in. (18 cm) thick with a minimum prestress equal to 255 psi (18 kg per sq cm) in both orthogonal directions (2, 3).

In determining the thickness of the second runway, recourse was made to data obtained from loading tests made in 1957 and 1958 at Paris-Orly Airport, on 10-ft (3.05-m) by 20-ft (6.1-m) prestressed slabs with thicknesses of 3.2 in. (8 cm), 4 in. (10 cm), and 4.80 in. (12 cm). The slabs were prestressed to 140 psi (10 kg per sq cm) longitudinally and 7 to 140 psi (0.5 to 10 kg per sq cm) transversely; the subgrade had a reaction modulus of 55 to 90 psi per in. (1.5 to 2.5 kg per sq cm per cm). These tests indicated that a 4-in. (10-cm) thick slab orthogonally prestressed at a rate of 140 psi (10 kg per sq cm) can support a repeated wheel load of 30 tons with a tire pressure equal to 280 psi (20 kg per sq cm).

Because the reaction modulus at Maison-Blanche was greater than that measured at Paris-Orly, a thickness of 5.6 in. (14 cm) would have provided an ample factor of safety. However, to allow for variations in thickness a 6.4-in. (16-cm) section was selected.

The maximum allowed prestress for the second runway was 1,700 psi (120 kg per sq cm). The specified minimum prestress was about 255 psi (18 kg per sq cm) in the longitudinal direction and 142 psi (10 kg per sq cm) in the transverse direction.

The thickness of conventional plain concrete pavement having a flexural strength of 525 psi (37 kg per sq cm) required to support the same traffic (27-ton single-wheel or 32-ton dual-wheel load) is 12 in. (30 cm).

Concrete Characteristics.—The coarse aggregates used for concrete were composed of hard crystalline limestone having a specific gravity of 2.50, an unconfined compressive strength of 14,000 psi (1,000 kg per sq cm measured on a 5-in. cube), and a Deval's coefficient of 9. A seashore sand was used. The mix design was as follows:

Crushed limestone:	
27 mm to 40 mm	1,210 lb (550 kg)
7 mm to 27 mm	1,650 lb (750 kg)
0 mm to 7 mm	1,100 lb (500 kg)
Sand	440 lb (200 kg)
Portland cement	770 lb (350 kg)
Water	41 to 42.5 gal

The 7-day compressive strength of 5-in. cubes was 3,500 psi (250 kg per sq cm) and the 28-day compressive strength was 4,400 psi (315 kg per sq cm).

Drainage

Three systems of drainage were provided. One system consists of the middle subbase layer with lateral collector pipes. Transverse drains were not used because it was felt that they would serve no purpose under the relatively impervious prestressed slab (high-density concrete and no joints). A second system consists of concrete drains

at the runway edges to collect surface water (Fig. 1). A third system involves paved shoulders along each edge of the runway. The 16.4-ft (5-m) wide and 12-in. (30-cm) thick shoulders (a) prevent excessive dust turbulence by aircraft, (b) permit better visibility of runway lights, (c) occasionally support a wheel of an aircraft, and (d) prevent rapid dessication of the clay below the edges of the pavement, thereby preventing excessive shrinkage or swelling.

PRESTRESSING OF SLABS

The concrete slabs were prestressed in the transverse direction by posttensioning wire tendons, and in the longitudinal direction by means of jacking, with Freyssinet flat jacks, against elastic abutments.

Transverse Prestressing

The specified prestress was obtained by posttensioning 12-wire tendons spaced at 4.36-ft (1.33-m) intervals. In the first runway metal conduits placed in the concrete formed the passageway for placement of the tendons. The tendons were not grouted. In the second runway these passageways were formed by use of cylindrical steel bars, which were removed after the concrete had partially hardened. The tendons in the second runway were grouted to prevent corrosion.

The tendons are located at mid-depth of the slab and were stressed simultaneously from both ends by double-acting jacks. After application of the jacking force, the tendons were anchored in place by means of Freyssinet cones. The tendons were stressed in pairs, leaving an interval of four tendons between successive tensionings. The two extreme tendons on each side of the joints were tensioned last.

In determining the required jacking force, consideration was taken of losses in tension resulting from (a) friction on the tendons in the conduits or passageways (the runways have a hipped-roof profile), (b) friction of the slab on its support during the contraction induced by the jacking force (a constant coefficient of friction was assumed), (c) re-entering of the wires during anchoring of the cones, (d) relaxation of the steel, (e) creep and contraction of the concrete, and (f) the fact that the instantaneous deformation is modified when untensioned tendons are finally tensioned. Computation of the prestress is discussed later.

Longitudinal Prestressing

The longitudinal prestressing of the pavements was obtained by poststressing with flat jacks and elastic abutments. The jacks are 20 ft (6 m) long, 6.7 in. (17 cm) high and operate under high water pressure.

The jacks were used to counterbalance the shrinkage of the concrete immediately after placement and to induce the specified prestress later. The jacking joints were filled with concrete before putting the pavement in operation.

For the first pavements the jacking joints were constructed at 987-ft (300-m) intervals with two intermediate temporary jacking joints; these two joints were used only to counterbalance the shrinkage of the concrete. On the second runway, the intervals were reduced to 645 ft (197 m). On these shorter panels temporary jackings were not required.

On the first runway the jacks were left in the permanent joints after placement of the cement grout. The joints contain three other lines of jacks, so it is possible to induce additional stress, as was done in 1958, to counterbalance the creep of the concrete.

For the second runway the jacks were taken out after inducing the specified stress. However, it is possible to use them again in the same joints, if necessary, to induce higher prestress. This can be done by removing a steel plate and inserting the jacks.

To avoid excessive curling of the slab at the joints a special "comb" system was used on the first pavements (Fig. 2), and dowels and bars were used for the last pavement (Fig. 3).

The elastic end abutments (Fig. 4) consist of curved concrete slabs buried beneath the pavements with one end joining the end of the pavement at ground level, and the

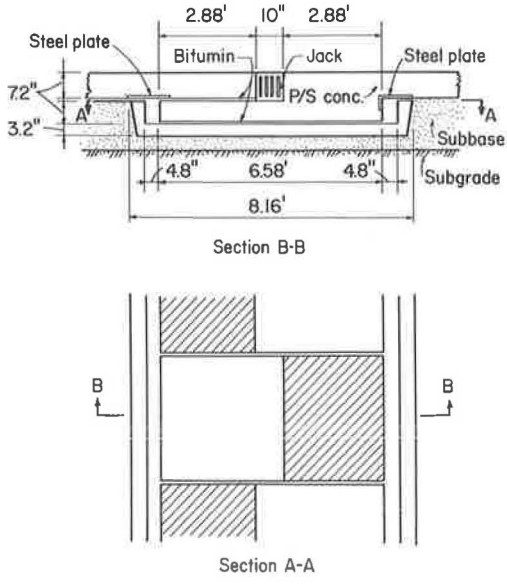

Figure 2. Details of comb joint.

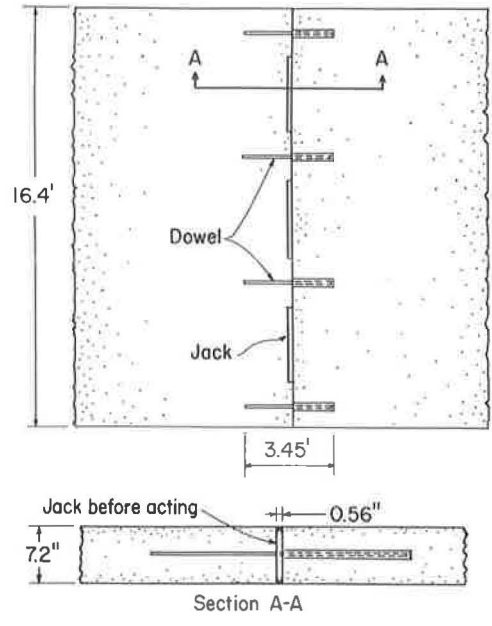

Figure 3. Details of doweled joint.

other end about 10 ft (3 m) in the ground. This buried end is designed to be restrained from any motion.

The wire tendons which give the abutment "elasticity" are anchored at the extremities of the pavement, pass freely through metal conduits at mid-depth of the concrete abutments, and are anchored underneath the end of these abutments. This type of abutment gives assurance that no permanent displacement of the extremities of the pavement can occur because the tension of the tendons is always counterbalanced by the friction of the concrete abutment on the ground and by the weight of the earth above this abutment. By this means, the prestressed condition can always be maintained.

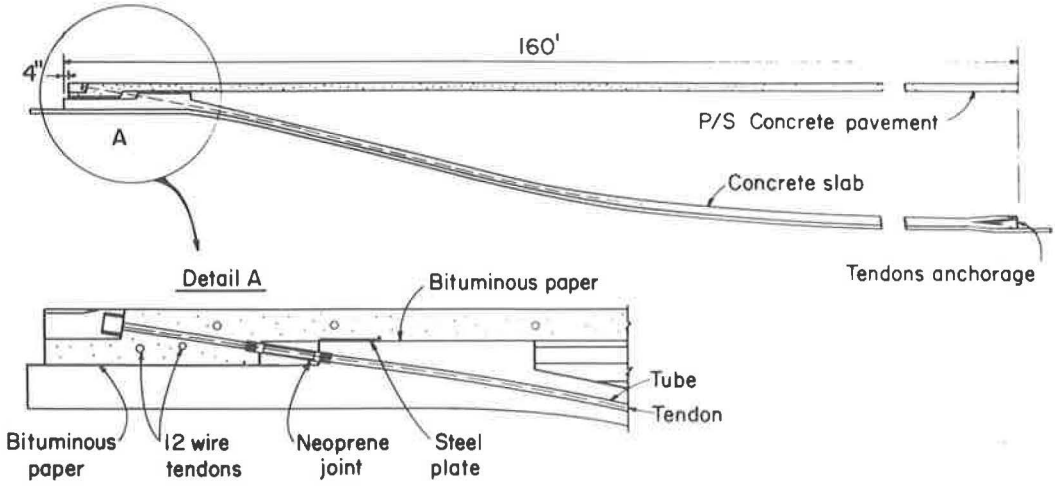

Figure 4. Details of elastic end abutment of second runway.

The small displacement of the ends of the pavement with the hygrothermal changes can be computed by hypothesis concerning the law of friction. This displacement is restrained by the friction of the pavement on the subgrade, and by the tendons.

The abutments were designed to support an average reaction equal to 966 psi (69 kg per sq cm), which corresponds to a total force of 4,968 tons for the second runway and allows the pavement to remain within the specified range of stresses for a temperature range of + 23F to + 122F (- 5C to + 50C).

PROBLEMS DURING CONSTRUCTION

Transverse Prestressing

One end of the tubes or bars which formed the conduits for the transverse tendons was placed in the corresponding conduit of the adjacent completed lane; the other end was placed in the hole in the side form. However, the completed lane was still under the stress of the initial prestress used to counterbalance the initial shrinkage of the concrete. When the new lane was put under stress, the conduits of the two adjacent lanes did not coincide. Thus, it became necessary to use conduits with a greater diameter to allow free passage of the tendons before the posttensioning. For the second runway, the diameter of the bars was 1.26 in. (32 mm) and the diameter of the tendons was only 0.63 in. (16 mm). This solved the problem.

Longitudinal Prestressing

End Abutments. —The tendons of the abutments were temporarily tensioned as soon as possible to prevent any definite displacement of the pavement, under the jacking force, during the construction.

To retain sufficient space between the upper end of the concrete abutment and the end of the pavement (to allow for future displacement of the pavement under the hygrothermal changes), temporary concrete blocks were used. These blocks were removed after construction.

Jacking Force. —At the beginning of the stressing operation the jacking force must be as low as possible to avoid excessive creep; however, it must be large enough to prevent any cracking caused by shrinkage of the concrete. When the concrete has hardened sufficiently, the force must be increased in order to reduce future creep. Empirical formulas for the stress in the slab were determined in the field during the first days of construction. For the second runway the following equations were used:

For the first day:

$$n = 2\,T \qquad (1)$$

For the following days:

$$n = 18 + 2\,(T + 5) + 10 \qquad (2)$$

In Eq. 2 the first term corresponds to the minimum allowed stress at + 23 F (- 5 C); the second term, to the correction for temperature; the last, to the estimated creep.

These equations had to be modified continuously to take other factors into account.

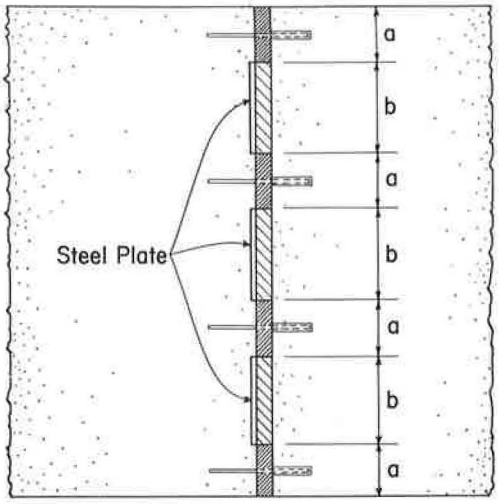

Step 1. Intervals "a" are filled up with concrete.
Step 2. Jack pressures are released and the jacks are removed.
Step 3. Steel plates are set into intervals "b" and they are filled with concrete.

Figure 5. Procedure for removing jacks.

For example, the jack width had to be continuously extended to avoid bursting, during which time the stress had to be maintained in the allowed range. When the thickness of the jacks increased from 0.4 in. (1 cm initial) to 1.0 in. (2.5 cm maximum), the jack was replaced by a steel plate and a new jack. The final stressing operation is explained in Figure 5.

SPECIFIC PROBLEMS

The most important experiments and observations made in Algiers concerned (a) distribution of the stresses between the jacking joints and the ends of the pavement at a given time; (b) variations of stresses with changes in temperature, moisture content, and time; and (c) distribution of stresses throughout the slab depth. For this purpose, the study included the volume variations of the pavement, which is restrained in movement by friction and by the tendons, Young's modulus, Poisson's ratio, the thermal expansion coefficient, and the whole past history of the pavement.

In the field, the following measurements were made (4, 5):

Distribution of Stresses in Central Section

The actual stress between two jacking joints was measured on the first runway when it became necessary to induce additional prestress after two years' creep of the concrete. Two jacking joints were activated and one jacking joint midway between these two joints was used for taking measurements. It was observed that the stresses at all of the joints became equal very quickly. This meant that the simple theory of a constant coefficient of friction must be revised. This also gave assurance that there was no section where the prestressed conditions were not satisfied. The actual behavior of the pavement was simpler than expected.

The same observation was made during construction of the second runway. The interval between the joints which induced the prestress was only 645 ft (197 m), and a special temporary joint was built in the middle of the pavement.

Displacement of Pavement Ends

The displacement of the ends of the pavements and of the upper end of the abutments was continuously observed. The upper end of the abutment is partially fixed; therefore, the displacement of the end of the pavement was small. There was perfect correlation of the observed displacements with the daily temperature changes in the slab. There was also a variation with the seasons. The daily variations were from 0.04 to 0.12 in. (1 to 3 mm) in winter, from 0.20 to 0.24 in. (5 to 6 mm) in spring, and up to 0.40 in. (10 mm) in summer. The average displacement was 0.0045 in. per °F (0.020 cm per °C). The seasonal variations did not exceed 0.4 in. (10 mm).

It follows that the stress remained practically constant, as expected. The maximum variation of stress in the concrete was less than 34 psi (2.4 kg per sq cm).

In the second runway a special joint was used to measure the stress in the vicinity of the ends of the pavement. This joint was 73 ft (22 m) from the end of the pavement. It appeared that the stress in this joint was closer to the stress in the central section, where there was no longitudinal displacement, than to the stress at the end of the pavement. Measurements made on the first pavements (4) indicated that there was no longitudinal displacement 500 ft (153 m) or more from the ends of the pavements.

Temperature in Slab

The temperature in the slab was systematically recorded in all the pavements. The gages are 1.76 in. (4.5 cm), 3.76 in. (9.5 cm), and 6.56 in. (16.7 cm) below the surface in the first pavements and 0.8 in. (2.0 cm), 3.2 in. (8.1 cm), and 5.6 in (14.2 cm) below the surface in the last pavement.

The daily variations of temperature of the air under roof 3 ft (0.9 m) above the ground and the daily variations of temperature in the concrete showed an approximate form of a sine function (Fig. 6). The variations were smaller and occurred later when the gages were farther from the surface of the concrete.

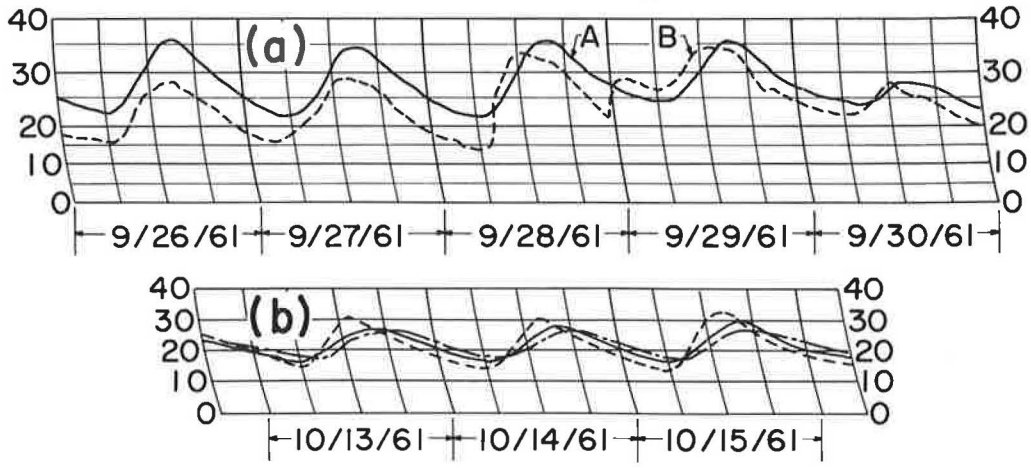

Figure 6. Typical temperature recordings (°C) of (a) gage at mid-depth of concrete (curve A) and gage in air under roof (curve B); and (b) three gages at different depths in concrete.

The temperature was approximately uniform throughout the slab depth regularly in the morning (about 7 A.M.); this uniformity occurred again, but less clearly, in the evening.

If it is assumed that the surface temperature obeys a sine law versus the time

$$T = T_0 \sin \frac{2\pi t}{H} \tag{3}$$

in which H is the period, the temperature at depth z (z = 0 at surface of slab) is given by

$$T = T_0 e^{-\beta z} - \sin\left(\frac{2\pi t}{H} - \beta z\right) \tag{4}$$

This can be shown (6) by integration of the Fourier equation

$$\frac{d^2T}{dz^2} = \frac{C\gamma}{K} \frac{dT}{dt} \tag{5}$$

in which

C = specific heat;
K = thermal conductivity coefficient;
γ = specific weight; and

$$\beta = \sqrt{\frac{\pi C \gamma}{H K}} \tag{6}$$

If this formula is used with the observations made on the second runway to take into account the decrease of the amplitude of the variations with the depth, $\beta = 5.62$; if the delay of the extreme variations is taken into account, $\beta = 5.75$. For the first pavements a good approximation could be made with $\beta = 5.75$ (4).

These values appear logical, inasmuch as the specific heat is small and the thermal conductivity is good, which results in a decrease of the thermal gradient in the slab. The following average approximate values, corresponding to the climatic conditions of Algiers, were determined:

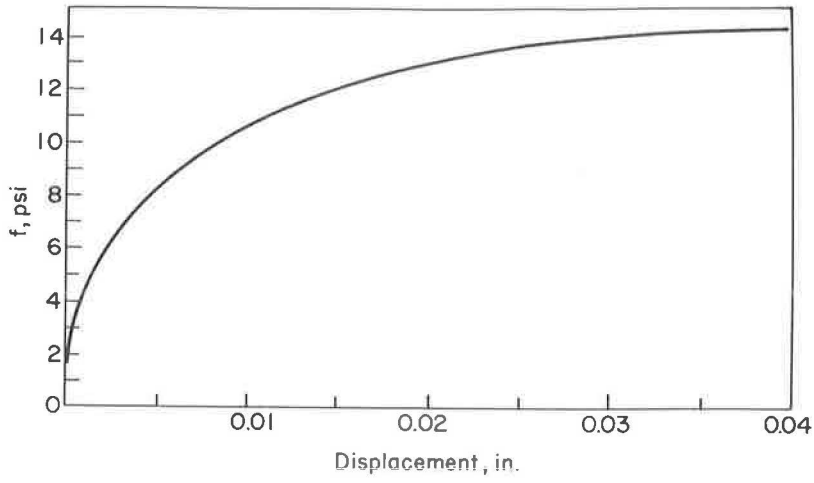

Figure 7. Measurement of slab friction.

Season	Air Temp.	Pavement Temp.
Winter	+ 50 F (10 C)	+ 41 F (5 C)
Spring	+ 59 F (15 C)	+ 68 F (20 C)
Summer	+ 77 F (25 C)	+ 86 F (30 C)

Friction

The law of friction is not simple. To gain a better understanding of friction a slab 132 ft (40 m) long was built in the same way as the first pavements and on the same subbase. The slab was pushed on one end by means of a jack, and the displacement of the other end was measured. The operation was conducted fast enough to prevent any effect of temperature changes.

The relationship obtained by plotting the observed slab displacements and the stress f, induced by the jack, is shown in Figure 7, which can be compared to a shear-stress curve for a sand. It can be used to determine a coefficient of friction; i.e., the ratio of the jacking force to the weight of the slab. As the stress increases the displacement increases; f tends to a limit which corresponds to the usual value of the friction coefficient obtained when there is a continuous sliding. Thus it can be assumed that f is a function of the displacement, ΔL, or

$$f = \phi (\Delta L) \tag{7}$$

It is possible to determine the distribution of stress in the slab when a jacking joint is acting for the first time (3), but this determination is only theoretical because temperature changes completely alter this ideal distribution.

Stress Variations with Hygrothermal Changes

By measuring the pressure in the jacks at the jacking joints of the first pavements it was possible to determine the stress variations with hygrothermal changes (3). This operation was conducted two years after construction of the pavements, a sufficient time for most of the creep in the concrete to occur. Therefore, the measured pressures corresponded to the variations of the stresses with the hygrothermal changes.

The relationship between stress variations and daily temperature changes was approximately linear, but the proportionality coefficient varied with the seasons (Fig. 9). The stresses shown correspond to the two instances during the day when the temperature throughout the slab depth was uniform (Fig. 6). The proportionality coefficient is ap-

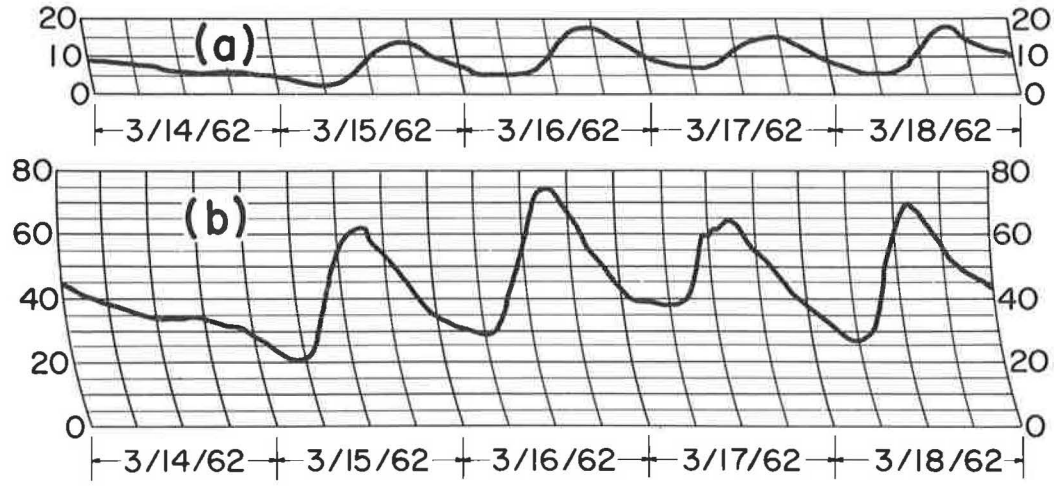

Figure 8. Typical recordings of (a) average slab temperature (°C), and (b) pressure in jacks (kg per sq cm).

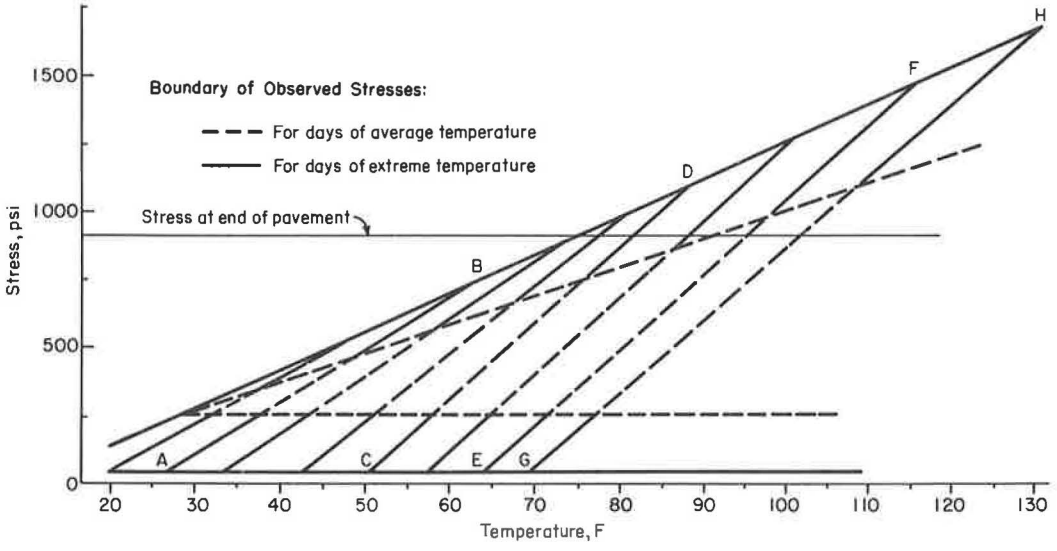

Figure 9. Stress-temperature relationship (4) in concrete pavement. AB is characteristic of a winter day; CD, of a spring day; EF, of a summer day; GH, of an extremely warm day.

proximately equal to 18 psi per deg F (2.35 kg per cm per deg C) in winter and 27 psi per deg F (3.5 kg per cm per deg C) in summer. The effective stresses were greater in winter than in summer; these results are discussed later.

For the second runway two special measuring joints were designed. The pressures of the jacks at these joints are permanently recorded; at present they give approximately the same results as those just described (Figs. 8 and 9).

The measuring joints were designed similar to the acting joints, but the entire surface between the dowels is occupied by the measuring jacks and the dowels are set closer. In these joints there are 6 dowels of 2-in. (51-mm) diameter for a 20-ft (6-m) wide lane, whereas the jacking joints have only 4 dowels of 1.6-in. (41-mm) diam-

eter for the same width of lane. Thus the force acting against flexure or curling is three times that of a jacking joint. They were so designed because they are not filled with concrete. The jacks remain in the joints and the joints are subjected to stresses induced by moving aircraft.

Attempts were made to use strain gages but, as has been shown (4, 7), it is not possible to obtain accurate results with these devices.

RELATIONSHIP BETWEEN STRESSES AND HYGROTHERMAL CHANGES

Determination of Theoretical Relationship

To simplify the problem it is assumed that (a) the pavement remains constantly on its support under its weight, (b) the vertical distribution of the temperature is the same in every point of the pavement, and (c) friction obeys the law $R = f(v)$, in which R is the resistance to the displacement induced by the friction, and $f(v)$ is a function only of the longitudinal displacement, v.

If the average rate of expansion of the slab is

$$\tau = \int_0^h \lambda \frac{dT}{dt} \frac{1}{h} dz \tag{8}$$

in which

τ = average expansion rate;
λ = thermal expansion coefficient of the concrete;
dT = temperature variation at point z, z defining the vertical position of this point; and
h = thickness of the slab.

Then the variations of stresses, n, are

$$n_3 = 0 \tag{9}$$

$$\frac{de_1}{dt} = 0 = -\frac{1}{E}\left[\frac{dn_1}{dt} - \sigma \frac{dn_2}{dt}\right] + \tau \tag{10}$$

$$\frac{de_2}{dt} = -\frac{1}{E}\left[\frac{dn_2}{dt} - \sigma \frac{dn_1}{dt}\right] + \tau \tag{11}$$

$$\frac{de_3}{dt} = \frac{\sigma}{E}\left[\frac{dn_1}{dt} + \frac{dn_2}{dt}\right] + \tau \tag{12}$$

(Axes 1, 2, 3 are directed, respectively, along the longitudinal, transverse, and vertical directions of the pavement.) These equations are implicitly valid if every cross-section remains a cross-section.

$$n_2 = \int_y^l R\, dy + N_2(t) \tag{13}$$

If origin of the y axis is in the middle of the pavement, it may be assumed that the transverse tendons give only a stress $N_2(t)$ at the edge of the pavement. Then

$$n_2 = \int_y^l f(v)\, dy + N_2(t) \text{ with } v \equiv v(y,t) \tag{14}$$

From Eqs. 8, 9, 10, 11 and 12,

$$\frac{de_2}{dt} = - \frac{(1 - \sigma^2)}{E} \frac{dn_2}{dt} + z (1 - \sigma) \tag{15}$$

The curve f (v) can be approximated by a straight line

$$f (v) \equiv A v \tag{16}$$

because the width of the pavements is such that for an average variation of temperature equal to ± 27 F (± 15 C) the displacement of the edge, without friction, should be small enough to maintain the value of f (v) corresponding to this maximum displacement below the maximum value of f (v) experimentally determined as indicated. It will be possible later to verify that all the displacements are small enough to assure that this approximation is sufficiently accurate.

The theoretical solution, if all of the preceding hypotheses are assumed, is

$$\frac{d^2 \frac{dv}{dt}}{dy^2} = (\frac{1 - \sigma^2}{E}) A \frac{dv}{dt} \tag{17}$$

If t_o is considered to be the instant when the transverse posttensioning was induced,

$$v = - \frac{(1 - \sigma^2)}{E} \int_0^y n_2 dy \tag{18}$$

because

$$n_1 - \sigma n_2 = 0 \tag{19}$$

$$e_2 = - \frac{1}{E} (n_2 - \sigma n_1) \tag{20}$$

with $\frac{dn_2}{dy} = - Av$, $V_{\left(\begin{smallmatrix} y = 0 \\ t = t_o \end{smallmatrix}\right)} = 0$, and $n_{2\left(\begin{smallmatrix} y = 0 \\ t = f_o \end{smallmatrix}\right)} = N_2(0)$,

$N_2(0)$ being the constant value specified for the construction and induced by the tensioning of the tendons.

It follows that

$$n_{2(t_o)} = \frac{N_2(0)}{\cosh l \sqrt{\frac{A}{E}(1 - \sigma^2)}} \cosh y \sqrt{\frac{A}{E}(1 - \sigma^2)} \tag{21}$$

$$V_{(t_o)} = - \frac{N_2(0)}{A} \sqrt{\frac{A}{E}(1 - \sigma^2)} \frac{\sinh y \sqrt{(1 - \sigma^2)\frac{A}{E}}}{\cosh l \sqrt{\frac{A}{E}(1 - \sigma^2)}} \tag{22}$$

Eq. 17 gives

$$\frac{dv}{dt} = \frac{dC(t)}{dt} \sinh y \sqrt{\frac{A}{E}(1 - \sigma^2)} \tag{23}$$

because $V_{(y = 0)} \equiv 0$ for every value of t.

Also,

$$V_{(t)} = C_{(t)} \sinh y \sqrt{\frac{A}{E}(1 - \sigma^2)} \tag{24a}$$

in which

$$C_{(t_0)} = - \frac{N_2(0)}{A} \frac{\sqrt{\frac{A}{E}(1 - \sigma^2)}}{\cosh l \sqrt{\frac{A}{E}(1 - \sigma^2)}} \tag{24b}$$

If it is assumed that the tendons are free in their conduits (neglecting the friction of the tendons in the conduits, which is justified considering the small variation of stress which corresponds to this friction), it is clear that

$$n_{2(y = l)}(t) = N_2(t) = \frac{N_2(0)}{\Delta L_0} (L_t - L_0 - L_t \lambda_a) \int_{t_0}^{t} \frac{dT}{dt} dt) \tag{25}$$

in which L_0 = length of the tendons before tensioning;

$$N_2(0) = E_a \frac{\Delta L_0}{L_0} \frac{S_a}{S_b} \tag{26}$$

$\frac{S_a}{S_b}$ = ratio of the cross-section of the steel tendons and the concrete;
L_0 = initial increase in length of tendons;
λ_a = thermal expansion coefficient of steel;
$\frac{dT}{dt}$ = rate of change of temperature of tendons;
$L_{(t)}$ = length of the tendons at time t;

$$L_{(t_0)} = \Delta L_0 + L_0 = l + v_{\substack{(y = l) \\ (t = t_0)}} \tag{27}$$

$$n_2 = \frac{AC(t)}{\sqrt{\frac{A}{E}(1 - \sigma^2)}} \left[\cosh l \sqrt{\frac{A}{E}(1 - \sigma^2)} - \cosh y \sqrt{\frac{A}{E}(1 - \sigma^2)} \right] + N_2(0) +$$

$$\frac{N_2(0)}{\Delta L_0} \left[(C_{(t)} - C_{(t_0)}) \sinh l \sqrt{\frac{A}{E}(1 - \sigma^2)} - L_{(t_0)} \lambda_a \int_{t_0}^{t} \frac{dT}{dt} dt \right] \tag{28}$$

But Eq. 15 gives

$$\frac{dC(t)}{dt} = \frac{\tau(1+\sigma) + \frac{N_2(0)}{\Delta L_0} L_{(t_0)} \lambda_a \frac{dT}{dt}\left(\frac{1-\sigma^2}{E}\right)}{\sqrt{\frac{A}{E}(1-\sigma^2)} \cosh l \sqrt{\frac{A}{E}(1-\sigma^2)} + \frac{N_2(0)}{\Delta L_0}\left(\frac{1-\sigma^2}{E}\right) \sinh l \sqrt{\frac{A}{E}(1-\sigma^2)}} \quad (29)$$

If it is assumed that

$$\lambda = \lambda \frac{dT}{dt} \quad (30)$$

and

$$\frac{dT}{dt_b} = \frac{dT}{dt_a} \quad (31)$$

$$C(t) = \left[\frac{\left[\lambda(1+\sigma) + \frac{N_2}{\Delta L_0} L_{(t_0)} \frac{(1-\sigma^2)}{E} \lambda_a\right] T}{\sqrt{\frac{A}{E}(1-\sigma^2)} \cosh l \sqrt{\frac{A}{E}(1-\sigma^2)} + \frac{N_2}{\Delta L_0} \frac{(1-\sigma^2)}{E} \sinh l \sqrt{\frac{A}{E}(1-\sigma^2)}}\right]_{T_0}^{T} - \frac{\frac{N_2(0)}{A}\sqrt{\frac{A}{E}(1-\sigma^2)}}{\cosh l \sqrt{\frac{A}{E}(1-\sigma^2)}} \quad (32)$$

or

$$C(t) = \alpha(T - T_0) - \beta \quad (33)$$

$$V = \left[\alpha(T - T_0) - \beta\right] \sinh y \sqrt{\frac{A}{E}(1-\sigma^2)} \quad (34)$$

$$n_{2_{av}} = C(t)\left[\frac{A}{\sqrt{\frac{A}{E}(1-\sigma^2)}} \cosh l \sqrt{\frac{A}{E}(1-\sigma^2)} - \frac{E}{l(1-\sigma^2)} \sinh l \sqrt{\frac{A}{E}(1-\sigma^2)} + \frac{N_2(0)}{\Delta L_0} \sinh l \sqrt{\frac{A}{E}(1-\sigma^2)}\right] - C_{(t_0)} \frac{N_2(0)}{\Delta L_0} \sinh l \sqrt{\frac{A}{E}(1-\sigma^2)} + N_2(0) - L_{(t_0)} \lambda_a (T - T_0) \frac{N_2(0)}{\Delta L_0} \quad (35)$$

Thus, the expression of average n_2 has the form

$$\gamma(T - T_0) + \delta \quad (36)$$

However, Eq. 36 is valid only if the tendons are free in the conduits and if Eqs. 9, 10, 11 and 12 are valid.

The creep gives a variation of e_1 when the longitudinal prestress is not definitively induced, and the deformation being plastic, Hooke's law is not valid. In any case, it is assumed that the preceding results are accurate enough to be used in the following developments.

At time t_0' the conduits are grouted and the tendons are bound to the concrete. Thus,

$$\frac{dN_a}{dy} = \frac{dn_2}{dy} + Av \tag{37}$$

in which N_a is the ratio of the tension force of the tendons to the corresponding section of the concrete. By convention, tension in the tendons is considered positive in this text. The change in length of a tendon is given by

$$\frac{S_b}{S_a}\frac{dN_a}{dt} = E_a\left[\frac{d^2v}{dt\,dy} - \lambda_a\frac{dT}{dt}\right] \tag{38}$$

From Eqs. 37, 38, and 15,

$$V = C_{(t)}\sinh y\sqrt{\frac{A}{\frac{E}{1-\sigma^2}+\frac{E_a S_b}{S_b}}} + V_{(t'_0)} \quad \text{with } V_{(t)\,(y=0)} \equiv 0 \tag{39}$$

$$n_2(t) = \frac{E}{1-\sigma}\lambda(T - T'_0) - \frac{E}{1-\sigma^2}C_{(t)}\sqrt{\frac{A}{\frac{E}{1-\sigma^2}+\frac{E_a S_b}{S_b}}} + \cosh y\sqrt{\frac{A}{\frac{E}{1-\sigma^2}+\frac{E_a S_a}{S_b}}} + n_2(t'_0) \tag{40}$$

$$N_2 = n_2(t) + \frac{AC_{(t)}}{\sqrt{\frac{A}{\frac{E}{1-\sigma^2}+\frac{E_a S_a}{S_b}}}}\cosh y\sqrt{\frac{A}{\frac{E}{1-\sigma^2}+\frac{E_a S_a}{S_b}}} - \left(\lambda_a\frac{S_a E_a}{S_b} + \frac{E}{1-\sigma}\lambda\right)(T - T'_0) \tag{41}$$

The boundary condition $N_a(l) = N_b(l)$ determines $C(t)$ and

$$n_2(t) = \frac{E}{1-\sigma}\lambda(T - T'_0) - \left[\frac{\frac{E}{1-\sigma^2}\left[\frac{\lambda_a S_a E_a}{S_b} + \frac{E}{1-\sigma}\lambda\right]}{\frac{E}{1-\sigma^2} + \frac{E_a S_a}{S_b}} + \frac{\cosh y\sqrt{\frac{A}{\frac{E}{1-\sigma^2} + \frac{E_a S_a}{S_b}}}}{\cosh l\sqrt{\frac{A}{\frac{E}{1-\sigma^2} + \frac{E_a S_a}{S_b}}}}\right](T - T'_0) + n_2(T'_0) \quad (42)$$

$$n_{2_{av}}(t) = \frac{E}{1-\sigma}\lambda(T - T'_0) - \left[\frac{\frac{E}{1-\sigma^2}\left[\frac{\lambda_a S_a E_a}{S_b} + \frac{E}{1-\sigma}\lambda\right]}{l\sqrt{A\left(\frac{E}{1-\sigma^2} + \frac{E_a S_a}{S_b}\right)}} + \tanh l\sqrt{\frac{A}{\frac{E}{1-\sigma^2} + \frac{E_a S_a}{S_b}}}\right](T - T'_0) + n_{2_{av}}(t_0) \quad (43)$$

It appears that the variation of $n_{2_{av}}$ is very small. If, for example, the approximate values for the second runway are $A = 1.75$ psi per in. (0.05 kg per sq cm), $E = 6.3 \times 10^6$ psi (450,000 kg per sq cm), $\sigma = 0.3$, $E_a = 28 \times 10^6$ psi (2×10^6 kg per sq cm), $\lambda = 5 \times 10^{-6}$, $\lambda_a = 10 \times 10^{-6}$, $S_a/S_b = 265/(1,330 \times 160)$, and $l = 885$ in. (2,250 cm), then $\Delta n_2 = 6.2\,\Delta T$ psi ($0.444\,\Delta T$ kg per sq cm). If $E\lambda$ is determined by

$$\Delta n_1 = E\lambda\Delta T \quad (44)$$

and not by

$$\Delta n_1 = E\lambda\Delta T + \sigma\Delta n_2 \quad (45)$$

the relative error is increased, but it is still less than 6 percent.

Thus, it can be assumed that the ratio of the rate of change of longitudinal prestress to the rate of change of temperature is equal to $E\lambda$, although the preceding developments require some assumptions which approximate the actual behavior.

The upper expression of n_2 is linear in λ, T, T'_0 and T_0; that is,

$$n_2 = (a_1\lambda + a_2\lambda_a)(T - T'_0) + (a_3\lambda + a_4\lambda_a)(T'_0 - T_0) + a_5 \quad (46)$$

As a result:

1. If, in two sections of the pavement, the temperatures corresponding, first, to the tensioning of the transverse tendons, and second, to the grouting of the conduits, are different, the transverse stress is not the same in these two sections. It follows that a systematic difference of longitudinal stress can eventually occur for these two sections. This difference is due chiefly to the initial induced prestress.
2. If the thermal expansion coefficient is not constant, it is possible that, for the same variation of temperature, different variations of transverse stress can be observed. Thus, the ratio of the rate of change of longitudinal prestress to the rate of change of temperature shows a variation greater than $E\lambda$, but remains linear in λ.
3. If the characteristics of the concrete remain constant, the preceding developments cannot be used to explain the observed variations of the stresses.

It could be possible to explain these observations by assuming (a) that no friction exists; that is,

$$\Delta n_2 = \left[\frac{E\lambda}{1-\sigma} - \frac{E}{1-\sigma^2} \frac{\frac{S_a S_b \lambda_a}{E_a} + \frac{E}{1-\sigma}}{\frac{S_a E_a}{S_b} + \frac{E}{1-\sigma^2}} \right] \Delta T \qquad (47)$$

and Δn is approximatively equal to $\lambda E \Delta T$; and (b) that an infinite amount of friction is developed; that is,

$$\Delta n_1 = \frac{\lambda E}{1-\sigma} \Delta T \qquad (48)$$

The ratio of these two coefficients ($\Delta n_1/\Delta T$) is approximately equal to the actual observed ratio (2.35/3.50). However, there is no reason to believe that in summer the friction completely restrains the pavement from movement and that in winter there is no friction. Thus it is clear that λE is not constant.

As a result, attempts were made to determine the variations of the thermal expansion coefficient and Young's modulus of the concrete with the three factors of stress, temperature, and moisture content.

Study of Variation of Modulus of Elasticity

Variation with Stress. —The modulus of elasticity of concrete varies with the stress, but the observed variations are small, especially for an old concrete such as the concrete at Maison-Blanche Airport. However, few of the experiments conducted to date by others are valid because the reversible elastic deformations were not separated from the total deformations.

Le Camus (8) shows that E decreases when the stresses increase; in the range of stresses observed in Algiers the variations of E are smaller than 5 percent of the dynamic modulus. The formula of the Zurich Laboratory, Vivian's formula, and the experiments of Santarelii cited by L'Hermite (9), are all in agreement.

The dynamic modulus of concrete remains constant for every static load; the measurement of the speed of sound in water made by the Laboratoire du Batiment et des Travaux Publics under stresses of 0, 700, and 1, 400 psi (0.50, and 100 kg per sq cm) on specimens of the Algiers concrete indicated no variation of the dynamic modulus. Thus the variations of the elastic modulus are smaller than 5 percent and this is true for every rate of loading.

Variation with Temperature. —The speed of sound was measured in the concrete at different times of the same day. No important variation was observed. It appears that E decreases slightly when the temperature increases, but the variations have the same magnitude as the possible error. On the other hand, the stress of a constrained concrete specimen increases with the temperature and the observations correspond to the simultaneous variations of these two factors.

The dynamic modulus being approximately constant, the variations of the elastic modulus are certainly not important, following the conclusions of the immediately preceding section.

The experiments of Theuer (10) seem to indicate that the modulus of instantaneous deformation considerably decreases when the temperature increases; however, the experiments were performed on new concrete without distinction between total deformation and reversible deformation and for only one increment of temperature.

Variation with Moisture Content. —A dry-air cured concrete does not possess, after soaking, the same modulus as a similar wet-air cured concrete, the modulus of the dry-air cured concrete always being smaller. On the other hand, if concrete is cured in water and then air-dried, the modulus is increased as if the concrete remained in the water (9). Therefore, it cannot be concluded that E increases with increases in moisture content.

The studies of Theuer (10) indicate that E decreases with temperature increases. This is more evident when the concrete is saturated, E being greater for a saturated concrete than for a dry concrete. But the moisture content of the concrete was, in these experiments, the storage moisture content; thus the concrete structure is not the same for all the specimens, and a true comparison of the different observed values of E is not possible. However, if a variation does exist, it certainly corresponds to an increase of E with the moisture content.

In conclusion, the observed variations of λE cannot be explained by the simple variation of E, which occurs in the opposite direction (it is shown later that small values of E were observed for concrete with a high moisture content). The explanation must be found in the variation of λ.

Study of Variation of Thermal Expansion Coefficient

Variation with Stress and Temperature. —To study the effect of stress and temperature, three series of experiments were conducted of 7 × 7 × 28-in. (17.8 × 17.8 × 71-cm) concrete specimens (27-40-mm aggregates were replaced by the same weight of 7-27-mm aggregates to avoid a wall (form) effect during the molding of the specimens).

The specimens were maintained in a relative humidity of 99 percent at 68 F (20 C). The molds were removed 48 hr after mixing and the specimens were put into water at 68 F (20 C).

First Experiment. —A compressive stress of 700 psi (50 kg per sq cm) was applied to two specimens for 4 weeks to eliminate most of the creep. During this time the specimens were maintained in water at 68 F (20 C). The specimens were then subjected to a stepwise variation of temperature from 68 F to 131 F (20 C to 55 C) and from 131 F to 68 F (55 C to 20 C) under a constant compressive stress of 700 psi (50 kg per sq cm). Equilibrium was maintained and length measurements made at 68 F (20 C), 86 F (30 C), 104 F (40 C), 131 F (55 C), 104 F (40 C), 86 F (30 C), and 68 F (20 C). Two unloaded specimens were subjected to the same variations of temperature. The results of these tests are given in Table 1 and Figure 10.

Second Experiment. —Two specimens were permitted to expand freely through the temperature cycles of 68 F (20 C) to 86 F (30 C), 68 F (20 C) to 104 F (40 C), and 68 F (20 C) to 140 F (60 C). When equilibrium was reached at a given temperature, a force sufficient to obtain the specimen's original length was applied. After measuring this force, the force was removed and the temperature decreased to 68 F (20 C) for the next cycle. The results are indicated in Table 2 and Figure 11.

Third Experiment. —Before testing, the specimens were subjected to the same increase in temperature and pressure as in the first experiment in order to eliminate part of the creep. During this operation the initial load was 280 psi (20 kg per sq cm).

The specimens were then subjected to a stepwise increase in temperature from 68 F to 133 F (20 C to 56 C), then a decrease of temperature from 133 F to 68 F (56 C to 20 C) with equilibrium at 104 F (40 C) and 86 F (30 C). The objective was to maintain a constant specimen length while measuring the variations of stress with the temperature changes. The results are given in Table 3 and Figure 12.

On the basis of these experiments it can be concluded that over a range of temperatures the deformation (length change) is not linear but shows the aspect of a curve (Fig.

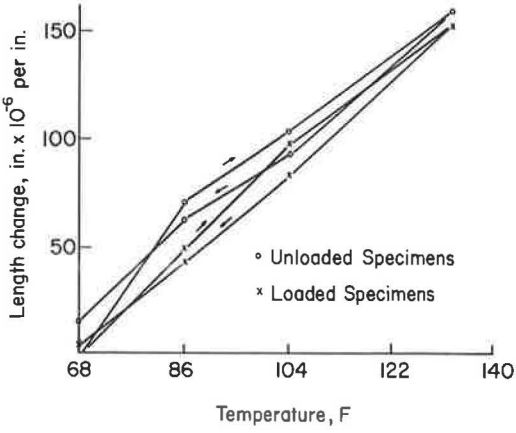

Figure 10. Length change-temperature relationships of constrained and unconstrained specimens.

TABLE 1

CHANGE IN LENGTH OF LOADED AND UNLOADED SPECIMENS DUE TO TEMPERATURE CHANGE

Temp. (° F)	Temp. (° C)	Length Change (10^{-6} in. per in.) Loaded Specimens[a] No. 1	Loaded Specimens[a] No. 2	Loaded Specimens[a] Avg.	Unloaded Specimens No. 1	Unloaded Specimens No. 2	Unloaded Specimens Avg.
68	20	0	0	0	0	0	0
86	30	+ 48	+ 51	+ 49.5	+ 66	+ 78	+ 72
104	40	+ 96	+ 102	+ 99	+ 96	+ 114	+ 105
132	55.5	+ 168	+ 144	+ 156	+ 150	+ 174	+ 162
104	40	+ 90	+ 78	+ 84	+ 90	+ 102	+ 96
86	30	+ 42	+ 48	+ 45	+ 54	+ 72	+ 63
68	20	- 6	+ 12	+ 3	+ 6	+ 24	+ 15

[a] Specimens loaded in compression to stress of 700 psi (50 kg per sq cm).

TABLE 2

STRESS REQUIRED TO OBTAIN ORIGINAL LENGTH OF EXPANDED SPECIMEN

Test	Var. of Temp. (° F)	Var. of Temp. (° C)	Stress (psi)[a] Spec. 1	Stress (psi)[a] Spec. 2	Stress (psi)[a] Avg.
First	68 to 86	20 to 30	294 (21)	350 (25)	322 (23)
	68 to 104	20 to 40	532 (38)	525 (37.5)	528 (38)
	68 to 140	20 to 60	770 (55)	770 (55)	770 (55)
Second	68 to 86	20 to 30	435 (31)	322 (23)	378 (27)
	68 to 104	20 to 40	616 (44)	560 (40)	588 (42)
	68 to 133	20 to 56	741 (53)	584 (56)	762 (54.5)

[a] Values in parentheses are in kg per sq cm.

13) which characterizes an adjustment or accommodation cycle; e.g., a completely reversible cycle is reached after all irreversible deformation has taken place. The accommodation cycle can be further defined by reference to Figure 14. If a force acts periodically on a material, the deformation generally follows the pattern shown in Figure 14. If after a series of such cycles, a final completely reproducible cycle is attained indefinitely, this is referred to as the accommodation cycle. It may be assumed that consecutive cycles progressively give a definite curve.

The form of the first-cycle curve is dependent on the stress. The greater the stress, the flatter the curve, but the average slope remains constant. The first experiment gives the curve indicated for the first cycles.

The third experiment showed that even though slight creep occurred, the curve obtained (stress-temperature) is in good agreement with the preceding consideration, because it is approximately the same as in the first experiment (length change-temperature, with a coefficient E/L). This experiment corresponds to a second cycle of temperature; therefore, it is difficult to assign the observed behavior to simple irreversible physico-chemical changes in the concrete. Creep is not a satisfactory explana-

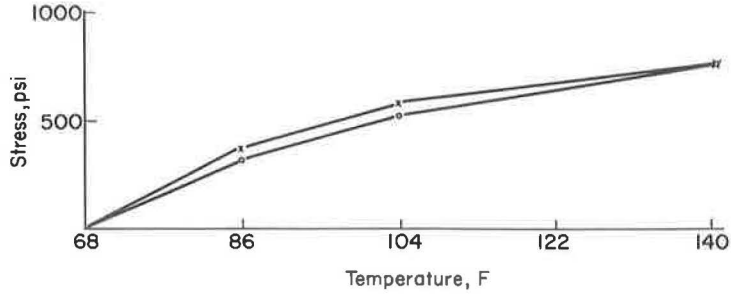

Figure 11. Stress-temperature relationships of constrained and unconstrained specimens.

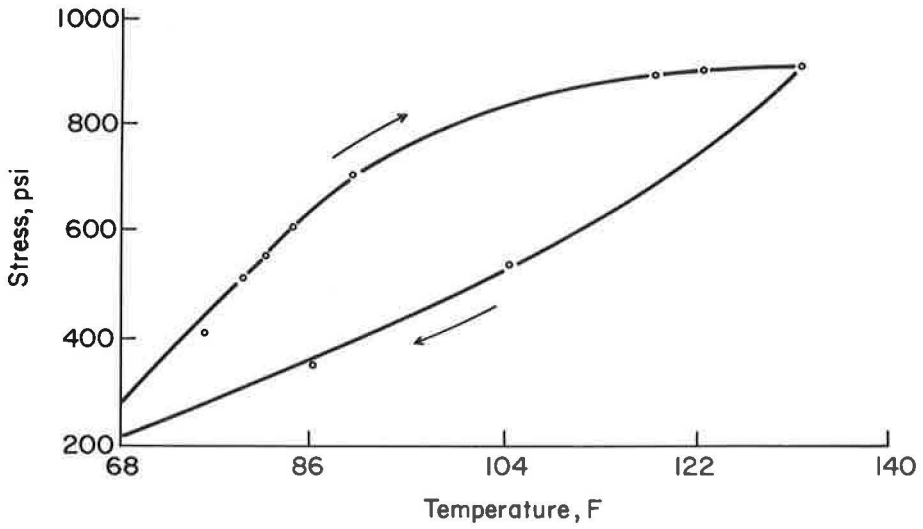

Figure 12. Stress-temperature relationship at constant specimen length.

TABLE 3

STRESS RESULTING FROM RESTRAINING SPECIMEN TO CONSTANT LENGTH DURING TEMPERATURE CHANGE

Temp.		Stress	
(° F)	(° C)	(psi)	(kg/sq cm)
68	20	280	20
76.1	24.5	413	29.5
79.7	26.5	518	37
81.5	27.5	560	40
84.2	29	616	44
89.6	32	714	51
117.5	47.5	902	64.5
122	50	881	63
131	55	923	66
104	40	546	39
86	30	357	25.5
68	20	217	15.5

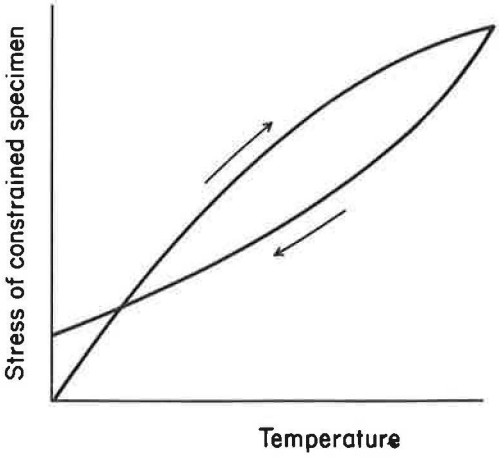

Figure 13. Theoretical relationship between temperature and stress of constrained specimen.

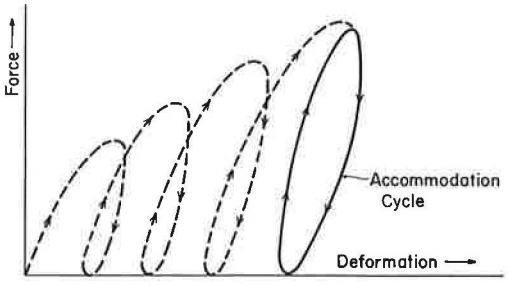

Figure 14. Adjustment or accommodation cycle.

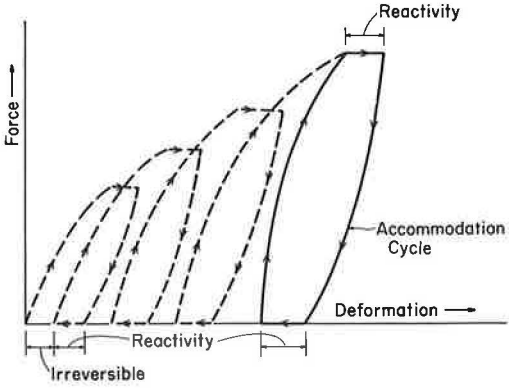

Figure 15. Effect of reactivity on accommodation cycle.

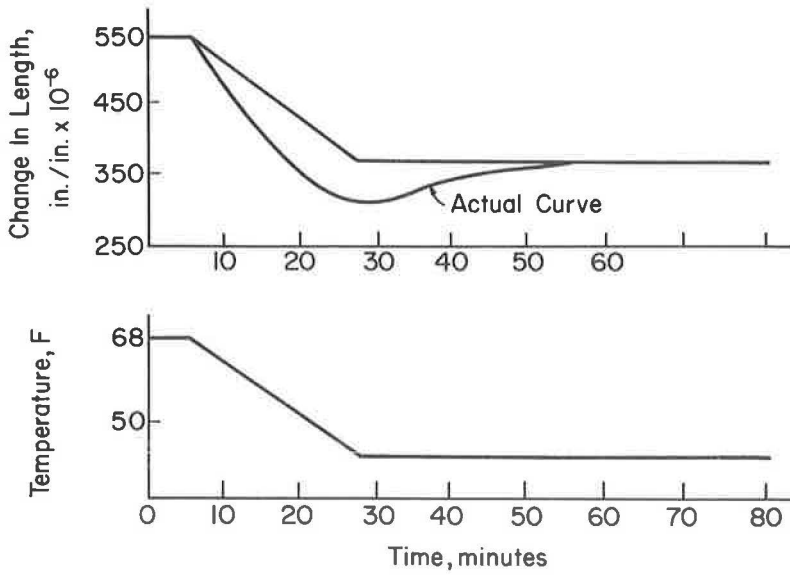

Figure 16. Effect of temperature variation on length change of specimen maintained in water.

tion because in this case the average slope of the curve should be, during the decrease of temperature, equal to or greater than the slope during the increase.

The second experiment is in good agreement with the preceding conclusions, but the importance of creep cannot be determined. In any case, the Algiers pavements are old enough so that it can be assumed that the accommodation cycle has occurred, and that the cycle is definitely flat. Therefore, it can result in only a smaller variation of the ratio of stress change to temperature change. Besides, the accommodation cycle is very often observed with reactivity. In Figure 15 the shape of the accommodation cycle is altered (see Fig. 14) by definite reversible deformations occurring with time; e.g., the total deformation does not occur immediately upon loading and does not disappear immediately upon unloading. These reversible deformations constitute reactivity, as defined in this paper, and are not to be confused with creep. Powers (11) indicates that some reactivity occurs for concrete.

Figure 16 shows the effect of the variation of temperature on the length change of a specimen maintained in water. The greater dT/dt is, the more pronounced is the phenomenon. Unfortunately, in this particular case for one of the two instances during which the temperature in the slab was uniform, dT/dt was a maximum.

Thus, this characteristic appears to be the most important among all the preceding developments discussed; it may result in a significant error and Eq. 44 may have to be replaced by

$$\Delta n_1 = E\lambda f\left(\frac{dT}{dt}\right)\Delta T \tag{49}$$

or even by

$$\Delta n_1 = E\lambda f\,(t,\ \Delta t)\,\Delta T \tag{50}$$

Variation with Moisture Content. —It is known that a variation in humidity at a constant temperature causes volume changes in concrete. This is due not only to physicochemical changes in the solid part of the concrete, but also to a modification of the

equilibrium between included water and this solid part. Three categories of included water may be observed (9, 12), as follows:

1. Chemically combined water.
2. Adsorbed and capillary water.
3. Free water.

The first category corresponds essentially to the non-evaporable water in the usual temperature range; the others to the evaporable water. The equilibrium which is disturbed by a variation of humidity concerns the adsorbed water and the capillary water.

At a given temperature and water vapor pressure, the cement gel water, the capillary water and the vapor water are in an equilibrium which seems to depend only on temperature and water vapor pressure. A change of this equilibrium induces a change of stresses caused by the interaction of water and solid. However, no such changes occur in the following two instances:

1. If the concrete is saturated and remains saturated (100 percent humidity).
2. If there is no adsorbed water or no capillary water, which appears to be true for a relative humidity less than 40 percent.

Under these conditions the thermal expansion coefficient remains the same. For a relative humidity between 40 and 100 a greater value is observed, as indicated by Bonnel and Harper (13), and Meyers (14). Figures 17 and 18 are characteristic of the values obtained. It should be noted that for a limestone-aggregate concrete (as used in Algiers), λ varies in a ratio equal to 23/36, not much different from the ratio of the two extreme values of λE observed in Algiers.

CONCLUSIONS

It can be concluded that the variation of the ratio of the stress rate to the temperature is mainly due to a variation of the thermal expansion. This variation is due either to a phenomenon of reactivity or, more likely, to a change in moisture content.

In Maison-Blanche, the average relative humidity of the air is approximately constant at 78 percent from October to February; then it decreases to 67 percent from March to May, and increases irregularly from June to September with an average value

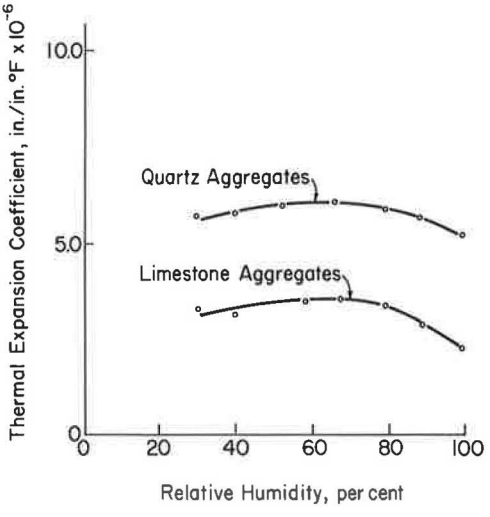

Figure 17. Thermal expansion coefficient-relative humidity relationship for two concrete aggregates (after Meyers, 14).

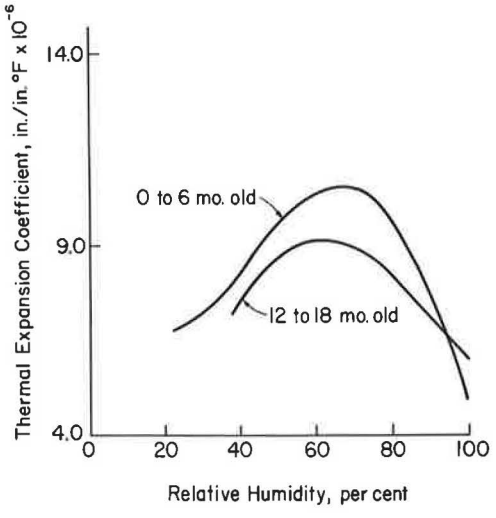

Figure 18. Effect of age on thermal expansion coefficient-relative humidity relationship (after Meyers, 14).

of 73 percent. This information is based on daily observations made every 3 hours during 1961.

Inasmuch as the variations of moisture content occur very slowly, the average daily humidity and temperature of the concrete can be used for calculating purposes. Under these ideal conditions there is an equilibrium between the vapor pressure of the air and the vapor pressure of the concrete only if the two entropies are equal; that is,

$$\int_{T_1}^{T_2} C_p \, d \log T + R \log \frac{p_1}{p_2} = 0 \qquad (51)$$

in which R is the constant of perfect gases.

In Algiers, the following average temperatures were observed:

	Temperature		
Location	Winter	Spring	Summer
Slab	41 F (5 C)	68 F (20 C)	122 F (50 C)
Air	50 F (10 C)	59 F (15 C)	77 F (25 C)

Using Eq. 51, it is possible to compute the vapor pressure in the concrete and to determine the relative humidity. This computation gives results which are in good agreement with actual observations. In winter the slab is in a saturated condition; in spring the relative humidity is approximately 52 percent; in summer it is approximately 58 percent.

These considerations give a satisfactory explanation of the observed variations of λE. They also explain why the stress is higher in winter than in summer at a given temperature.

Unfortunately, it was not possible to make all the experiments and observations hoped for. The preceding developments, however, are in good agreement with the actual behavior of the pavement and explain the observations made in Algiers. They give assurance that the stresses will remain in the specified range and that the design of the pavement is adequate for the expected traffic.

The design of these pavements is a direct application of the theories of Freyssinet. The method was used with success because of the experience and competency of the contractor, Entreprises Campenon-Bernard.

The design was selected competitively from three possible designs: asphalt pavement, ordinary concrete pavement, and prestressed concrete pavement. Bids on these designs were approximately equal. The prestressed concrete pavement was chosen because of the easy and cheap maintenance and smooth riding surface that results from the elimination of joints. Because the most expensive part of the construction is the end abutments, it is quite likely that for a longer pavement, the prestressed concrete would cost less than the other designs.

ACKNOWLEDGMENTS

The preceding developments summarize many studies and experiments led by Messrs. J. Gabriel, J. Block and J. G. Claudon under the direction of Mr. Pousse, and by the contractor's engineers.

The author is pleased to acknowledge the assistance of Les Laboratoires des Batiments et des Travaux Publics, which conducted many of the tests, and of those who aided in the construction of the pavements of Algiers Airport.

E. L. Kawala, Engineer with the Portland Cement Association, was of inestimable assistance in the preparation of this paper, including assembly, editing and presentation.

REFERENCES

1. Pousse, M., "L'Aeroport d'Alger-Maison-Blanche et ses Noveaux Ouvrages vue d'Ensemble sur les Principles de Construction." Revue Generale des Routes et des Aerodromes (Paris), 26: No. 296, 53-75 (Sept. 1956).
2. Gabriel, J., and Pigeot, R., "La Construction de la Nouvelle Piste NE-SW d'Alger-Maison-Blanche et de ses Anneres." Revue Travaux (Paris), 39: No. 249, 617-634 (July 1955).
3. Claudon, J. G., and du Sorbier, M., "La Nouvelle Piste en Beton Precontraint d'Alger-Maison-Blanche et ses Ouvrages Annexes." Revue Travaux (Paris), 46: No. 332, 465-476 (June 1962).
4. Block, J., "Revetements Precontraints: Comportement des Ouvrages de l'Aerodrome d'Alger-Maison-Blanche." Spec. publ., Aeroport de Paris (Dec. 1958).
5. Claudon, J. G., "Le Revetement en Beton Precontraint de la Nouvelle Piste de l'Aeroport d'Alger-Maison-Blanche." Revue Generale des Routes et des Aerodromes (Paris), 32: No. 364, 101-116 (May 1962).
6. Jeuffroy, G., "Consideration Theoretiques sur le Calcul des Chaussees en Beton." Revue Generale des Routes et des Aerodromes, 25: No. 276, 57-58 (Jan. 1955).
7. Claudon, J. G., "Pistes et Voie de Circulation en Beton Precontraint de l'Aerodrome d'Alger-Maison-Blanche." Spec. Report.
8. le Camus, B., "Recherches Experimentales sur la Deformation du Beton et du Beton Arme." Compte Rendu des Recherches des Laboratoires du Batiment et des Travaux Publics (Paris) (1945-6).
9. l'Hermite, R., "Les Deformations du Beton." Cahiers de la Recherche, Assn. Francaise de Recherches et d'Essais sur les Materiaux et les Contructions.
10. Theuer, A. U., "Effect of Temperature on the Stress Deformation of Concrete." Jour. of Research, U. S. Natl. Bur. of Standards, 18: No. 2, 195-204 (Feb. 1937).
11. Powers, T. C., "The Physical Structure and Engineering Properties of Concrete." Res. Bull. 90, Portland Cement Assn., 28 pp. (July 1958).
12. Powers, T. C., and Brownyard, T. L., "Studies of the Physical Properties of Hardened Portland Cement Pastes." Jour. Amer. Conc. Inst., 18: No. 8, 933-992 (Apr. 1947).
13. Bonnell, D. G. R., and Harper, F. C., "The Thermal Expansion of Concrete." Tech. Paper No. 7, National Building Studies, Building Research Station, Gt. Brit., 24 pp. (1951).
14. Meyers, S. L., "Thermal Expansion Characteristics of Hardened Cement Paste of Concrete." Proc. HRB, 30: 193-203 (1950).